

COMPRESSIVE SENSING FOR RADAR TARGET DETECTION

A THESIS SUBMITTED TO  
THE GRADUATE SCHOOL OF NATURAL AND APPLIED SCIENCES  
OF  
MIDDLE EAST TECHNICAL UNIVERSITY

BY

FIRUZE ÇAĞLIYAN

IN PARTIAL FULFILLMENT OF THE REQUIREMENTS  
FOR  
THE DEGREE OF MASTER OF SCIENCE  
IN  
ELECTRICAL AND ELECTRONICS ENGINEERING

FEBRUARY 2014



Approval of the thesis:

**COMPRESSIVE SENSING FOR RADAR TARGET DETECTION**

Submitted by **FİRuze ÇAĞLIYAN** in partial fulfillment of the requirements for the degree of **Master of Science in Electrical and Electronics Engineering Department, Middle East Technical University** by,

Prof. Dr. Canan ÖZGEN

Dean, Graduate School of **Natural and Applied Sciences**

\_\_\_\_\_

Prof. Dr. Gönül Turhan SAYAN

Head of Department, **Electrical and Electronics Engineering**

\_\_\_\_\_

Assoc. Prof. Ali Özgür YILMAZ

Supervisor, **Electrical and Electronics Engineering Dept., METU**

\_\_\_\_\_

**Examining Committee Members:**

Prof. Dr. Yalçın TANIK

Electrical and Electronics Engineering Dept., METU

\_\_\_\_\_

Prof. Dr. Tolga ÇİLOĞLU

Electrical and Electronics Engineering Dept., METU

\_\_\_\_\_

Assoc. Prof. Dr. Çağatay CANDAN

Electrical and Electronics Engineering Dept., METU

\_\_\_\_\_

Assoc. Prof. Dr. Ender Mete EKŞİOĞLU

Electronics and Communication Engineering Dept., İTÜ

\_\_\_\_\_

Assoc. Prof. Dr. Ali Özgür YILMAZ

Electrical and Electronics Engineering Dept., METU

\_\_\_\_\_

**Date:**

07.02.2014

**I hereby declare that all information in this document has been obtained and presented in accordance with academic rules and ethical conduct. I also declare that, as required by these rules and conduct, I have fully cited and referenced all material and results that are not original to this work.**

Name, Last Name: FİRUZE ÇAĞLIYAN

Signature :

## ABSTRACT

### COMPRESSIVE SENSING FOR RADAR TARGET DETECTION

Çağlıyan, Firuze

M.S., Department of Electrical and Electronics Engineering

Supervisor: Assoc. Prof. Dr. Ali Özgür Yılmaz

February 2014, 64 pages

Compressive sampling, also known as compressive sensing and sparse recovery, is a new type of sampling theory, which predicts that sparse signals and images can be reconstructed from far less amount of data than what was traditionally considered necessary (i.e. Nyquist/Shannon sampling theory). The theory has many applications such as design of new imaging systems, cameras, sensor networks and analog to digital converters. Several algorithms have been proposed for the measurement and recovery process of the theory. The theory uses only a small amount of measurements which are linear, nonadaptive and suitably designed. The reconstruction process is nonlinear and simply depends on searching for the sparsest vector that is coherent with the measurements. The compressive sensing theory and its key points are explained in detail.

In this thesis, compressive sensing (CS) is used to reconstruct the target scene of a radar. The target scene is discretized so that a total of  $N$  possible target locations exist. The number of targets  $K$  is assumed to be small (i.e.,  $K \ll N$ ) meaning that the target scene is sparsely populated. A theoretical lower bound on the number of measurements  $M$  depending on the sparsity  $K$  and the total number of data  $N$  is presented based on the results in the literature. The target scene reconstruction results for different noise levels are compared. Three different compressive sensing reconstruction methods are described and their performances are compared. The compressive sensing radar target detection and the classical radar detection performance difference is investigated. The change in probability of detection due to SNR variation under constant false alarm rate (FAR) is analyzed. Finally, the effect of Doppler to the compressive sensing radar target detection is analyzed. When the number of measurements is limited, i.e.,  $M < N$ , there is an SNR loss in detection performance. The CS method roughly attains the performance of classical detection when received SNR is boosted by  $M/N$  either with higher power at the transmitter or lower noise figure at the receiver.

**Keywords:** Compressive sensing, sparsity, radar target scene, detection

# ÖZ

## RADAR HEDEF TESPİTİNDE SIKIŞTIRILMIŞ ÖRNEKLEME

Çağlıyan, Firuze

Yüksek Lisans, Elektrik Elektronik Mühendisliği Bölümü

Tez Yöneticisi: Doç. Dr. Ali Özgür Yılmaz

Şubat 2014, 64 sayfa

Yeni bir çeşit örnekleme teorisi olan Sıkıştırılmış Örnekleme sıkıştırılabilir (seyrek) sinyallerin gerekli olduğu düşünülenden (Nyquist/Shannon örnekleme teorilerinde belirtilen) çok daha az sayıda örnek ile tekrar elde edilebileceğini öngörmektedir. Bu teorinin yeni görüntü sistemleri, kameralar, sensör ağları, örnekselden sayısala dönüştürücü dizaynı gibi birçok uygulama alanı bulunmaktadır. Ölçüm ve geri alma aşamaları için geliştirilmiş çeşitli algoritmalar mevcuttur. Teori, doğrusal ve uyarlanabilir olmayan ölçümlerden az sayıda, uygun şekilde tasarlanmış olanları kullanmaktadır. Geri alma işlemi ise doğrusal olmamakla birlikte, temel olarak ölçümlerle uyumlu olan en seyrek vektörü bulmayı amaçlamaktadır. Bu çalışmada, sıkıştırılmış algılama teorisi önemli noktaları ile birlikte detaylı bir şekilde açıklanmıştır.

Bu tezde, sıkıştırılmış algılama metodu kullanılarak bir radarın hedef sahnesinin yeniden oluşturulması ele alınmıştır. Hedef sahnesi, toplamda  $N$  sayıda hedef yeri olacak şekilde ayrıştırılmıştır. Hedef sayısının ( $K$ )  $N$ 'ye göre çok az olduğu varsayılmıştır ( $K \ll N$ ), bu durumda hedef sahnesi seyrek nüfusludur. Literatürdeki sonuçlar kullanılarak, ölçüm sayısı  $M$  için hedef sayısı  $K$  ve toplam veri sayısı  $N$ 'ye bağlı teorik bir alt sınır belirtilmiştir. Gürültü seviyesindeki değişimler karşısında hedef sahnesinin yeniden oluşturulması durumlarının karşılaştırılması grafiklerle sunulmuştur. Farklı sıkıştırılmış algılama metodları tanımlanmış ve bu metodların performansları karşılaştırılmıştır. Sıkıştırılmış algılama ile radar hedef tespiti ve klasik radar hedef tespiti performans farkları incelenmiştir. Hatalı alarm olasılığı (FAR) sabit tutularak SNR değişimine karşılık hedef tespit olasılığının değişimi durumları incelenmiştir. Son olarak, Doppler'in sıkıştırılmış algılama ile radar hedef tespitine etkisi incelenmiştir. Ölçüm sayısı az olduğunda, öyle ki  $M < N$ , hedef tespit performansında SNR kaybı oluşmaktadır. Alınan SNR vericide daha fazla güç ya da alıcıda daha düşük gürültü seviyesi kullanılarak  $M/N$  oranında artırıldığında Sıkıştırılmış Algılama metodu klasik tespit metodu ile yaklaşık olarak aynı tespit sonuçlarını vermektedir.

**Anahtar Kelimeler:** Sıkıştırılmış algılama, seyreklik, radar hedef sahnesi, tespit

*To my family*

## **ACKNOWLEDGEMENTS**

I would like to express my sincere gratitude and appreciation to my supervisor Assoc. Prof. Dr. Ali Özgür YILMAZ for his encouragement and support throughout this study. Without him, this work could never have been completed.

I am deeply grateful to my family for their endless love and support.

I would thank all members of my project team in MilSOFT Software Technologies Inc. for providing the tolerance and assistance I need throughout this study.

Finally, my special thanks go to my friends, Rabia Aburus, Baran Ersin Özilhan, Mustafa Genç, Erkan Ersin Yıldırım, and Sermet Reha Yavuz for their help, support and cheerful presence through not only the course of this study but also any course of my life. Thanks for giving me a shoulder to lean on, whenever I need.

## TABLE OF CONTENTS

ABSTRACT .....	iv
ÖZ. ....	v
ACKNOWLEDGEMENTS .....	vii
TABLE OF CONTENTS .....	viii
LIST OF FIGURES.....	x
LIST OF ABBREVIATIONS .....	xiv
1 INTRODUCTION.....	1
1.1 Compressive Sensing .....	1
1.2 Contributions and Motivation .....	1
1.3 Organization of the Thesis .....	2
2 RELATED WORK ON COMPRESSIVE SENSING .....	3
2.1 Sparse and Compressible Signals.....	3
2.2 Incoherence and the Restricted Isometry Property .....	4
2.3 Compressive Sensing Theory.....	4
3 COMPRESSIVE SENSING RECONSTRUCTION ALGORITHMS .....	7
3.1 Classical Reconstruction Algorithm ( $l_1$ minimization).....	7
3.2 Orthogonal Matching Pursuit (OMP).....	8
3.3 Backtracking-Based Adaptive Orthogonal Matching Pursuit (BAOMP).....	9
4 COMPRESSIVE SENSING RADAR .....	13
4.1 Classical Radar Detection .....	13

4.2 Compressive Sensing Radar Detection .....	14
5 RESULTS AND EVALUATION .....	17
5.1 Simulation Model .....	17
5.1.1 Classical Detection Model .....	17
5.2 Simulation Results .....	18
5.2.1 $l_1$ Minimization Simulations for Different Transmitted Signals ..	18
5.2.2 Choice of Transmitted Signal .....	22
5.2.3 OMP - BAOMP Comparisons .....	25
5.2.4 BAOMP Simulations .....	27
5.2.5 Classical – $l_1$ Minimization – BAOMP Comparison .....	30
5.2.6 Detection of Close Targets .....	34
5.2.7 FAR Calculations .....	36
5.2.8 Detection Threshold Calculations for Constant FAR .....	39
5.2.9 Probability of Detection vs Convergence Threshold .....	41
5.2.10 Probability of Detection (Pd) vs SNR .....	44
5.2.11 False Detections Around the Target Position .....	45
5.2.12 Doppler Effect .....	46
5.3 Summary of Simulation Results .....	58
6 CONCLUSION AND FUTURE WORK .....	61
7 REFERENCES .....	63

## LIST OF FIGURES

Figure 2-1 The Classical sampling approach [22] .....	5
Figure 2-2 The CS approach [22].....	5
Figure 5-1 Optimal detector when the absolute signal phase is unknown .....	18
Figure 5-2 N=2209, M=47, K=10 for noiseless case .....	19
Figure 5-3 N=2209, M=47, K=10 for SNR=15dB.....	19
Figure 5-4 N=2209, M=47, K=10 for noiseless case .....	20
Figure 5-5 N=2209, M=47, K=10 for SNR=15dB.....	20
Figure 5-6 N=1000, M=300, K=10 for noiseless case .....	21
Figure 5-7 N=1000, M=300, K=10 for SNR=15dB.....	21
Figure 5-8 Autocorrelation function of the good signal.....	23
Figure 5-9 The BAOMP detection result of the good signal, SNR=10dB .....	23
Figure 5-10 Autocorrelation function of the bad signal.....	24
Figure 5-11 The BAOMP detection result of the bad signal, SNR=10dB.....	24
Figure 5-12 OMP&BAOMP for N=256, M=100, K=10 with no noise.....	25
Figure 5-13 OMP&BAOMP for N=256, M=100, K=10 with SNR=20dB .....	26
Figure 5-14 OMP&BAOMP for N=256, M=100, K=10 with SNR=15dB .....	27
Figure 5-15 BAOMP Simulations for N=1000, M=200, K=2, SNR=20dB and $\alpha = 0.0001$ .....	28

Figure 5-16 BAOMP Simulations for $N=1000$ , $M=200$ , $K=2$ , $SNR=20dB$ and $\alpha = 0.007$ .....	29
Figure 5-17 BAOMP Simulations for $N=1000$ , $M=200$ , $K=2$ , $SNR=20dB$ and $\alpha = 0.05$ .....	29
Figure 5-18 BAOMP Simulations for $N=1000$ , $M=200$ , $K=2$ , $SNR=20dB$ and $\alpha \geq 0.01$ .....	30
Figure 5-19 l1 minimization simulation for $N=1000$ , $M=200$ , $K=2$ with no noise ..	31
Figure 5-20 MF simulation for $N=1000$ , $M=200$ , $K=2$ with no noise .....	31
Figure 5-21 BAOMP simulation for $N=1000$ , $M=200$ , $K=2$ with no noise.....	32
Figure 5-22 l1 minimization simulation for $N=1000$ , $M=200$ , $K=2$ with $SNR=20dB$ .....	33
Figure 5-23 MF simulation for $N=1000$ , $M=200$ , $K=2$ with $SNR=20dB$ .....	33
Figure 5-24 BAOMP simulation for $N=1000$ , $M=200$ , $K=2$ with $SNR=20dB$ .....	34
Figure 5-25 The BAOMP result for $N=1000$ , $M=200$ , $K=3$ with no noise .....	35
Figure 5-26 Closer view of the BAOMP result.....	35
Figure 5-27 The MF result for $N=1000$ , $M=200$ , $K=3$ with no noise .....	36
Figure 5-28 BAOMP simulation for $N=1000$ , $M=200$ , no target and $\alpha = 0.007$ ....	37
Figure 5-29 BAOMP simulation for $N=1000$ , $M=200$ , no target and $\alpha = 0.01$ .....	37
Figure 5-30 BAOMP simulation for $N=1000$ , $M=200$ , no target and $\alpha = 0.05$ .....	38
Figure 5-31 BAOMP simulation for $N=1000$ , $M=200$ , no target and $\alpha = 0.1$ .....	38
Figure 5-32 Detection threshold vs $\alpha$ for constant FAR .....	40

Figure 5-33 BAOMP simulation for $N=1000$ , $M=200$ , $K=1$ with $SNR=20dB$ and $\alpha = 0.01$ .....	41
Figure 5-34 $P_d$ vs $\alpha$ for $SNR=20dB$ .....	42
Figure 5-35 $P_d$ vs $\alpha$ for $SNR$ values .....	42
Figure 5-36 $P_d$ vs $\alpha$ for $SNR$ values with 8 PSK transmitted signal .....	43
Figure 5-37 $P_d$ vs $SNR$ by choosing the transmitted signal as the signal which gives the best $P_d$ for $SNR=10dB$ , $FAR=10^{-3}$ .....	44
Figure 5-38 $P_d$ vs $SNR$ by choosing the transmitted signal as the signal which gives the best $P_d$ for $SNR=5dB$ , $FAR=10^{-3}$ .....	45
Figure 5-39 $P_d$ vs $SNR$ graphs for classical, exact target position, 1_shifted target position and 2_shifted target position cases, $FAR=10^{-3}$ .....	46
Figure 5-40 One target at 90 <sup>th</sup> bin, 16 Doppler, 16 pulse, $N=100$ , $M=20$ , $K=1$ with $SNR=22dB$ .....	47
Figure 5-41 One target at 90 <sup>th</sup> bin, 16 Doppler, 16 pulse, $N=100$ , $M=20$ , $K=1$ with $SNR=17dB$ .....	48
Figure 5-42 One target at 90 <sup>th</sup> bin, 16 Doppler, 16 pulse, $N=100$ , $M=20$ , $K=1$ with $SNR=12dB$ .....	48
Figure 5-43 One target at 750 <sup>th</sup> bin, 16 Doppler, 16 pulse, $N=100$ , $M=20$ , $K=1$ with $SNR=10dB$ .....	49
Figure 5-44 One target at 750 <sup>th</sup> bin, 16 Doppler, 16 pulse, $N=100$ , $M=20$ , $K=1$ with $SNR=15dB$ .....	49
Figure 5-45 $P_d$ vs $SNR$ comparison for 16 Doppler, 16 pulses, $FAR=10^{-3}$ .....	50
Figure 5-46 One target at 2601 <sup>th</sup> bin, 32 Doppler, 16 pulse, $N=100$ , $M=20$ , $K=1$ with $SNR=10dB$ .....	51

Figure 5-47 Single run for one target at 2601 <sup>th</sup> bin, 32 Doppler, 16 pulse, N=100, M=20, K=1 with SNR=10dB .....	52
Figure 5-48 Single run for one target at 2601 <sup>th</sup> bin, 32 Doppler, 16 pulse, N=100, M=20, K=1 with SNR=10dB .....	52
Figure 5-49 Single run for one target at 2601 <sup>th</sup> bin, 32 Doppler, 16 pulse, N=100, M=20, K=1 with SNR=10dB .....	53
Figure 5-50 Single run for one target at 2601 <sup>th</sup> bin, 32 Doppler, 16 pulse, N=100, M=20, K=1 with SNR=10dB .....	53
Figure 5-51 One target at 2601 <sup>th</sup> bin, 32 Doppler, 16 pulse, N=100, M=20, K=1 with SNR=15dB .....	54
Figure 5-52 Single run for one target at 2601 <sup>th</sup> bin, 32 Doppler, 16 pulse, N=100, M=20, K=1 with SNR=15dB .....	55
Figure 5-53 Single run for one target at 2601 <sup>th</sup> bin, 32 Doppler, 16 pulse, N=100, M=20, K=1 with SNR=15dB .....	55
Figure 5-54 One target not at any Doppler frequency, 32 Doppler, 16 pulse, N=100, M=20, K=1 with SNR=15dB .....	56
Figure 5-55 Pd vs SNR comparison for 32 Doppler, 16 pulses, FAR=10 <sup>-3</sup> .....	57

## LIST OF ABBREVIATIONS

<b>CS</b>	Compresssive Sensing
<b>RIP</b>	Restricted Isometry Property
<b>iid</b>	independent and identically distributed
<b>MP</b>	Matching Pursuit
<b>OMP</b>	Orthogonal Matching Pursuit
<b>BAOMP</b>	Backtracking-based Adaptive Orthogonal Matching Pursuit
<b>PRF</b>	Pulse Repetition Frequency
<b>FAR</b>	False Alarm Rate
<b>SNR</b>	Signal to Noise Ratio
<b>Pd</b>	Probability of Detection
<b>MF</b>	Classical Method
<b>PRI</b>	Pulse Repetition Interval
<b>MIMO</b>	Multiple-input multiple-output



# CHAPTER 1

## INTRODUCTION

### 1.1 Compressive Sensing

The common knowledge in data acquisition is the usage of Nyquist/Shannon sampling theorem. This theorem states that the number of samples needed to reconstruct a signal with no error is determined by its bandwidth. In other words, the sampling rate of the signal should be at least twice of its bandwidth, the so called Nyquist rate [4]. In the last nine years or so, an alternative sensing/sampling theory to the common knowledge in data reconstruction has emerged. This theory, called “compressive sensing”, states that super-resolved signals and images can be reconstructed from far fewer data/measurements than what is usually considered necessary.

The key point is that in real-world, many signals have sparsity or compressibility property. In other words, they have a sparse representation in a fixed basis. Therefore, there is no need to acquire the full signal, compute all transform coefficients, and then take only the largest coefficients while discarding all others. Since it is known that the most of the acquired data will be discarded, the effort of acquiring all data is unnecessary. This raises the question of whether it is possible to directly measure the part of the data that will not end up being thrown away. Compressive sensing theory shows that this is possible [8].

Compressive sensing theory has two key points: sparse representation and incoherent measurements of the signal to extract the maximum amount of information by taking minimum number of measurements. In this theory, reconstruction of the full signal from the small amount of collected incomplete data is done by numerical optimization.

### 1.2 Contributions and Motivation

Our study is centered on the application of the CS theory to the radar target detection problem. For using the CS approach for radar target detection there are some key points to be aware of: First, the target scene should be sparsely populated. Second, the transmitted signal should be incoherent. Finally, a matched filter is not used in this approach. [18]

A 1-dimensional, monostatic, far-field radar system is used in this study.

In general, the target scene of a radar is sparsely populated since the number of targets in the target scene is so small compared to the number of possible target locations in the target scene. Therefore, the sparsity condition is achieved. The transmitted signal should be chosen

properly so that the incoherence property is satisfied. A random signal is incoherent with any fixed basis with high probability, so a random signal can be chosen as the transmitted signal to satisfy this condition [6]. Since these two key points of CS can be easily applied to radar target detection process, the CS theory can be used for radar target detection.

CS theory states that, under certain conditions, radar target detection using compressive sensing achieves better target detection performance than classical detection approach. Exact reconstruction of the target scene can be achieved by taking far less number of measurements than that of the classical detection. The detection performance of the CS is as good as the classical approach when the SNR loss which is proportional with the  $M/N$  ratio is compensated.

### **1.3 Organization of the Thesis**

The rest of the thesis is organized as follows: Chapter 2 gives relevant information about compressing sensing theory and key points of this theory, which are sparse and compressible signals, incoherence and the Restricted Isometry Property. Chapter 3 describes three CS reconstruction algorithms;  $l_1$  minimization, OMP and BAOMP. In Chapter 4, classical radar target detection method and compressive sensing radar target detection methods are explained. In Chapter 5, simulation results and their evaluation are presented. Finally, Chapter 6 includes a conclusion and discussion for future work.

## CHAPTER 2

### RELATED WORK ON COMPRESSIVE SENSING

Compressive sensing (CS), also called compressive sampling, is a novel data acquisition approach for finding solutions to underdetermined linear systems. CS theory states that recovery of certain signals and images is possible by taking far fewer measurements or samples than traditional methods use if sparsity and incoherence conditions are satisfied.

In this chapter, we first describe sparse and compressible signals. In Section 2.2, incoherence and the Restricted Isometry Property will be discussed. In the last section, CS theory will be explained in detail.

#### 2.1 Sparse and Compressible Signals

Let  $\mathbf{x}$  be a one-dimensional, finite-length, discrete time signal of length  $N$  in  $\mathbb{C}^N$ . We regard  $\mathbf{x}$  as an  $N \times 1$  column vector, and call it the information vector. Any signal  $\mathbf{x}$  in  $\mathbb{C}^N$  can be represented in terms of a basis matrix  $\Psi$  which is an  $N \times N$  matrix with the vectors  $\{\psi_j\}_{j=1}^N$  as its columns and assume that the basis is orthonormal. This signal  $\mathbf{x}$  can be written in  $\Psi$  domain as

$$\mathbf{x} = \Psi \mathbf{s} \quad \text{or} \quad \mathbf{x} = \sum_{j=1}^N s_j \psi_j. \quad (1)$$

We can say that  $\mathbf{x}$  and  $\mathbf{s}$  are equivalent representations of the signal [1]. If  $\mathbf{s}$  is an  $N \times 1$  coefficient vector and has only  $K$  nonzero values for  $K \ll N$ , then we say that the signal  $\mathbf{x}$  is  $K$ -sparse.

Many natural signals are not strictly sparse but can be approximated as sparse. Signals which have a few large coefficients and many small coefficients are called compressible. In other words, a compressible signal  $\mathbf{x}$  has coefficients  $s_i$  decreasing rapidly in magnitude according to a power law. Compressible signals can be approximated by  $K$ -sparse signals due to this rapid decay by keeping just the  $K$ -largest coefficients of  $\mathbf{x}$ . Keeping just the  $K$ -largest (in magnitude) coefficients of  $\mathbf{x}$  is the best approximation to a sparse signal [2].

According to these definitions, we can say that the information content of a sparse/compressible signal  $\mathbf{x}$  resides in at most  $K$  dimensions rather than  $N$  [3]. So that, throwing away a large part of the coefficients is possible without much loss and CS theory mainly uses this fact.

## 2.2 Incoherence and the Restricted Isometry Property

**Definition 1 (Coherence)** Let  $(\Psi, \Phi)$  be a pair of bases in  $\mathbb{C}^n$ . The *coherence* between  $\Psi$  and  $\Phi$  is defined as

$$\mu(\Phi, \Psi) = \sqrt{n} \max_{1 \leq k, j \leq n} |\langle \varphi_k, \psi_j \rangle|. \quad (2)$$

From this definition, we can say that coherence equals to the largest correlation between any two elements of  $\Phi$  and  $\Psi$ . When the bases  $\Phi$  and  $\Psi$  are orthonormal, it follows that the coherence is  $1 \leq \mu(\Phi, \Psi) \leq \sqrt{n}$  [4]. The correlated elements of  $\Phi$  and  $\Psi$  determine how coherent the bases are. For example, when  $\Phi = \Psi$ , the bases are fully coherent and  $\mu = \sqrt{n}$ . The bases are called ‘incoherent’ when  $\mu \cong 1$  which means they are nearly independent on the dimension  $n$ .

Compressive sensing theory is mainly interested in largely incoherent pairs as it will be described in Section 2.3. For example, when  $\Phi$  is *the identity basis* and  $\Psi$  is *the Fourier basis*, maximal incoherence is obtained and  $\mu = 1$ . Also, a random matrix  $\Phi$  has very small coherence with any fixed basis  $\Psi$ . When we choose  $\Phi$  uniformly at random as an orthonormal basis, then the coherence between  $\Phi$  and any fixed basis  $\Psi$  is about  $\sqrt{2 \log(n)}$  with high probability [4, 5] which is smaller than  $\sqrt{n}$ .

**Definition 2 (Restricted Isometry Property)** Let  $K$  be an integer and  $\mathbf{x}$  be a  $K$ -sparse vector. For all such  $\mathbf{x}$ , a matrix  $\Phi$  satisfies the Restricted Isometry Property (RIP) with parameter  $\delta_K \geq 0$ , called the restricted isometry constant, as the smallest value such that

$$1 - \delta_K \leq \frac{\|\Phi \mathbf{x}\|_2^2}{\|\mathbf{x}\|_2^2} \leq 1 + \delta_K \quad (3)$$

The matrix  $\Phi$  is said to have the RIP of order  $K$  if  $\delta_K$  is not too close to 1. Restricted isometry constants are a measure of how much the length/Euclidean norm of a  $K$ -sparse vector can be changed by transformation described by  $\Phi$  [2, 6]. A random matrix  $\Phi$  satisfies the RIP with high probability.

## 2.3 Compressive Sensing Theory

Compressive Sensing is a technique which finds sparse solutions to underdetermined linear systems. Generally, an underdetermined linear system has infinite number of solutions since it has more unknowns than equations. However, if an underdetermined linear system has a unique sparse solution, CS theory states that recovery of that solution is possible. In the CS technique, measurements are a weighted linear combination of samples and taken in a basis different from the basis of the sparse signal where the two bases are incoherent. The main advantage of CS theory is that the number of these measurements can be small and they can still contain all the useful information. Thus, the probability of recovering the unique sparse signal is very high.

Consider a length  $N$  signal  $\mathbf{x}$  which is  $K$ -sparse in basis  $\Psi$ , as defined in Section 2.1. In the classical sampling approach, this  $N \times 1$  sparse signal  $\mathbf{x}$  is multiplied by the measurement matrix  $\Phi$ , where the measurement matrix is an  $N \times N$  identity matrix. So, an  $N \times 1$  observation matrix is obtained by taking  $N$  measurements as shown in the figure below.

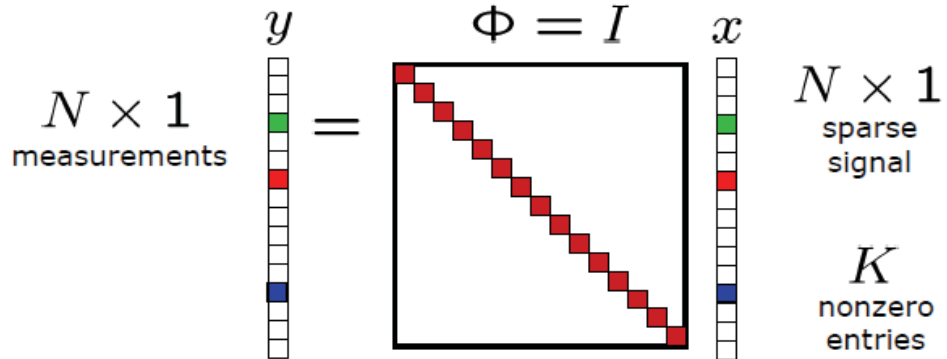


Figure 2-1 The Classical sampling approach [22]

However, in the CS approach, the measurement matrix  $\Phi$  is  $M \times N$ , where  $M$  is the number of measurements and  $M \ll N$ . So only  $M$  measurements are taken and an  $M \times 1$  observation matrix is obtained as shown in Figure 2-2. In the CS, the aim is to reconstruct the  $N \times 1$  sparse signal  $\mathbf{x}$  from these  $M$  measurements.

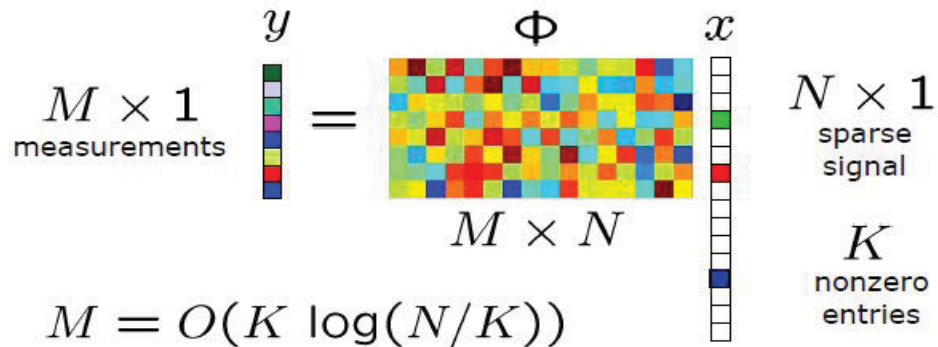


Figure 2-2 The CS approach [22]

In the CS approach, the signal  $\mathbf{x}$  is measured by sampling it with respect to  $\Phi$ . Let  $\varphi_i$  for  $1 \leq i \leq M$  be the rows of the measurement matrix  $\Phi$ . The measurement process computes observations  $y_i$ , inner products of  $\mathbf{x}$  with  $\varphi_i$ , as in  $y_i = \langle \varphi_i, \mathbf{x} \rangle$ . The observation vector  $\mathbf{y}$  can be written in matrix notation as

$$\mathbf{y} = \Phi \mathbf{x} = \Phi \Psi \mathbf{s} = \Theta \mathbf{s}. \quad (4)$$

It has been shown that when  $\mathbf{x}$  is sparse and the measurement matrix  $\Phi$  satisfies the RIP, the solution  $\hat{\mathbf{x}}$  to

$$\hat{\mathbf{x}} = \operatorname{argmin} \|\tilde{\mathbf{x}}\|_1 \quad \text{such that} \quad \Phi \tilde{\mathbf{x}} = \mathbf{y} \quad (5)$$

recovers  $\mathbf{x}$  exactly with a very high probability [23].

The focus in the theory is the case where  $\mathbf{x}$  is sparse. So, it is reasonable to try to find the sparsest solution of  $\Phi\tilde{\mathbf{x}} = \mathbf{y}$  by solving

$$\hat{\mathbf{x}} = \operatorname{argmin} \|\tilde{\mathbf{x}}\|_{l_0} \quad \text{such that} \quad \Phi\tilde{\mathbf{x}} = \mathbf{y} \quad (6)$$

However, solving this problem is numerically unstable and hard. Researches show that the  $l_0$  and  $l_1$  problems give equivalent solutions if the measurement matrix satisfies the RIP, as explained in [23] and [24]. As a result, there is no need to resort to  $l_0$  optimization. Instead of  $l_0$ , a much easier  $l_1$  optimization which is based on linear programming techniques can be used [25].

In CS theory, there are two key points:

- 1) Designing the measurement matrix  $\Phi$ :  $\Phi$  should be designed so that rows of  $\Phi$  are incoherent with the columns of  $\Psi$  and  $\Theta$  satisfies the RIP. This makes the measurement process non-adaptive, which means  $\Phi$  is fixed and does not depend on the signal  $\mathbf{x}$  [1]. Incoherence is important for the number of measurements needed. When  $\Phi$  and  $\Psi$  have large coherence, then each row of  $\Phi$  only gives information about how much of one particular basis element  $\psi_i$  is present in the signal, and thus we would need to make all  $N$  measurements to reconstruct the signal  $\mathbf{x}$  correctly [5]. When  $\Phi$  and  $\Psi$  are incoherent, the information in the  $K$ -sparse signal is not lost by the dimensionality reduction from  $N$  to  $M$ . For example, when the elements of  $\Phi$  are independent and identically distributed (iid) Gaussian random variables, then  $\Phi$  is incoherent with any fixed basis  $\Psi$  with high probability (universality) [6].
- 2) Choosing the reconstruction algorithm: Most of the existing studies in the literature are using optimization based methods for reconstruction, especially  $l_1$ -minimization. Other methods used for reconstruction are Greedy reconstruction algorithms, like Matching Pursuit (MP). These algorithms will be explained in detail in the following chapters.

An  $M \times N$  iid, Gaussian measurement matrix  $\Phi$  satisfies the incoherence and RIP with high probability when  $M \geq cK \log(N/K)$  with  $c \geq 1$ . Therefore, only  $M \geq cK \log\left(\frac{N}{K}\right)$  or more basically  $M \geq O(K \log(N))$  random measurements are needed to exactly recover a  $K$ -sparse signal  $\mathbf{x}$  of length- $N$ . [7, 8, 9] One may observe that  $O(K \log(N))$  is much smaller than  $O(N)$ . We can say that the parameter  $K$  is for determination of the amplitudes of the  $K$ -nonzero coefficients, and  $\log(N)$  is for determination of the locations of the nonzero coefficients.

Eqn. (4) is for noiseless case. When there is noise, the equation becomes

$$\mathbf{y} = \Phi\mathbf{x} + \mathbf{n} = \Phi\Psi\mathbf{s} + \mathbf{n} = \Theta\mathbf{s} + \mathbf{n} \quad (7)$$

for an  $M \times 1$  noise vector  $\mathbf{n}$ . Throughout this thesis, the noise vector  $\mathbf{n}$  is taken as iid Gaussian noise. In the noisy case, the number of measurements needed to exactly recover the signal  $\mathbf{x}$  is somewhat larger than the noiseless case since the observation vector  $\mathbf{y}$  contains noise added observations [8, 9].

## CHAPTER 3

### COMPRESSIVE SENSING RECONSTRUCTION ALGORITHMS

As mentioned in the previous chapter, there are different reconstruction algorithms used in Compressive Sensing. In this chapter, some of these methods will be explained in detail. First, the classical optimization-based reconstruction algorithm, called  $l_1$  minimization will be described. Then, two Greedy reconstruction algorithms, Orthogonal Matching Pursuit (OMP) and Backtracking-based Adaptive Orthogonal Matching Pursuit (BAOMP) will be explained.

#### 3.1 Classical Reconstruction Algorithm ( $l_1$ minimization)

Suppose we have a  $K$ -sparse signal  $\mathbf{x}$  of length  $N$ , in basis  $\Psi$ . The  $M \times N$  measurement matrix  $\Phi$  is designed such that it is incoherent with  $\Psi$ . We have the observation vector  $\mathbf{y}$  as defined in Eqn. (4). Also, the matrix  $\Theta = \Phi\Psi$  satisfies the RIP. As CS theory states, the signal  $\mathbf{x}$  can be recovered by making only  $M$  ( $M \geq O(K \log(N)) \ll N$ ) random measurements out of  $N$ . Under these conditions, exact recovery of  $\mathbf{x}$  (or  $\mathbf{s}$  equivalently) is possible by using  $l_1$  minimization algorithm for reconstruction.

$l_1$  minimization algorithm recover the signal by solving the convex optimization problem of finding

$$\hat{\mathbf{s}} = \operatorname{argmin} \|\tilde{\mathbf{s}}\|_{l_1} \quad \text{such that} \quad \Theta\tilde{\mathbf{s}} = \mathbf{y} \quad (8)$$

where  $\|\mathbf{s}\|_{l_1} \stackrel{\text{def}}{=} \sum_{i=1}^N |s_i|$ . The solution  $\hat{\mathbf{s}}$  will give the most sparse and exact vector  $\mathbf{s}$  with very high probability [7, 10].

For the noisy case, the observation vector  $\mathbf{y}$  is as defined in Eqn. (5) and the  $l_1$  minimization problem becomes as defined below:

$$\hat{\mathbf{s}} = \operatorname{argmin} \|\tilde{\mathbf{s}}\|_{l_1} \quad \text{such that} \quad \|\mathbf{y} - \Theta\tilde{\mathbf{s}}\|_{l_2}^2 \leq \beta^2 \quad (9)$$

where  $l_2$ -norm,  $\|\mathbf{s}\|_{l_2} \stackrel{\text{def}}{=} \sqrt{\sum_{i=1}^N s_i^2}$ , forces the residual term  $(\mathbf{y} - \Theta\tilde{\mathbf{s}})$  to be small [11].

Solving the  $l_1$  minimization problem through convex optimization has some computational complexity. There are some Matlab packages that solve convex optimization problems so as to find the minimum  $l_1$ -norm solution under given constraints. Two of these packages used

in this thesis work are CVX: Matlab Software for Disciplined Convex Programming [12] and  $l_1$ -magic [13].

### 3.2 Orthogonal Matching Pursuit (OMP)

Algorithms based on convex optimization, like  $l_1$  minimization, are computationally intractable and complex. This results in finding alternative algorithms that are not based on convex optimization, like Greedy pursuit algorithms. Greedy pursuit algorithms use iterative search mechanisms and they are usually faster and simpler than optimization based methods.

In OMP, the estimate of the signal  $\mathbf{x}$  is initialized as  $\hat{\mathbf{x}} = 0$  and nonzero components of  $\mathbf{x}$  are recovered sequentially at each iteration [14].

Similar to the scenario in  $l_1$  minimization algorithm, suppose we have a  $K$ -sparse signal  $\mathbf{x}$  of length  $N$ , and  $M \times N$  measurement matrix  $\Phi$ . The columns of  $\Phi$  are denoted as  $\varphi_j$ ,  $j = 1, \dots, N$ .  $M$ -dimensional observation vector  $\mathbf{y} = \Phi \mathbf{x}$ . Since the signal  $\mathbf{x}$  has only  $K$ -nonzero components, we can say that the observation vector  $\mathbf{y}$  is a linear combination of  $K$  columns of the measurement matrix  $\Phi$ . For reconstruction of  $\mathbf{x}$ , determination of the columns of  $\Phi$  which participate in the observation vector  $\mathbf{y}$  is necessary. In OMP algorithm, most strongly correlated column of  $\Phi$  with  $\mathbf{y}$  is chosen first. Then, its contribution to  $\mathbf{y}$  is subtracted and the same procedure is applied to the residual iteratively. The algorithm states that; after  $K$  iterations, the correct set of columns ( $\varphi_j$ 's) will be identified. The OMP algorithm is explained in detail in Algorithm 1 [15].

#### Algorithm 1 (Orthogonal Matching Pursuit)

INPUT:

- $\Phi$ : An  $M \times N$  measurement matrix
- $\mathbf{y}$ : An  $M$ -dimensional observation vector
- $K$ : Sparsity level of the signal  $\mathbf{x}$
- $t$ : Iteration counter

OUTPUT:

- $\hat{\mathbf{x}}$ : Estimate of the signal  $\mathbf{x}$
- $\Lambda_K$ : An index set of  $K$  elements from  $\{1, \dots, N\}$
- $\Phi_t$ : The matrix of chosen columns
- $\mathbf{a}_K$ : An  $M$ -dimensional approximation of the observation data  $\mathbf{y}$
- $\mathbf{r}_K = (\mathbf{y} - \mathbf{a}_K)$ : An  $M$ -dimensional residual vector

INITIALIZATION:

- $\mathbf{r}_0 = \mathbf{y}$
- $\Lambda_K = \emptyset$

- $t = 1$
- $\Phi_0 = \emptyset$

ITERATION:

1. Find the index  $\lambda_t$  that solves the following optimization problem.  $\lambda_t$  gives the column of  $\Phi$  which is most strongly correlated with the residual  $\mathbf{r}_{t-1}$ .

$$\lambda_t = \operatorname{argmax}_{j=1,\dots,N} |\langle \mathbf{r}_{t-1}, \varphi_j \rangle| \quad (10)$$

2. Augment the index set.

$$\Lambda_t = \Lambda_{t-1} \cup \{\lambda_t\} \quad (11)$$

3. Augment the matrix of chosen columns.

$$\Phi_t = [\Phi_{t-1} \quad \varphi_{\lambda_t}] \quad (12)$$

4. Obtain a new signal estimate by solving a least squares problem.

$$\mathbf{x}_t = \operatorname{argmin}_{\hat{\mathbf{x}}} \|\mathbf{y} - \Phi_t \hat{\mathbf{x}}\|_{l_2} \quad (13)$$

5. Calculate the new approximation of the observation data.

$$\mathbf{a}_t = \Phi_t \mathbf{x}_t \quad (14)$$

6. Calculate the new residual.

$$\mathbf{r}_t = \mathbf{y} - \mathbf{a}_t \quad (15)$$

7. If  $t < K$ , increment  $t$  by one and return to Step 1 to continue with a new iteration.

The residual  $\mathbf{r}_t$  is always orthogonal to columns of the matrix  $\Phi_t$ . At every new iteration ( $t$ ), when the residual of the previous iteration ( $t - 1$ ) is nonzero, a new column of  $\Phi$  is chosen and the matrix  $\Phi_t$  has full column rank (it has independent columns). Therefore, the signal estimate  $\mathbf{x}_t$ , solution to the least squares problem in Step 4, is unique. Also, the approximation  $\mathbf{a}_t$  and the residual  $\mathbf{r}_t$  are unique [15].

At the end of the algorithm, the estimate  $\hat{\mathbf{x}}$  of the signal  $\mathbf{x}$  has nonzero entries at the components listed in the index set  $\Lambda_t = \Lambda_K$ , since  $t=K$  at last iteration.

### 3.3 Backtracking-Based Adaptive Orthogonal Matching Pursuit (BAOMP)

BAOMP algorithm is a Greedy pursuit algorithm like the OMP algorithm. The BAOMP algorithm is an extended version of the OMP algorithm. In the BAOMP algorithm, unlike OMP, more than one atoms (columns of the measurement matrix) can be chosen at each iteration. Additionally, at each iteration, the BAOMP algorithm uses a backtracking technique to detect the reliability of the previously chosen atoms and deletes unreliable atoms. Another extension of the BAOMP algorithm is that this algorithm does not require the sparsity level  $K$  of the signal  $\mathbf{x}$  to be known a priori. These modifications make performance of the BAOMP algorithm much better than the OMP and  $l_1$  minimization algorithms.

We have the same scenario as defined in Section 3.2. We aim to reconstruct the  $K$ -sparse, length  $N$  signal  $\mathbf{x}$  from length  $M$  observation vector  $\mathbf{y} = \Phi \mathbf{x}$  by using BAOMP. The BAOMP algorithm is explained in detail in Algorithm 2 [16].

## Algorithm 2 (Backtracking-based Adaptive Orthogonal Matching Pursuit)

INPUT:

- $\Phi$ : An  $M \times N$  measurement matrix
- $\mathbf{y}$ : An  $M$ -dimensional observation vector
- $\mu_1$ : A preset atom-adding constant threshold in  $[0,1]$
- $\mu_2$ : A preset atom-deleting constant threshold in  $[0,1]$
- $\varepsilon$ : Convergence threshold to stop the iterations
- $t$ : Iteration counter
- $t_{\max}$ : maximum number of iterations allowed

OUTPUT:

- $\mathbf{x}^t$ : Estimate of the signal  $\mathbf{x}$
- $\Lambda$ : Estimated support set
- $\mathbf{C}_t$ : Candidate set
- $\Gamma_t$ : Atom-deleting set
- $\mathbf{r}_t$ : An  $M$ -dimensional residual vector
- $\Phi_{\Lambda}$ : A matrix of chosen columns (indices listed in the set  $\Lambda$ ) of  $\Phi$

INITIALIZATION:

- $\mathbf{x}^0 = 0$
- $\Lambda = \emptyset$
- $\mathbf{C}_0 = \emptyset$
- $\Gamma_0 = \emptyset$
- $\mathbf{r}_0 = \mathbf{y}$
- $t = 1$
- $\Phi_0 = \emptyset$

ITERATION:

Find the candidate set  $\mathbf{C}_t$  that consist of the atoms solving the following optimization problem.  $\mathbf{C}_t$  contains the columns  $\varphi_j$ 's of  $\Phi$ , which are most strongly correlated with the residual  $\mathbf{r}_{t-1}$  and satisfy the following inequalities.

$$|\langle \mathbf{r}_{t-1}, \varphi_{C_t} \rangle| \geq \mu_1 \cdot \max_{j=1, \dots, N} |\langle \mathbf{r}_{t-1}, \varphi_j \rangle| \quad \text{with cardinality } |\mathbf{C}_t| \leq M - |\Lambda| \quad (16)$$

Obtain a signal estimate by solving the following equation where  $^T$  sign means matrix transpose.

$$\mathbf{x}_{\Lambda \cup \mathbf{C}_t}^t = \Phi_{\Lambda \cup \mathbf{C}_t}^T \cdot \mathbf{y} \quad (17)$$

Find atom-deleting set  $\Gamma_t$  that consist of the atoms satisfying the following inequality.

$$|\mathbf{x}_{\Lambda \cup \mathbf{C}_t}^t| < \mu_2 \cdot \max |\mathbf{x}_{\mathbf{C}_t}^t| \quad \text{where} \quad \mathbf{x}_{\mathbf{C}_t}^t = \Phi_{\mathbf{C}_t}^T \cdot \mathbf{y} \quad (18)$$

Update the support set.

$$\Lambda = \{\Lambda \cup \mathbf{C}_t\} \setminus \Gamma_t \quad (19)$$

Calculate the new signal estimate.

$$\mathbf{x}_{\Lambda}^t = \Phi_{\Lambda}^T \cdot \mathbf{y} \quad (20)$$

Calculate the new residual.

$$\mathbf{r}_t = \mathbf{y} - \Phi_{\Lambda} \cdot \mathbf{x}_{\Lambda}^t \quad (21)$$

If  $\|\mathbf{r}_t\|_{l_2} < \varepsilon$  or  $t = t_{\max}$ , quit the iteration. If not, increment  $t$  by one and return to Step 1 to continue with a new iteration.

In BAOMP, first a candidate set is found by adaptively choosing several atoms at each iteration. The adaptive decision of how many atoms are chosen at each iteration is made by a pre-defined constant  $\mu_1$ . When  $\mu_1 = 1$ , only the most strongly correlated atom is chosen at each iteration, like the OMP method. When  $\mu_1 = 0$ , all  $N$  atoms, which means the full measurement matrix, are chosen. Choosing  $\mu_1$  smaller speeds up the algorithm but increases complexity. There is a constraint  $|\mathbf{C}_t| \leq M - |\Lambda|$  for the candidate set to guarantee the existence of the inverse matrix of  $\Phi_{\Lambda \cup \mathbf{C}_t}$ , since the measurement matrix is  $M \times N$ . Then, an atom-deleting set is found by choosing the atoms whose estimated coefficients  $\mathbf{x}_{\Lambda \cup \mathbf{C}_t}^t$  are smaller than a pre-defined constant,  $\mu_2$  times the maximum amplitude of the coefficients  $\mathbf{x}_{\mathbf{C}_t}^t$  in the current candidate set  $\mathbf{C}_t$ . Also, the pre-defined constant  $\mu_2$  controls the adaptive decision of how many atoms are deleted at each iteration. Ideally, the estimated coefficients of recently chosen atoms are expected to be smaller than that of the previously chosen atoms. If the estimated coefficients of recently chosen atoms are larger than that of the previously chosen atoms, those previously chosen atoms were chosen wrongly with high probability. This backtracking step removes the previously chosen atoms with smaller estimated coefficients than the recently chosen atoms, so it corrects the previous wrong decisions. The support set is updated by deletion of the atoms in the atom-deleting set from the support set. Then, a new signal estimate and a new residual is found by using this support set. Iterations of the BAOMP method will stop when the maximum number of iterations allowed is reached, or when  $l_2$ -norm of the residual is less than a threshold value,  $\varepsilon$  [16].



## CHAPTER 4

### COMPRESSIVE SENSING RADAR

In radar, detection is one of the most basic functions. A radar signal processor performs detection of the presence of targets in the target scene of interest. The main difficulty is analyzing whether the received signal contains a real target echo, if so, finding its range, angle and velocity, or it contains only the effects of interference; such as noise and clutter. In the simplest case, detection decisions are made for each range bin (fast-time sample) for each pulse to decide the presence of a target at the range of the corresponding range bin and the spatial angle of the antenna pointing direction for the corresponding pulse. This results in the need of making millions of detection decisions per second, because of the existence of thousands of range bins and high PRFs (Pulse Repetition Frequency) of multiple kilohertz. The optimal solution to this detection decision problem is the technique of *threshold detection*. In this method, the amplitude of each sample of the received radar echo signal is compared to a predefined threshold value. If the signal amplitude is above this threshold, it is assumed that a target is present. If it is below the threshold, the echo is assumed to be due to interference only and no target is present [17].

Threshold detection decisions are the result of a statistical process, so the probability of a wrong decision is not zero and there could be false alarms, i.e., a false target declaration. In real-world systems, interference statistics are not known a priori, so they cannot be used to compute a predefined threshold value. Instead, the threshold is estimated using interference statistics estimated from the data itself, by keeping FAR (False Alarm Rate) constant [17].

In this thesis, a 1-dimensional, monostatic, far-field, single-pulse radar system is used. Monostatic means the transmitter and the receiver are colocated. The far-field property allows modelling of targets as point sources. We assume that the targets are radially aligned with the transmitter and receiver, so only the range and velocity of targets will be of concern [18].

#### 4.1 Classical Radar Detection

The *cross-ambiguity function* of  $\tau, \omega \in \mathbb{R}$  for two finite energy functions  $f, g \in L^2(\mathbb{R})$  is defined as [19]

$$A_{f,g}(\tau, \omega) = \int_{\mathbb{R}} f\left(t + \frac{\tau}{2}\right) \overline{g\left(t - \frac{\tau}{2}\right)} e^{-2\pi i \omega t} dt \quad (22)$$

where  $\overline{\cdot}$  denotes complex-conjugate of the function.

The (*self*) ambiguity function is obtained when  $f = g$  in (20), and denoted as  $A_f(\tau, \omega)$ .

**Definition 3 (Radar Uncertainty Principle)** For some support set  $U \subseteq \mathbb{R}^2$  and  $\epsilon \geq 0$ , if

$$\iint_U |A_{f,g}(\tau, \omega)|^2 d\tau d\omega \geq (1 - \epsilon) \|f\|_2^2 \|g\|_2^2 \quad (23)$$

then the area  $|U| \geq (1 - \epsilon)$  [20].

The radar uncertainty principle states that, in classical radar detection, the ability to detect two close targets in the time-frequency plane is limited by the support of the ambiguity function  $A_f(\tau, \omega)$ . Therefore, the ambiguity function of  $f$  is fundamental in determining the resolution between targets [21].

For our radar model, suppose there is a target at distance  $x$  moving with velocity  $v$ . The reflection coefficient of the target is  $s_{xv}$ . The transmitted signal is  $f(t)$  and the received signal is  $r(t)$ .  $r(t)$  is defined as

$$r(t) = s_{xv} f(t - \tau_x) e^{2\pi i \omega_v t} \quad (24)$$

where  $\tau_x = 2x/c$  is the round trip time of flight,  $c$  is the speed of light,  $\omega_v \cong -2\omega_0 v/c$  is the Doppler shift, and  $\omega_0$  is the carrier frequency. Thus, the time-frequency shift  $(\tau_x, \omega_v)$  of the transmitted signal is used to gather range-velocity  $(x, v)$  information of the target.

In classical detection, a matched filter is used at the receiver which corresponds to correlation of the received signal  $r(t)$  with a time-frequency shifted version of the transmitted signal  $f$ . This correlation equals the cross-ambiguity function:

$$A_{r,f}(\tau, \omega) = \int_{\mathbb{R}} r(t) \overline{f(t - \tau)} e^{-2\pi i \omega t} dt \quad (25)$$

$$= s_{xv} A_f(\tau - \tau_x, \omega - \omega_v) \quad (26)$$

From (24), we can say that the ambiguity region of  $f$  with its center at target's location  $(\tau_x, \omega_v)$  and scaled by its reflection coefficient  $|s_{xv}|$  is included in the time-frequency plane. Targets that are close to each other can have overlapping ambiguity regions. This results in problems like detection of two or more targets as a single target, or inability to detect the exact location of a target [18].

## 4.2 Compressive Sensing Radar Detection

Radar target detection using CS can have better detection performance than classical detection under appropriate conditions for CS. As mentioned in Section 2.3, the CS method is based on two conditions: sparsity and incoherence. Therefore, these conditions should be satisfied in order to use CS in radar target detection. In CS radar detection, when incoherency increases, the number of measurements needed for detection decreases. Also, the CS method does not use a matched filter in radar target detection.

Assume that there exists  $K$  targets in the time-frequency plane. All targets have unknown range, velocity and reflection coefficients. We discretize the time-frequency plane, the target scene, such that the total number of points is equal to  $N$ . If  $K \ll N$ , we can say that the target scene is sparsely populated, so it can be represented as a  $K$ -sparse vector of length  $N$ . Each point on the target scene represents a possible target location, meaning a unique time-frequency shift,  $\mathbf{H}_i$  with a related reflection coefficient,  $x_i$ . Assume that  $\mathbf{H}_i$  is an orthonormal basis for  $\mathbb{C}^N$  and consider that  $\mathbf{H}$  is an unknown matrix in  $\mathbb{C}^N$ . If the target scene is represented by a matrix  $\mathbf{H}$ , and the transmitted signal is  $\mathbf{p}$ , then the observation vector  $\mathbf{y}$  is defined as

$$\mathbf{H} = \sum_{i=1}^N x_i \mathbf{H}_i \quad (27)$$

$$\mathbf{y} = \mathbf{H}\mathbf{p} = \sum_{i=1}^N x_i \mathbf{H}_i \mathbf{p} = \sum_{i=1}^N x_i \boldsymbol{\varphi}_i = \boldsymbol{\Phi}\mathbf{x} \quad (28)$$

In Eqn.(26),  $\boldsymbol{\varphi}_i$ 's are the columns of the measurement matrix  $\boldsymbol{\Phi}$  and defined as  $\boldsymbol{\varphi}_i = \mathbf{H}_i \mathbf{p}$ . Also,  $\mathbf{x}$  is the  $N \times 1$  coefficient vector defined as  $\mathbf{x} = [x_1, x_2, \dots, x_N]^T$  in  $\mathbb{C}^N$  where  $^T$  denotes transpose. If  $\mathbf{x}$  is sparse, the target scene of the radar can be reconstructed by solving the underdetermined system of equations in Eqn.(26) with the CS method. [3]

After sparsity, the second condition that the CS is based on; incoherence, should also be satisfied. To satisfy the incoherence property of measurement matrix  $\boldsymbol{\Phi}$ , the transmitted signal  $\mathbf{p}$  should be chosen appropriately. The transmitted signal should be chosen such that it is incoherent with a fixed basis  $\mathbf{H}_i$ . Some deterministic signals, like Alltop sequence are incoherent [18]. But, as mentioned in Section 2.3, *random signals*, which are uniform iid Gaussian distributed, satisfy incoherence property with any fixed basis. Therefore, we prefer to use random signals in most of the simulations in this thesis. After choosing the transmitted signal, the measurement matrix should be designed so that it satisfies the RIP.

In this study, for forming the measurement matrix, a convolution matrix  $\mathbf{A}$  is generated from the transmitted signal first. The convolution matrix is generated as an  $(N+L-1) \times N$  matrix and its columns are formed by the transmitted signal  $\mathbf{p}$ .

If we take the transmitted signal  $\mathbf{p}$  as a length  $L$  column vector as  $\mathbf{p} = [p_1, p_2, \dots, p_L]^T$ , the form of the convolution matrix is as shown below:

$$\mathbf{A} = \begin{bmatrix} p_1 & 0 & & 0 & 0 \\ p_2 & p_1 & & 0 & 0 \\ \vdots & p_2 & \dots & 0 & 0 \\ p_L & \vdots & & \vdots & \vdots \\ 0 & p_L & & 0 & 0 \\ 0 & 0 & & 0 & 0 \\ \vdots & \vdots & \ddots & \vdots & \\ 0 & 0 & & p_1 & 0 \\ 0 & 0 & & p_2 & p_1 \\ \vdots & \vdots & \dots & \vdots & p_2 \\ 0 & 0 & & p_L & \vdots \\ 0 & 0 & & 0 & p_L \end{bmatrix}$$

After forming this convolution matrix, the measurement matrix is generated by taking  $M$  rows of the matrix  $\mathbf{A}$  randomly.

The choice of these  $M$  rows affects the performance of the CS algorithm since, together with the transmitted signal, the incoherence and the RIP of the measurement matrix is also depends on this choice. When incoherence of the measurement matrix increases, the amount of information extracted by the measurements gets larger. Together with this, the number of measurements needed to be taken gets smaller. Therefore, we can extract the maximum amount of information by taking minimum number of measurements with a fully incoherent measurement matrix.

Since we take only  $M$  measurements out of  $N$ , our observation vector  $\mathbf{y}$  is a length  $M$  vector consisting of noise added measurements. From this observation vector, the target scene of the radar is reconstructed by using the CS theory. Reconstruction performance analyses of a radar target scene for different noise levels, when Doppler is present, with different transmitted signals and reconstruction algorithms are given in the following chapter.

## CHAPTER 5

### RESULTS AND EVALUATION

#### 5.1 Simulation Model

In this thesis, a 1-dimensional, monostatic, far-field radar system is used for simulations as details are given in Chapter 4. The target scene is discretized such that the total number of points is equal to  $N$  where each point on the target scene represents a possible target location. We have  $K$  targets and  $K \ll N$ , so that the target scene is sparsely populated, and it is represented as a  $K$ -sparse vector of length  $N$ .

Assume that the radar transmitter transmits a signal of length  $L$  where  $L < N$ . An  $N \times N$  convolution matrix is generated by using the transmitted signal as a column vector.  $M$  rows of this convolution matrix are randomly chosen which means taking  $M$  measurements out of  $N$ , and an  $M \times N$  measurement matrix is constructed with these rows.

For all scenarios in which noise is present, independent and identically distributed (iid) proper complex Gaussian noise is used.

Signal to noise ratio (SNR) is defined as the ratio of the received signal energy to noise variance. Therefore, the length  $L$  of the transmitted signal is taken into account while choosing the transmitted signal. Transmitted signal power and target amplitudes are normalized to obtain a received signal energy of 1 (dB). Also, the noise power is set to  $1/\text{SNR}$  (dB) in order to reach the SNR (dB).

In the simulation results, the label ‘real data’ means the targets in the target scene.

##### 5.1.1 Classical Detection Model

The Classical method for radar target detection is described in Section 4.1. In our simulation model, radar receives a random signal with an unknown phase and the matched filter used at the receiver is an ideal matched filter. In this case, when the absolute received signal phase is unknown, the magnitude of the signal is used and the structure of optimal detector is as shown below in Figure 5-1. The magnitude of the matched filter output is taken and then the result is compared to a threshold [17].

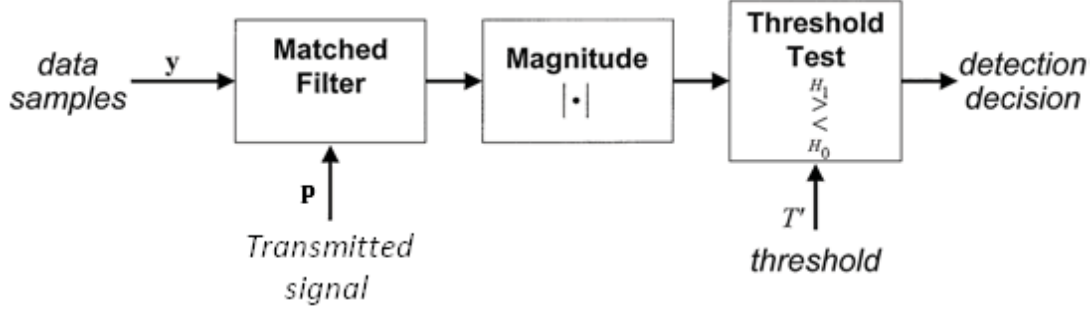


Figure 5-1 Optimal detector when the absolute signal phase is unknown

For this case, the probability of detection is defined as [17]

$$Pd = Q_M(\sqrt{2 \cdot \text{SNR}}, \sqrt{-2 \cdot \ln \text{FAR}}) \quad (29)$$

where Pd is probability of detection, SNR is signal to noise ratio, FAR is false alarm rate and  $Q_M$  is the Marcum-Q function defined as  $Q_M(a, b) = \int_b^\infty \text{texp}\left[-\frac{t^2+a^2}{2}\right] I_0(at) dt$  where  $I_0$  is the modified Bessel function of the first kind defined as  $I_0(z) = \frac{1}{\pi} \left(\int_0^\pi e^{\pm z \cos \theta} d\theta\right)$ .

Unlike the CS method, measurements are taken for all range bins in the target scene for the classical model. This results in N measurements for a vectorized target scene of length N. However, the CS method takes only M measurements which correspond to a number much less than N. While graphs including SNR are plotted, this SNR loss in CS method is compensated.

## 5.2 Simulation Results

Simulations in this section are mainly based on the simulation model explained in Section 5.1.

During our work on Compressive Sensing, we utilized various algorithms. These algorithms are the  $l_1$  minimization algorithm, the OMP algorithm and the BAOMP algorithm. We started with the  $l_1$  minimization algorithm then, we moved to the OMP and the BAOMP algorithms, chronologically. The reason for this change is that we read about the usage of some different algorithms during our literature survey. Comparisons of these algorithms will be given in following sections of this chapter. When we compare these algorithms, we see that the BAOMP algorithm is the best with its performance and complexity features as explained in Chapter 3. Depending on these results, the BAOMP algorithm is used for most of the analysis in this thesis.

### 5.2.1 $l_1$ Minimization Simulations for Different Transmitted Signals

The choice of the transmitted signal is an important factor in the CS. As mentioned before, the transmitted signal should satisfy the incoherence property. As an example, random

signals satisfy this property. In this section,  $l_1$  minimization algorithm is run with different transmitted signals which satisfy incoherence property. These signals are the Alltop sequence, Barker Code, P4 Code and Random signal. The simulations are done with  $l_1$  minimization algorithm because this study is performed at early times of our work, so we were using  $l_1$  minimization algorithm. As a result, it is seen that there is no major difference in the performance of the CS, so random signals will be used as the transmitted signal from now on.

In simulations below, the Alltop sequence with length- $M$  is used as transmitted signal which is written into the columns of  $M \times N$  Measurement matrix. Simulations are performed for noiseless and noisy case. It is seen that, with the Alltop sequence, exact recovery is also possible even when iid Gaussian noise is added:

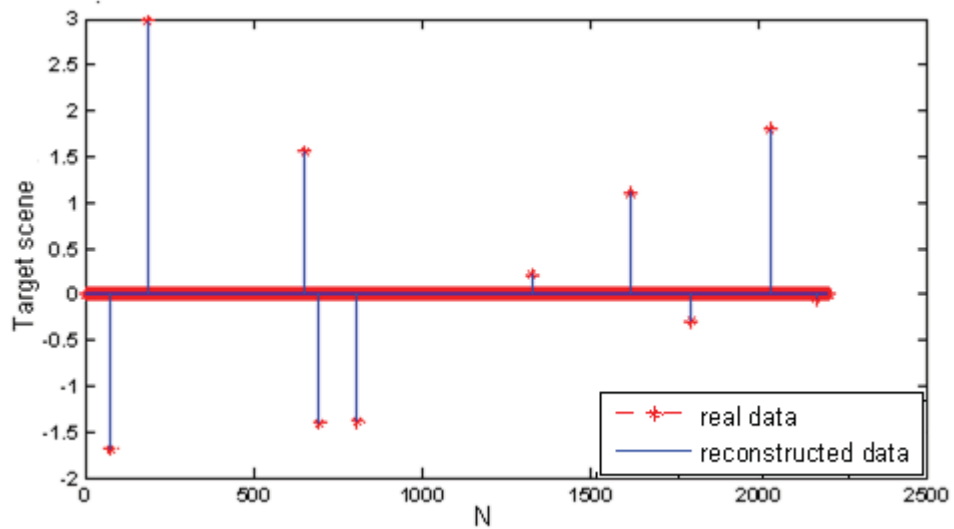


Figure 5-2  $N=2209, M=47, K=10$  for noiseless case

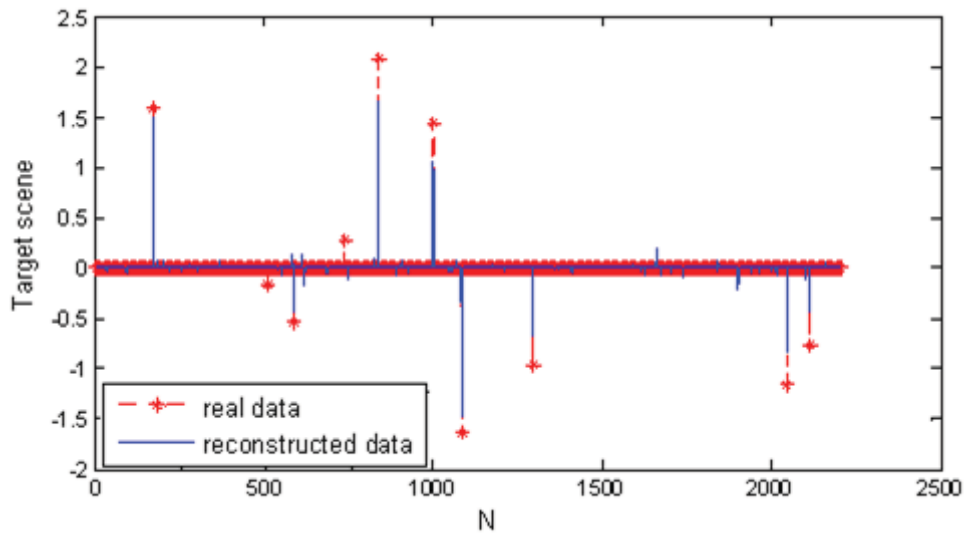


Figure 5-3  $N=2209, M=47, K=10$  for  $SNR=15dB$

In simulations below, the Barker Code of length-13 is used as transmitted signal which is written into the columns of  $M \times N$  Measurement matrix. Simulations are performed for

noiseless and noisy case. When iid Gaussian noise is added, the performance of the algorithm decreases as expected. When Barker Code is used as the transmitted signal, the number of measurements needed for exact recovery is larger than that when the transmitted signal is random or Alltop sequence. When SNR=15dB, three of the targets can not be detected. As a result, the Barker Code is not a good choice for the transmitted signal in CS theory.

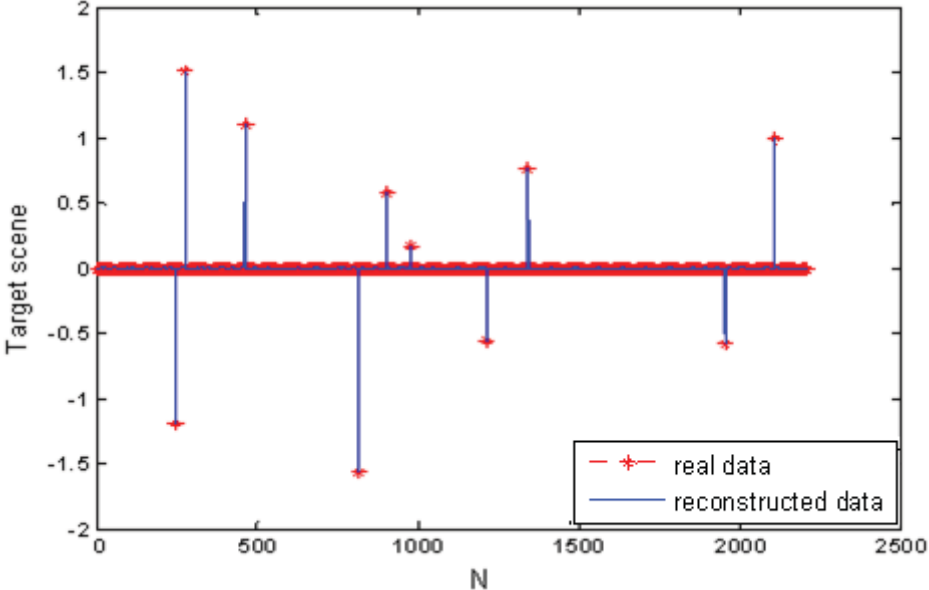


Figure 5-4 N=2209, M=47, K=10 for noiseless case

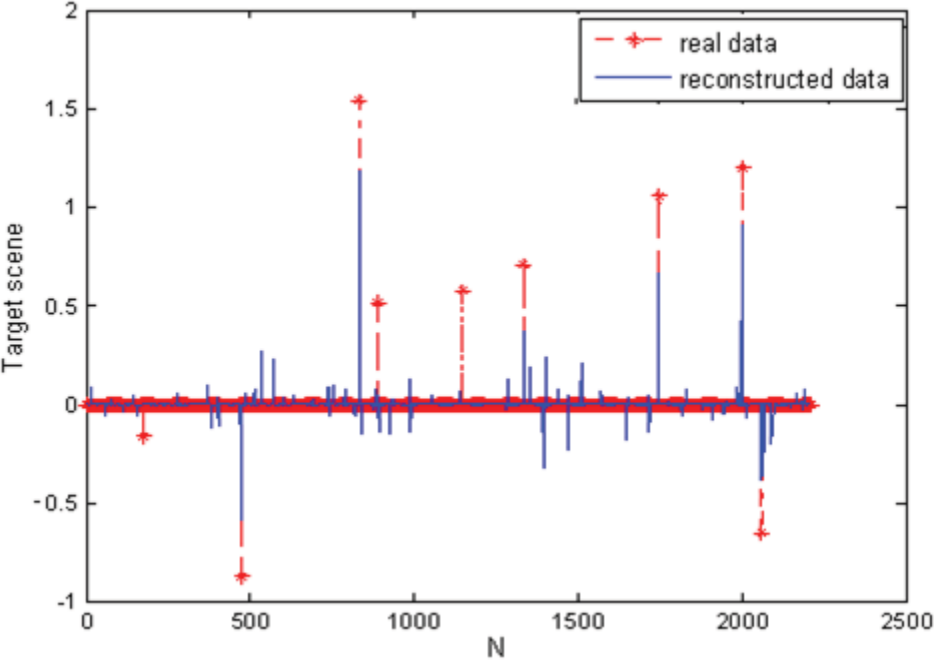


Figure 5-5 N=2209, M=47, K=10 for SNR=15dB

As the third case, the P4 Code of length-60 is used as transmitted signal which is written into the columns of  $M \times N$  Measurement matrix. Simulations are performed for noiseless and noisy case. It is seen that, similar to the Alltop sequence, exact recovery is also possible with the P4 Code even when iid Gaussian noise is added as shown below:

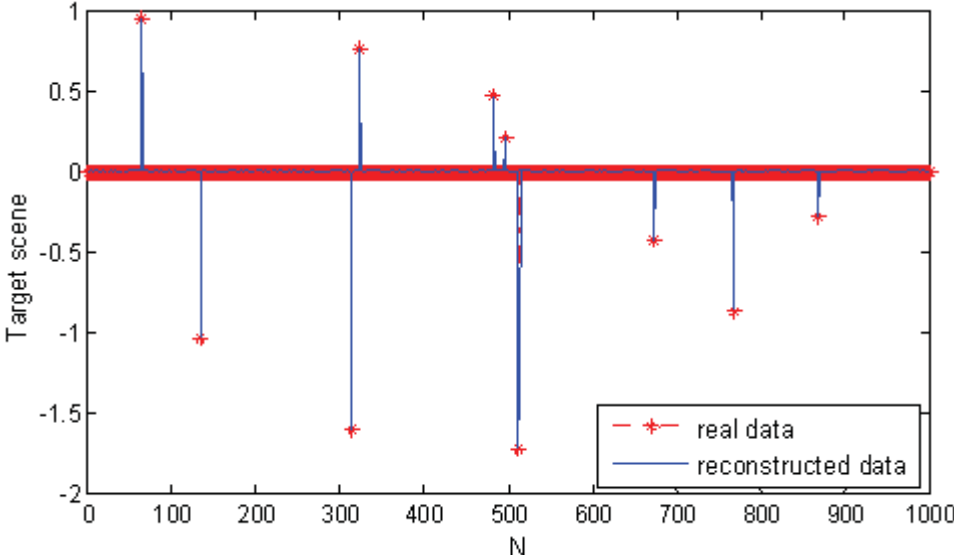


Figure 5-6  $N=1000, M=300, K=10$  for noiseless case

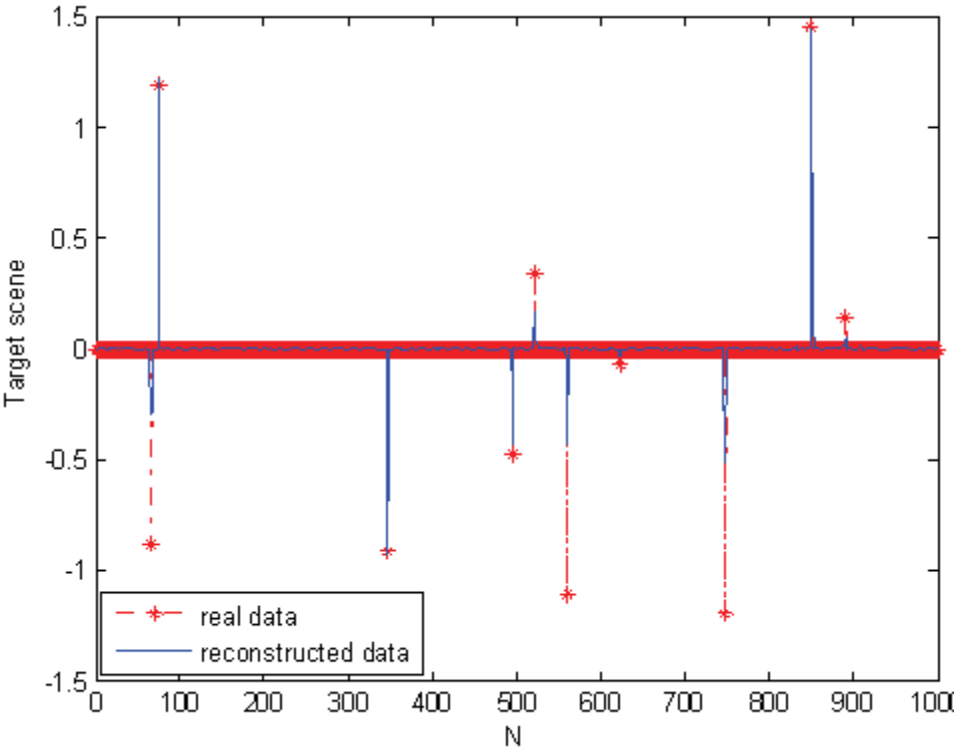


Figure 5-7  $N=1000, M=300, K=10$  for SNR=15dB

### 5.2.2 Choice of Transmitted Signal

As mentioned before, random codes of length 60 is used as transmitted signal in simulations. The transmitted signal affects the reconstruction performance of the CS. Simulations show that a scenario which results in a bad detection performance can have a good detection performance when the transmitted random signal is changed. In this section, autocorrelation functions and Restricted Isometry Properties of different transmitted signals are analyzed as shown below. Different random codes and measurement matrices are generated for 100 times. For each of these, the algorithm is run for no target, only noise is present case. Then, a detection threshold value is determined for constant False Alarm Rate (FAR)= $10^{-3}$  for each. Using this threshold value, the algorithm is run 100 times for each measurement matrix for  $N=1000$ ,  $M=200$ ,  $K=1$  and  $SNR=10dB$  to obtain the probability of detection ( $P_d$ ) for each case. A signal is called a ‘good signal’ if when used, the reconstruction performance of the BAOMP algorithm is good, meaning  $P_d$  is large. Similarly, a signal is called a ‘bad signal’ if when used, the reconstruction performance of the BAOMP algorithm is bad, meaning  $P_d$  is small. Simulations show that autocorrelation function is not a measure of a good signal or a bad signal. The measure of a good signal or a bad signal is the RIP. This means that together with the transmitted signal, the chosen rows of the measurement matrix are also important. If the measurement matrix has smaller restricted isometry constant, the performance of the BAOMP algorithm is better. When restricted isometry constant becomes closer to 1, the performance gets worse. These results are shown in below simulations:

a) Good signal:

Restricted isometry constant is found as 0.5612. Pd is found as 0.78.

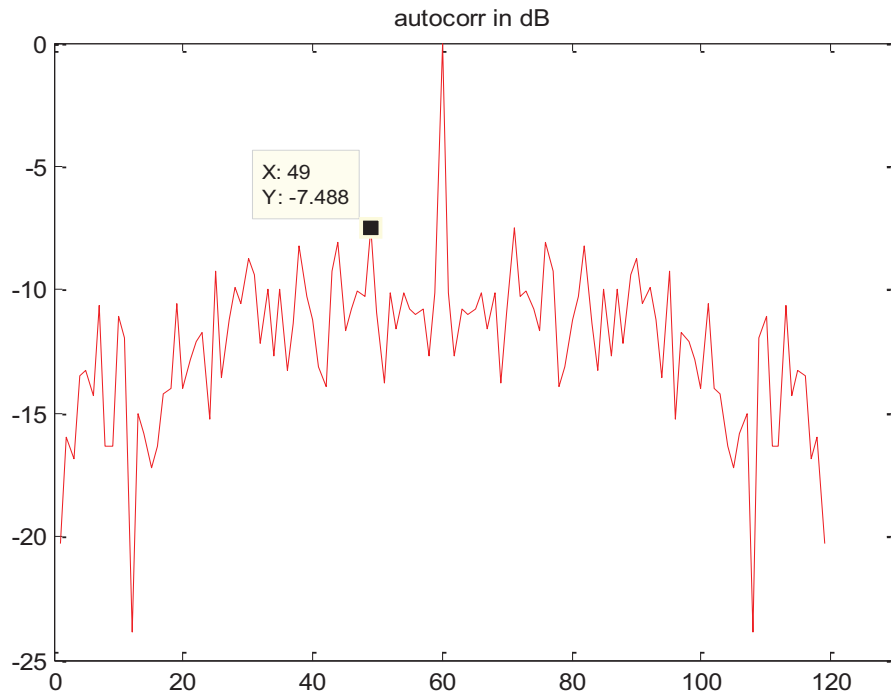


Figure 5-8 Autocorrelation function of the good signal

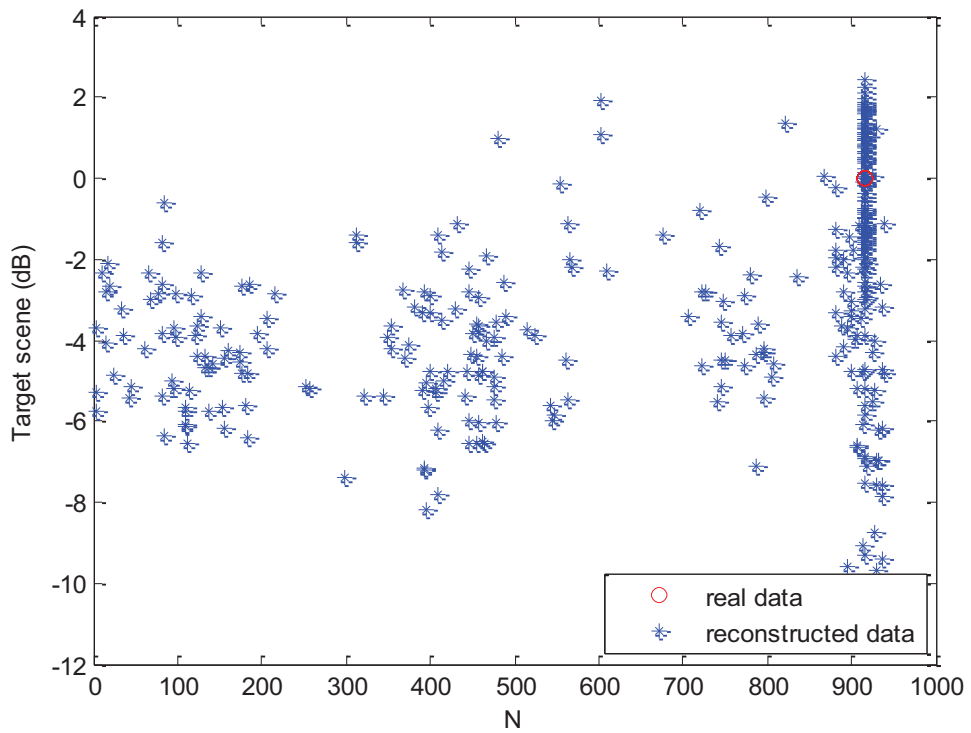
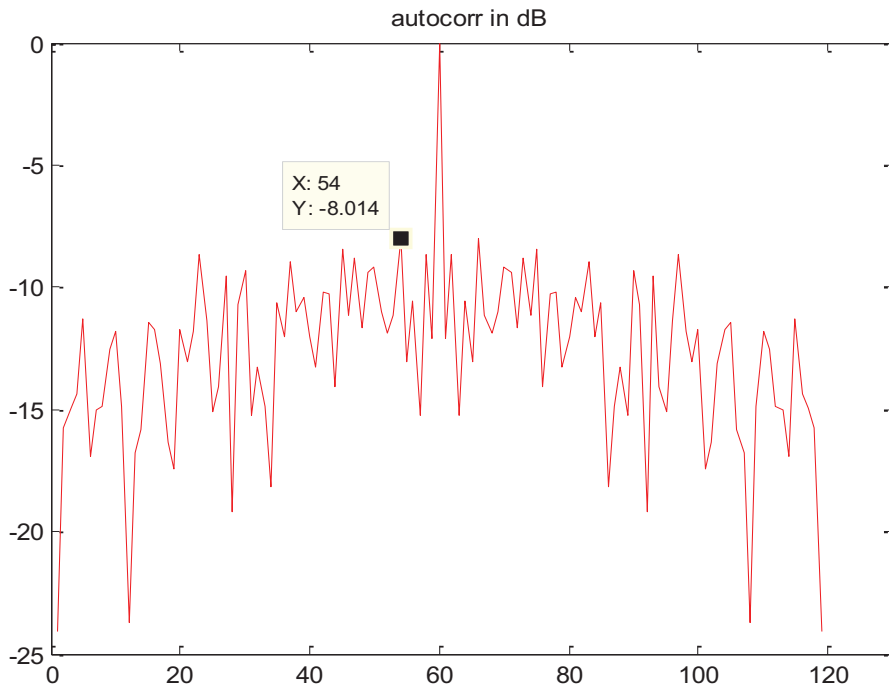


Figure 5-9 The BAOMP detection result of the good signal, SNR=10dB

**b) Bad signal:**

Restricted isometry constant is found as 0.8402. Pd is found as 0.03.



**Figure 5-10 Autocorrelation function of the bad signal**

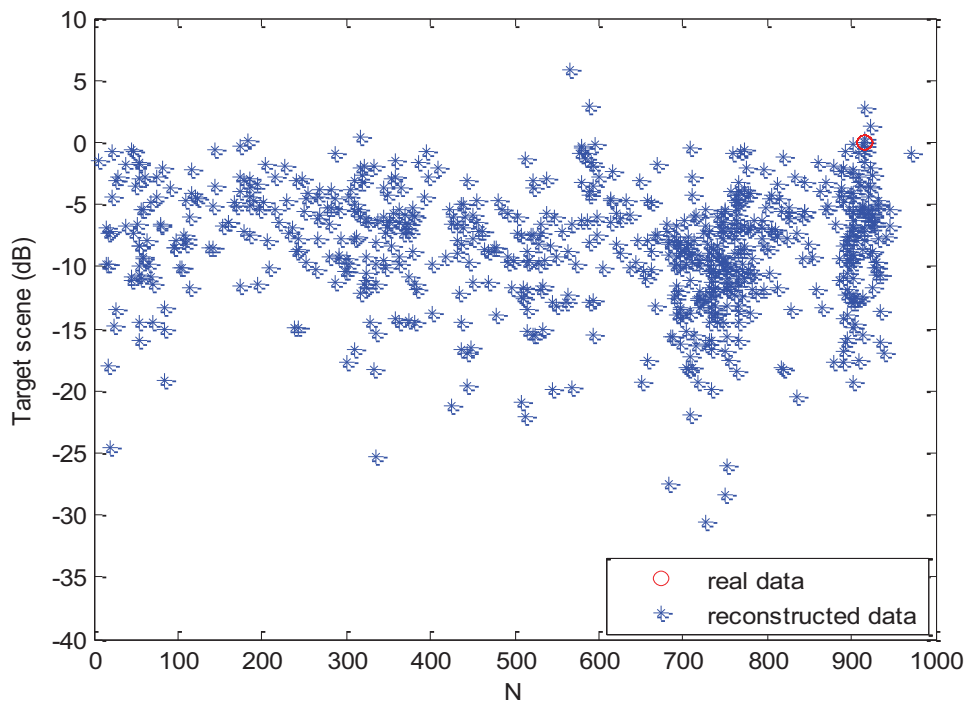


**Figure 5-11 The BAOMP detection result of the bad signal, SNR=10dB**

### 5.2.3 OMP - BAOMP Comparisons

As denoted at the beginning of Section 5.2, when we compare some of the algorithms used in the CS, the BAOMP algorithm is found to be the best with its performance and complexity features. This section gives results of one of these comparisons; detection performances of the OMP and the BAOMP algorithms are compared. The OMP and the BAOMP algorithms are executed with same  $N$ ,  $M$  and  $K$  values for noiseless case. Targets have amplitude equal to 1 and random phase. The transmitted signal is random code of length-60 with unit energy. Graphs are drawn using absolute values. Exact recovery is achieved in both algorithms as shown below, but the number of iterations needed to achieve exact reconstruction is different. The OMP algorithm finds the solution at 10 iterations whereas the BAOMP algorithm finds the solution only at 2 iterations. This result is not surprising since in the BAOMP algorithm, more than one atom can be chosen at each iteration. However, in the OMP algorithm, only one atom is chosen at each iteration. The number of iterations of the BAOMP is smaller, but one can say that the BAOMP is more complex because of choosing more than one atom at each iteration and the backtracking step. When the CPU times of these two algorithms are analyzed for the case above, CPU time of the OMP is found as 13.3438 whereas CPU time of the BAOMP is found as 0.9376. We can say that the BAOMP is more advantageous also in terms of the CPU times.

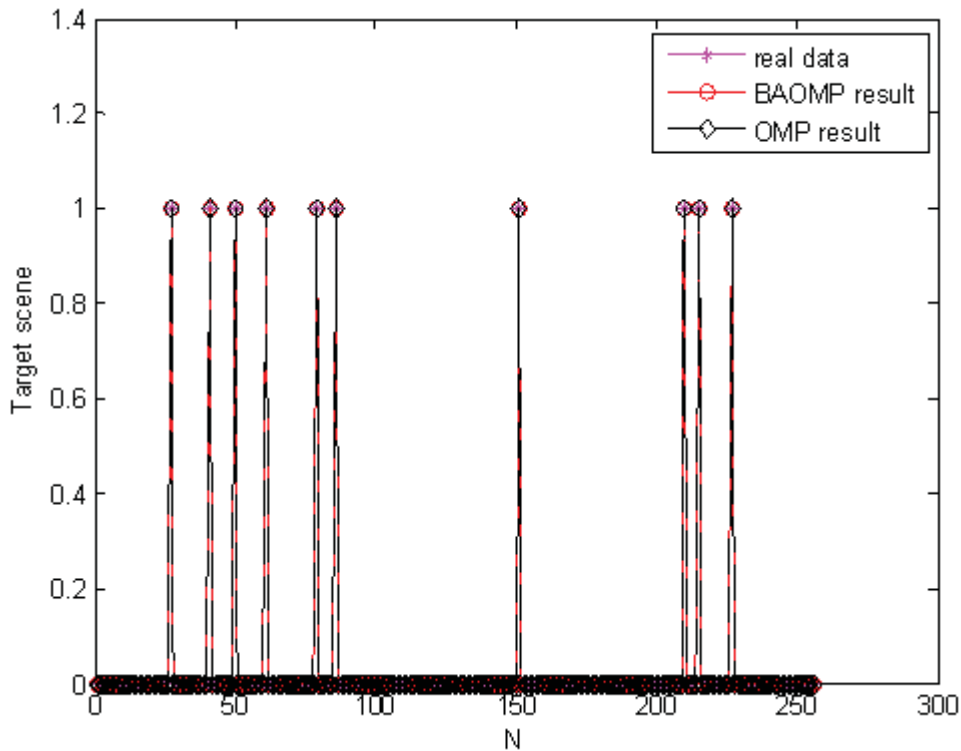


Figure 5-12 OMP&BAOMP for  $N=256$ ,  $M=100$ ,  $K=10$  with no noise

When there is noise, the results are similar. The result below is achieved by 10 iterations of the OMP, and by only 1 iteration of the BAOMP for SNR=20dB.

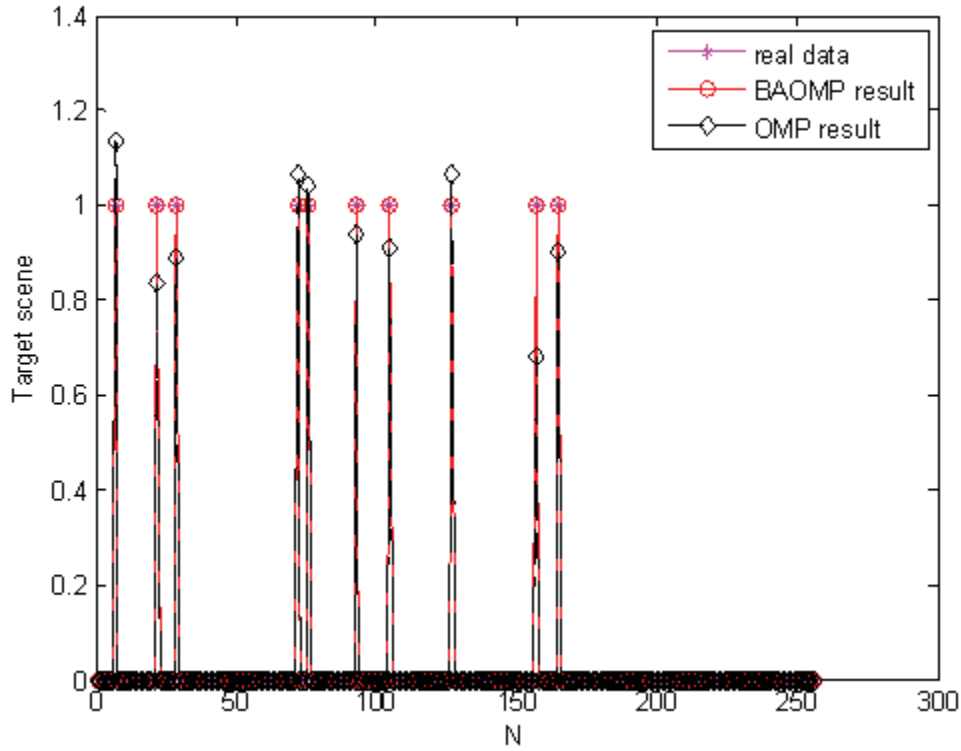


Figure 5-13 OMP&BAOMP for N=256, M=100, K=10 with SNR=20dB

Also, the reconstruction performance of the BAOMP algorithm is better than the OMP as expected, because of the backtracking step in the BAOMP algorithm. An example of this is shown in below figure. All targets are detected with the BAOMP, but the OMP algorithm cannot detect 1 target and makes 1 wrong detection. The number of iterations used is 5 in the BAOMP and 10 in the OMP.

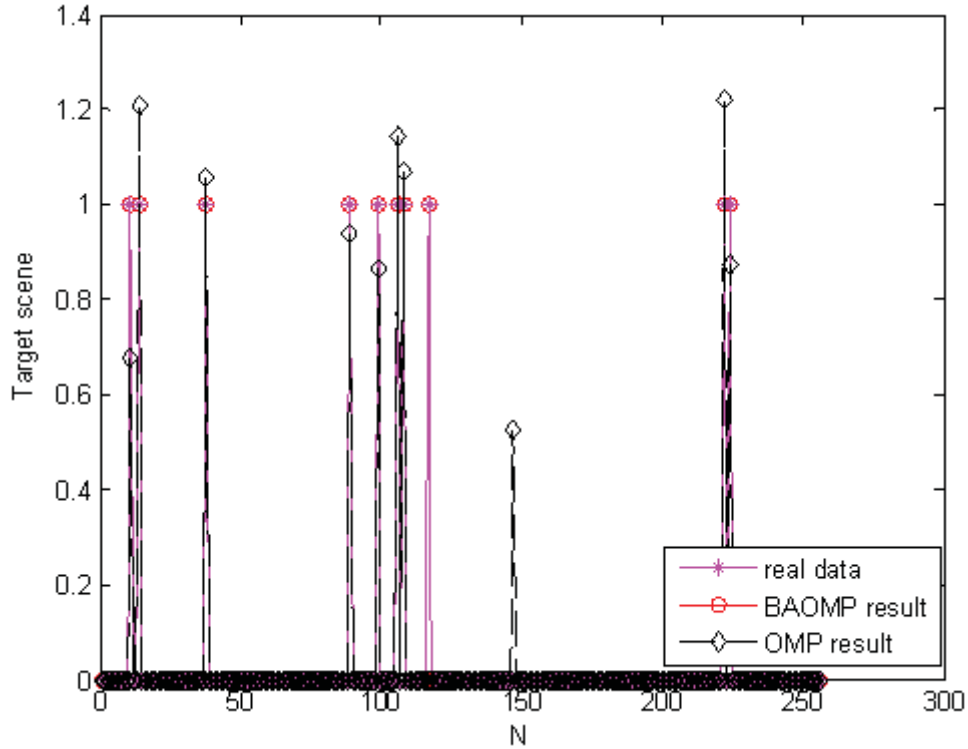


Figure 5-14 OMP&BAOMP for N=256, M=100, K=10 with SNR=15dB

#### 5.2.4 BAOMP Simulations

**Scenario 1:** All data is complex. The good signal, random code of length 60, found in Section 5.2.2 is used as transmitted signal, iid Gaussian noise added for noisy case, N=1000, M=200, K=2 and SNR=20dB.

Reconstruction results of the BAOMP algorithm for Scenario 1 are given below for different values of the convergence threshold  $\varepsilon$ . The convergence threshold value is one of the determining factors for the number of iterations in BAOMP. When  $l_2$ -norm of the residual vector is smaller than  $\varepsilon$  before reaching the maximum number of iterations allowed, the iterations stop. Choosing  $\varepsilon$  large means performing a smaller number of iterations.  $\varepsilon = \alpha * N * \text{var}(\text{noise})$  [16], where  $\alpha$  is a chosen constant. The choice of  $\alpha$  effects the performance of the BAOMP algorithm. This effect is analyzed in this section.

Every simulation is repeated 100 times for each convergence threshold value. Reconstruction performances are compared by using the terms defined below:

**correct1:** The first target is reconstructed at correct position with an amplitude greater than a predefined threshold value

**correct2:** The second target is reconstructed at correct position with an amplitude greater than a predefined threshold value

**false**: Number of detections which are at neither first nor second target's position

**falsebig**: Number of detections which are at neither first nor second target's position with an amplitude greater than a predefined threshold value

After 100 run, we can say that the target scene is reconstructed exactly when correct1 and correct2 are equal to 100 and falsebig is equal to zero. The threshold value is taken as 8dB at simulations.

Changing  $\alpha$  effects the performance of BAOMP algorithm as shown in the following figures. When  $\alpha$  is greater than 0.05, exact recovery is observed.

a)  $\alpha = 0.0001$ : correct1=53, correct2=53, false=77, falsebig=0

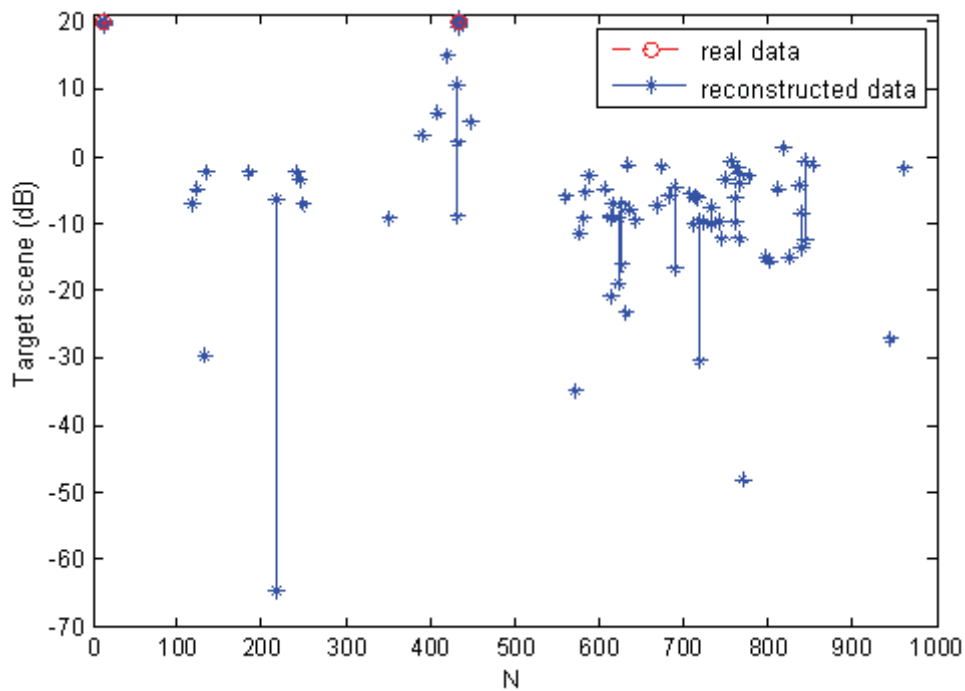


Figure 5-15 BAOMP Simulations for  $N=1000$ ,  $M=200$ ,  $K=2$ ,  $SNR=20dB$  and  $\alpha = 0.0001$

b)  $\alpha = 0.007$ : correct1=54, correct2=54, false=64, falsebig=0

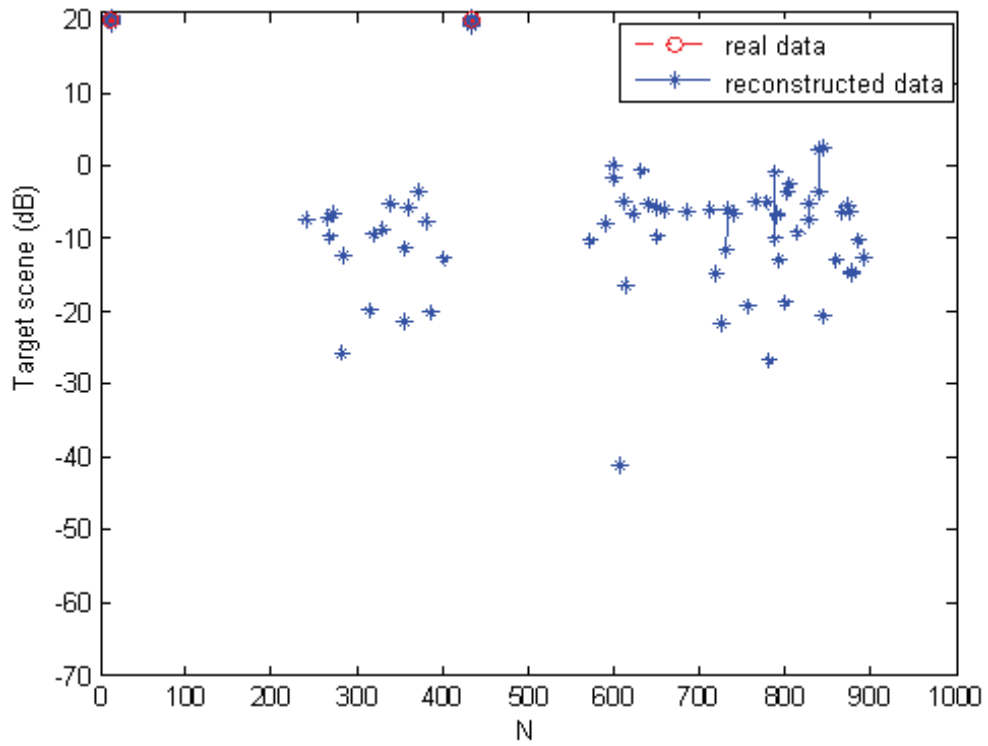


Figure 5-16 BAOMP Simulations for  $N=1000$ ,  $M=200$ ,  $K=2$ ,  $SNR=20dB$  and  $\alpha = 0.007$

c)  $\alpha = 0.05$ : correct1=100, correct2=99, false=0, falsebig=0

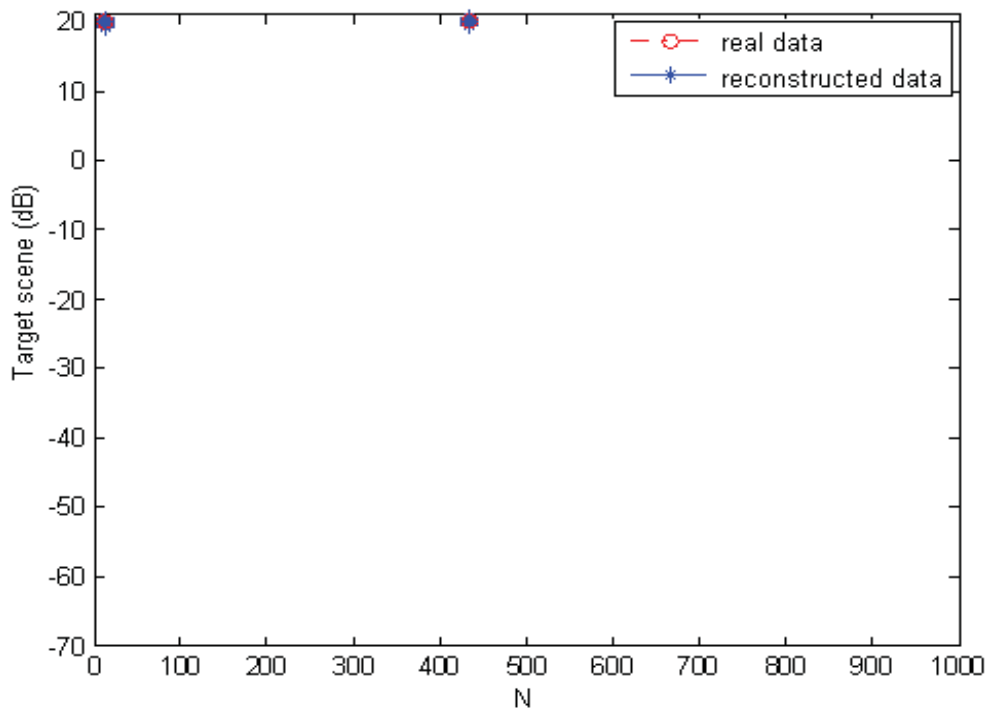


Figure 5-17 BAOMP Simulations for  $N=1000$ ,  $M=200$ ,  $K=2$ ,  $SNR=20dB$  and  $\alpha = 0.05$

d)  $\alpha = \{0.01, 0.02, 0.1, 1\}$ : correct1=100, correct2=100, false=0, falsebig=0

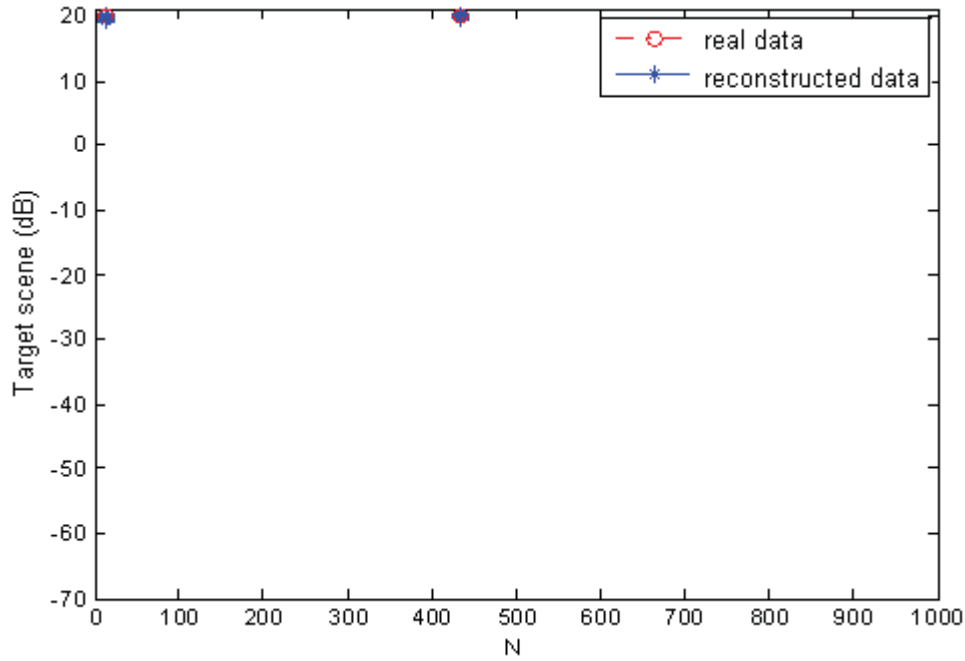


Figure 5-18 BAOMP Simulations for  $N=1000$ ,  $M=200$ ,  $K=2$ ,  $SNR=20dB$  and  $\alpha \geq 0.01$

### 5.2.5 Classical – $l_1$ Minimization – BAOMP Comparison

Comparison of detection performances of the classical method (MF), the  $l_1$  minimization method with  $l_1$  Magic and the BAOMP method for same transmitted signal and target scene is given in this section. The three algorithms are executed with the same  $N$ ,  $M$  and  $K$  values. Targets have amplitudes equal to 1 and random phase. The transmitted signal is random code of length-60 with unit energy. Graphs are drawn using absolute values.

Comparison for noiseless case is given in below figures. The CS method (both  $l_1$  minimization and BAOMP algorithm) gives better reconstruction results than the classical method, even by using less number of measurements. Classical method cannot detect the exact target position and detects false alarms around the target position, in other words has larger side-lobes compared to CS result. There exist false detections in  $l_1$  minimization simulation but their amplitudes are very small compared to the target amplitude, so they cannot be called as false alarm. In the BAOMP simulation, exact reconstruction is observed.

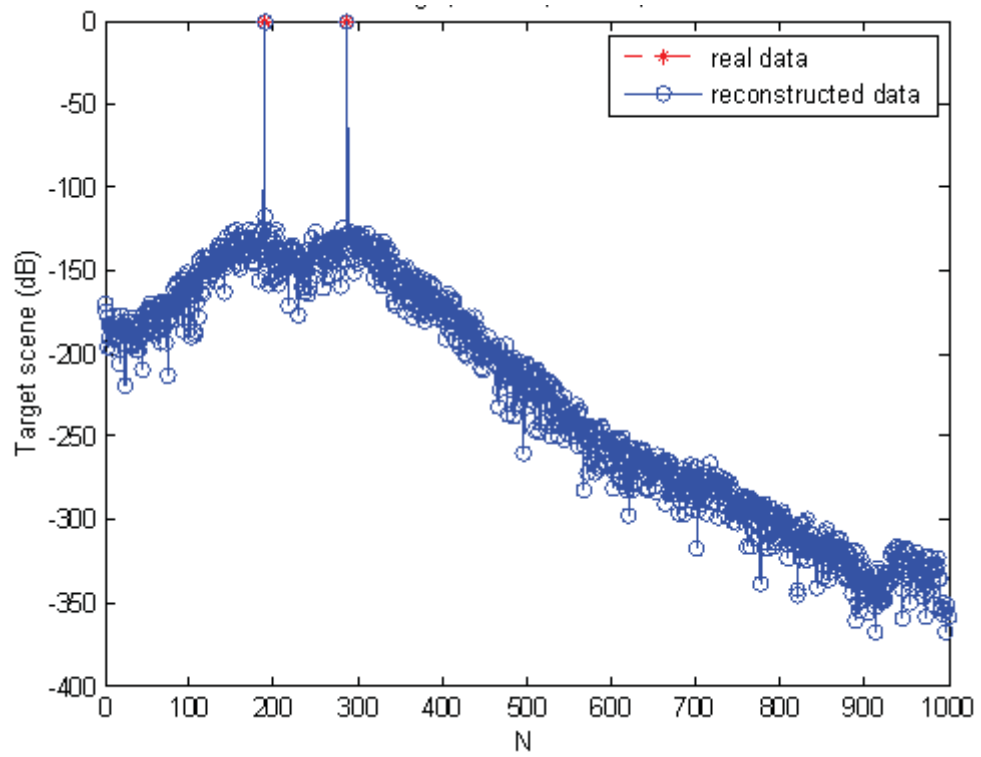


Figure 5-19  $l_1$  minimization simulation for  $N=1000$ ,  $M=200$ ,  $K=2$  with no noise

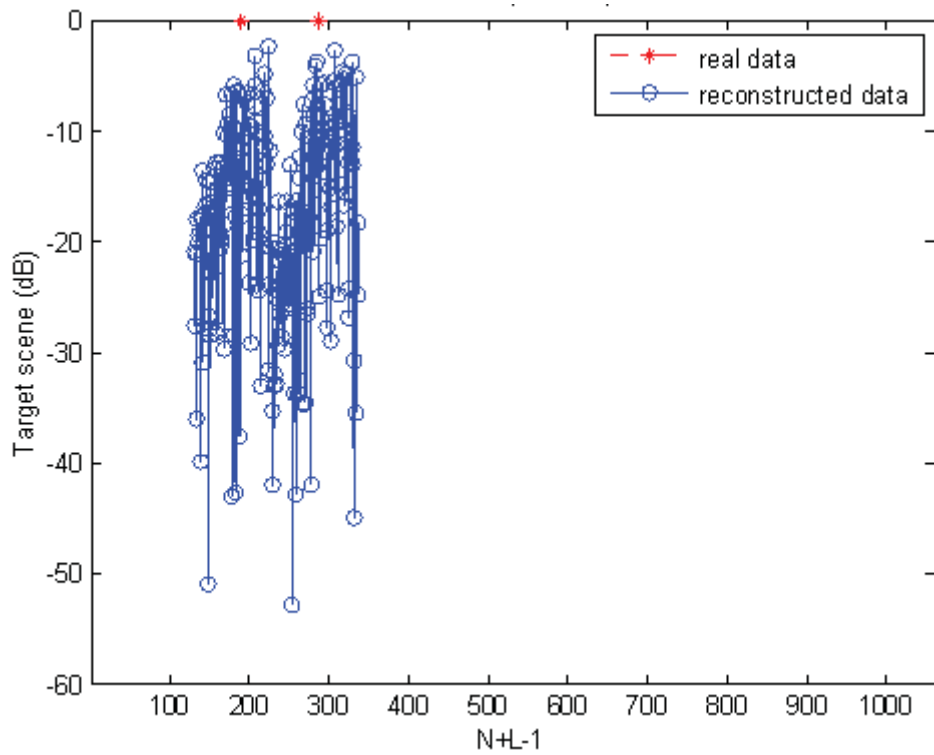


Figure 5-20 MF simulation for  $N=1000$ ,  $M=200$ ,  $K=2$  with no noise

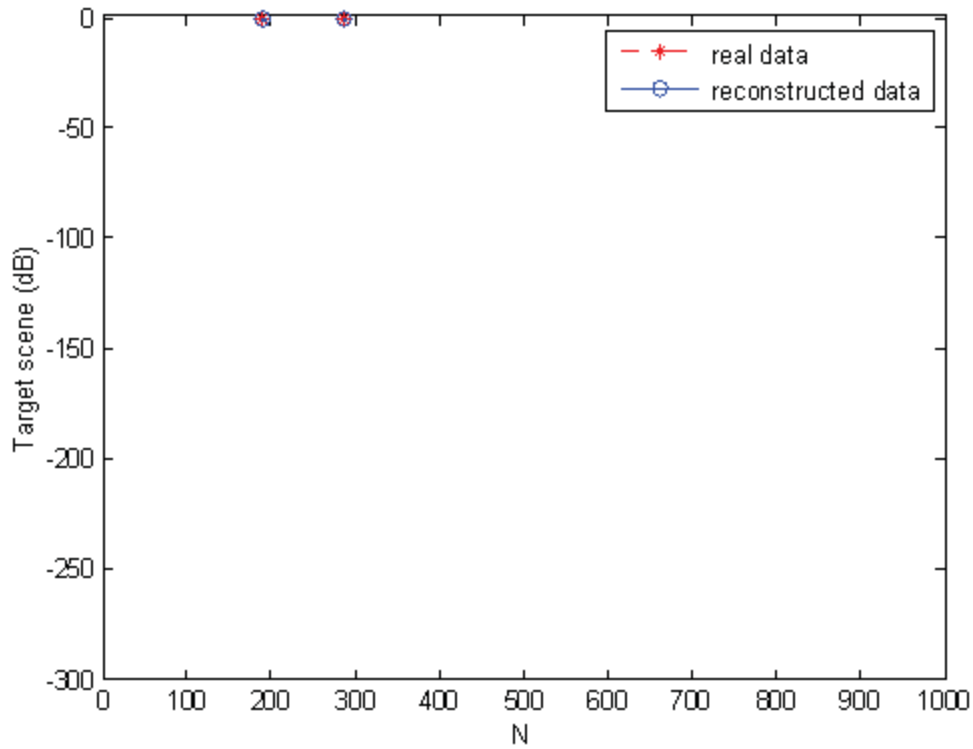


Figure 5-21 BAOMP simulation for  $N=1000$ ,  $M=200$ ,  $K=2$  with no noise

Comparison for noise added case is given in below figures.  $SNR=20dB$  in all simulations. The CS method (both  $l_1$  minimization and BAOMP algorithm) gives better reconstruction results than the classical method, even when noise is present. Similarly, classical method cannot detect the exact target position and detects false alarms around the target position. There exist false detections in the  $l_1$  minimization simulation with amplitudes greater than those in the noiseless case but their amplitudes are still very small compared to the target amplitude, so they cannot be called as false alarm. Again, in the BAOMP simulation, exact reconstruction is observed.

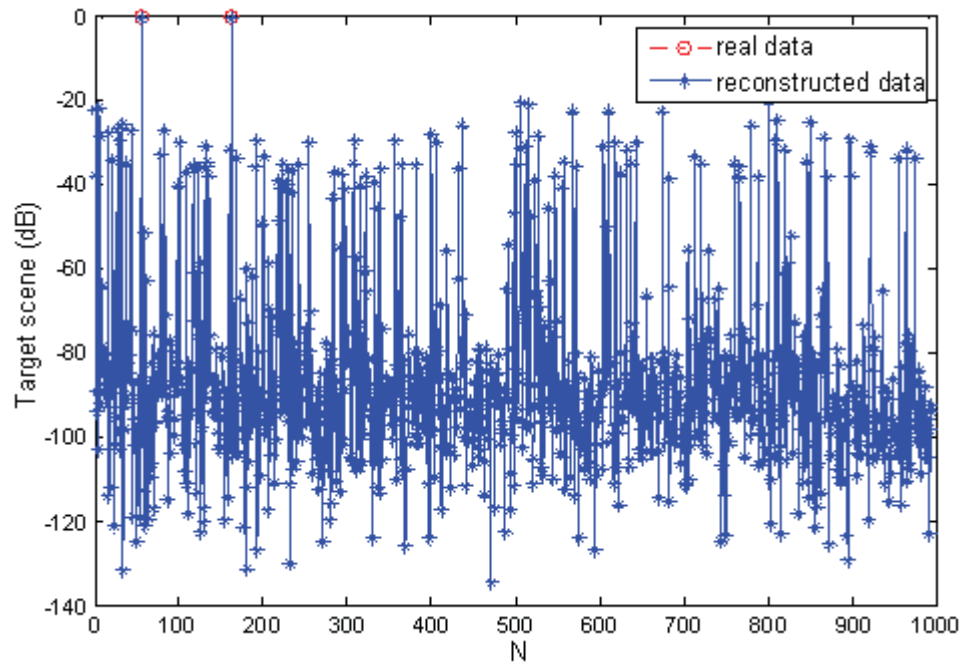


Figure 5-22  $l_1$  minimization simulation for  $N=1000$ ,  $M=200$ ,  $K=2$  with  $SNR=20dB$

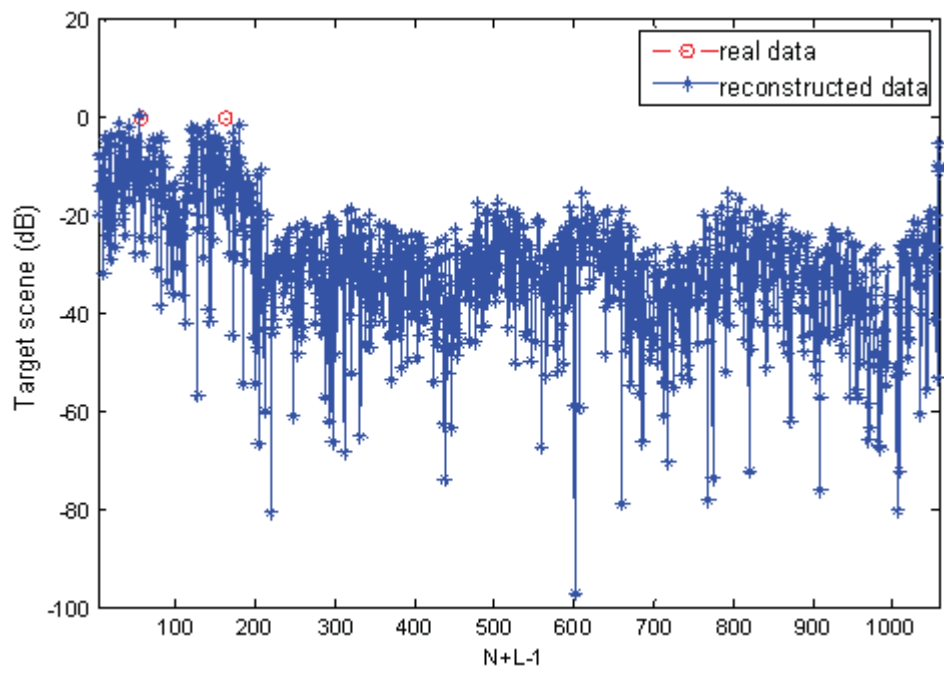


Figure 5-23 MF simulation for  $N=1000$ ,  $M=200$ ,  $K=2$  with  $SNR=20dB$

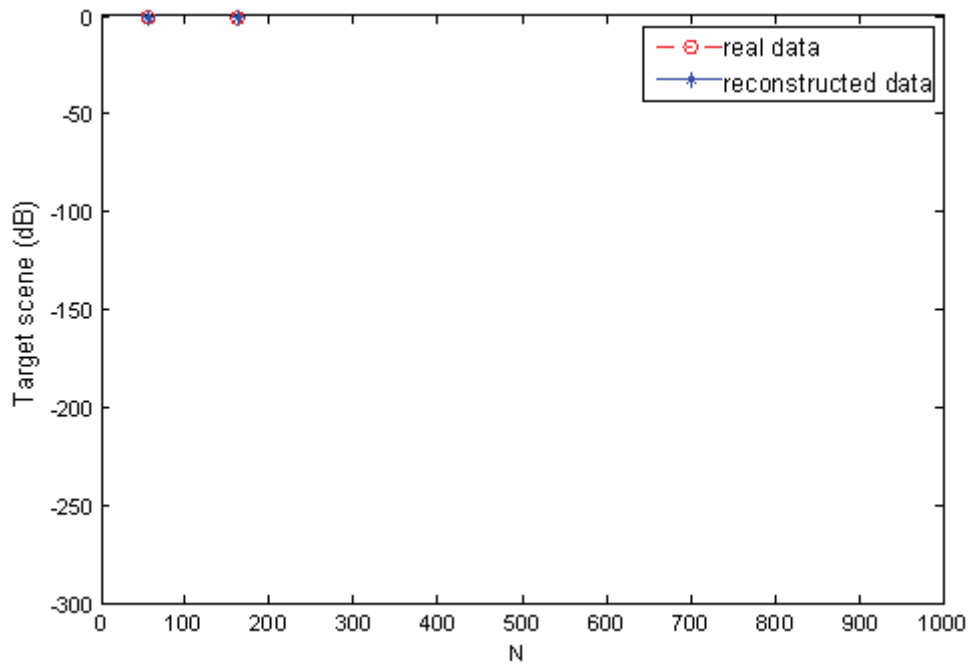


Figure 5-24 BAOMP simulation for  $N=1000$ ,  $M=200$ ,  $K=2$  with  $SNR=20dB$

### 5.2.6 Detection of Close Targets

Performance of the CS at detection of close targets is analyzed in this section. The detection performance of the BAOMP method when there are close targets is compared with that of the classical method for noiseless case. Targets have amplitude equal to 1 and random phase. The transmitted signal is a random code of length-60 with unit energy. Graphs are drawn using absolute values. There exists three targets in the target scene, at 910, 915 and 917th range bins. The CS with the BAOMP algorithm detects targets at exactly correct positions as shown in below figures. However, the classical method cannot detect the exact target positions.

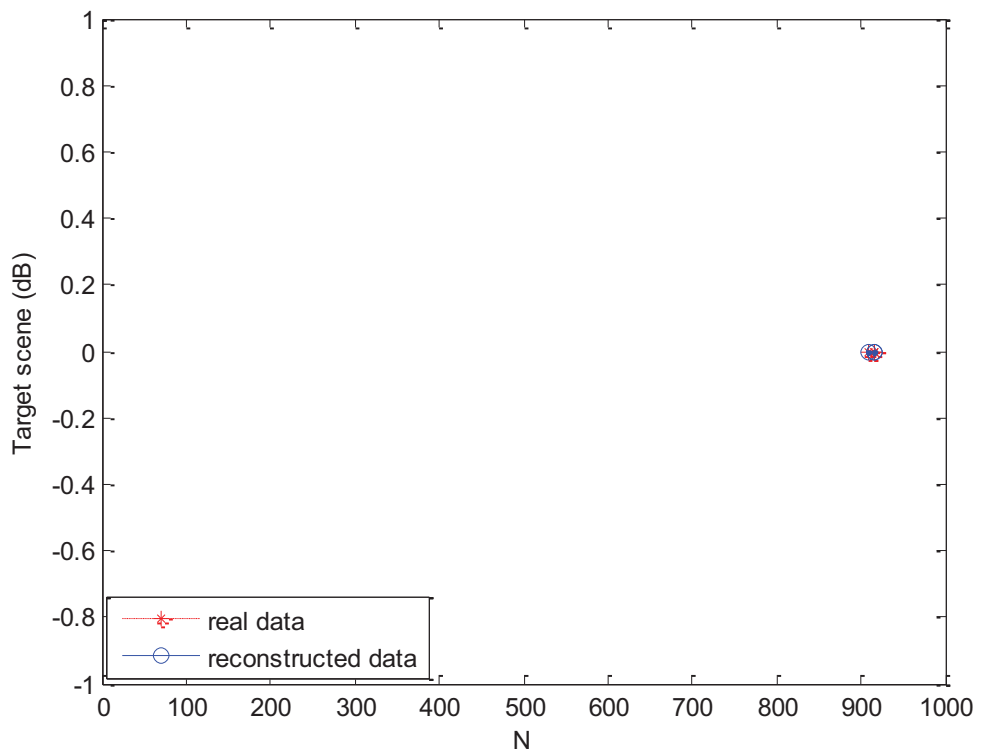


Figure 5-25 The BAOMP result for  $N=1000$ ,  $M=200$ ,  $K=3$  with no noise

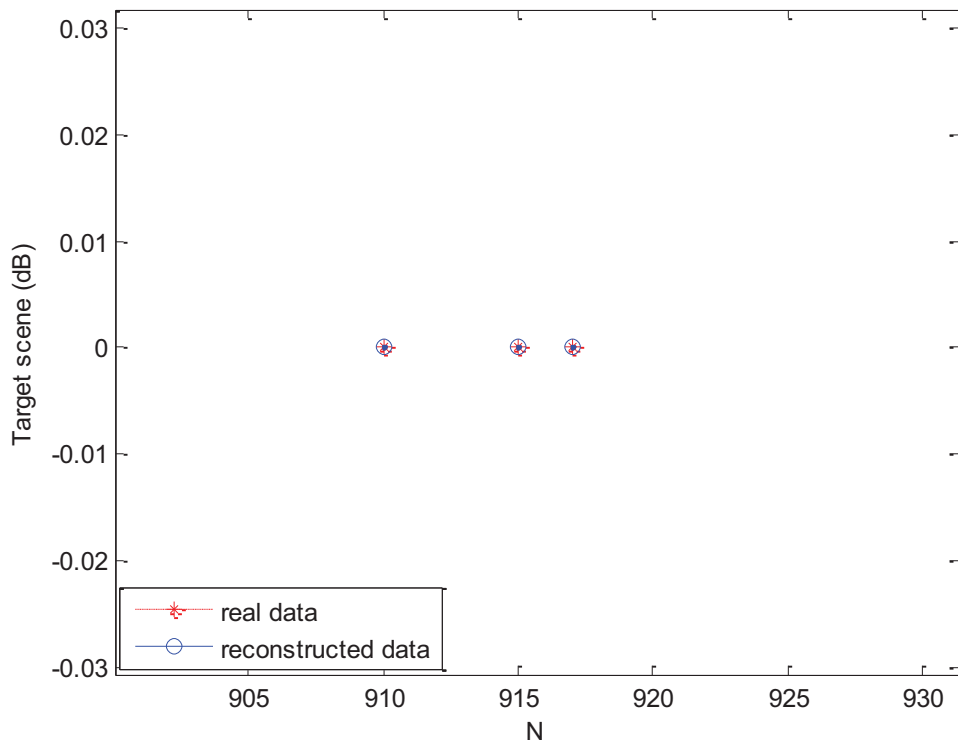


Figure 5-26 Closer view of the BAOMP result

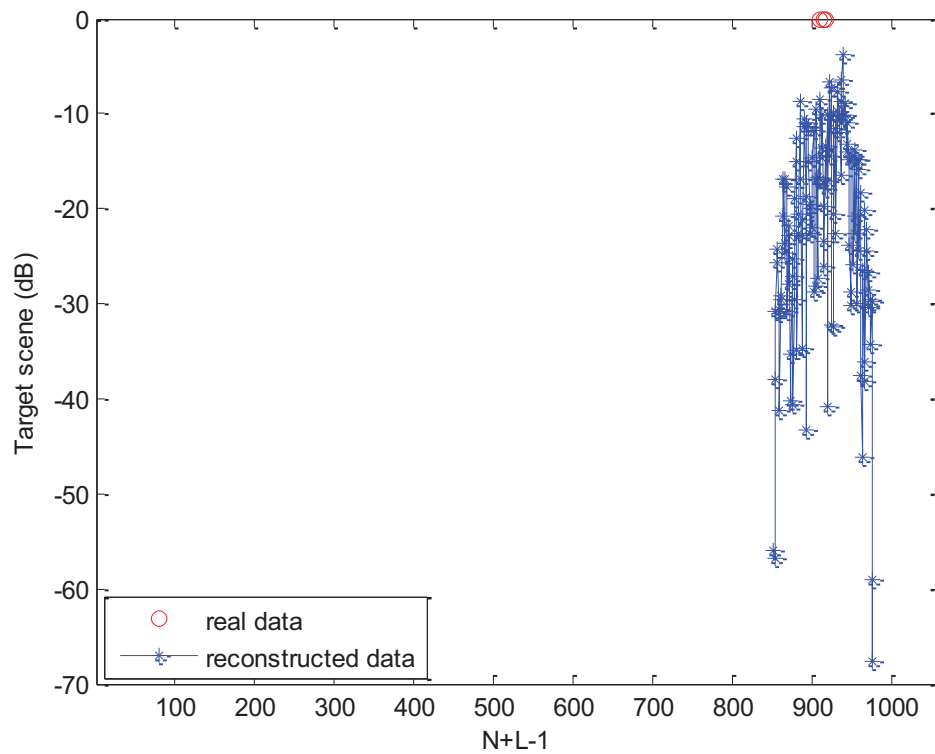


Figure 5-27 The MF result for  $N=1000$ ,  $M=200$ ,  $K=3$  with no noise

### 5.2.7 FAR Calculations

In this section, FAR is calculated for different  $\alpha$  values and constant predefined detection threshold value using the BAOMP algorithm. The scenario is the same as Scenario 1, except there is no target, only noise is present, meaning  $K=0$ . For calculating FAR, there should be only noise no targets in the target scene. FAR is calculated for different  $\varepsilon$  (meaning different  $\alpha$ ) values. The threshold value is taken as 8dB in simulations. As a result, for  $\alpha \geq 0.05$ , the BAOMP method detects no false alarms above the detection threshold, so  $FAR=0$ . Therefore, choosing  $\alpha$  value greater than 0.05 is a good choice for the BAOMP algorithm.

a)  $\alpha = 0.007$ : FAR = 0.1238:

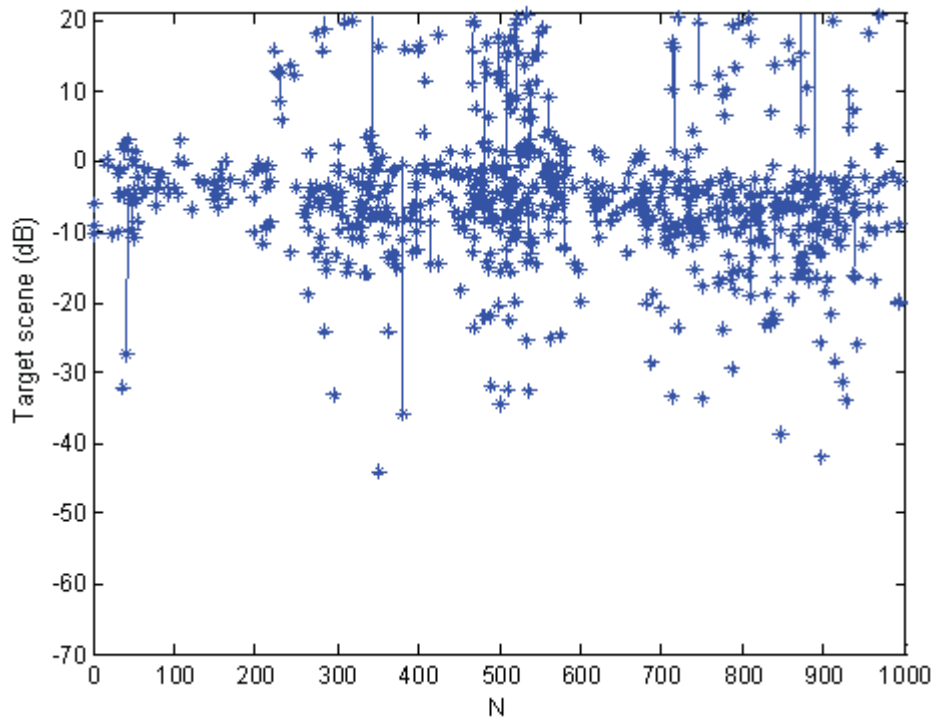


Figure 5-28 BAOMP simulation for  $N=1000$ ,  $M=200$ , no target and  $\alpha = 0.007$

b)  $\alpha = 0.01$ : FAR = 0.0059:

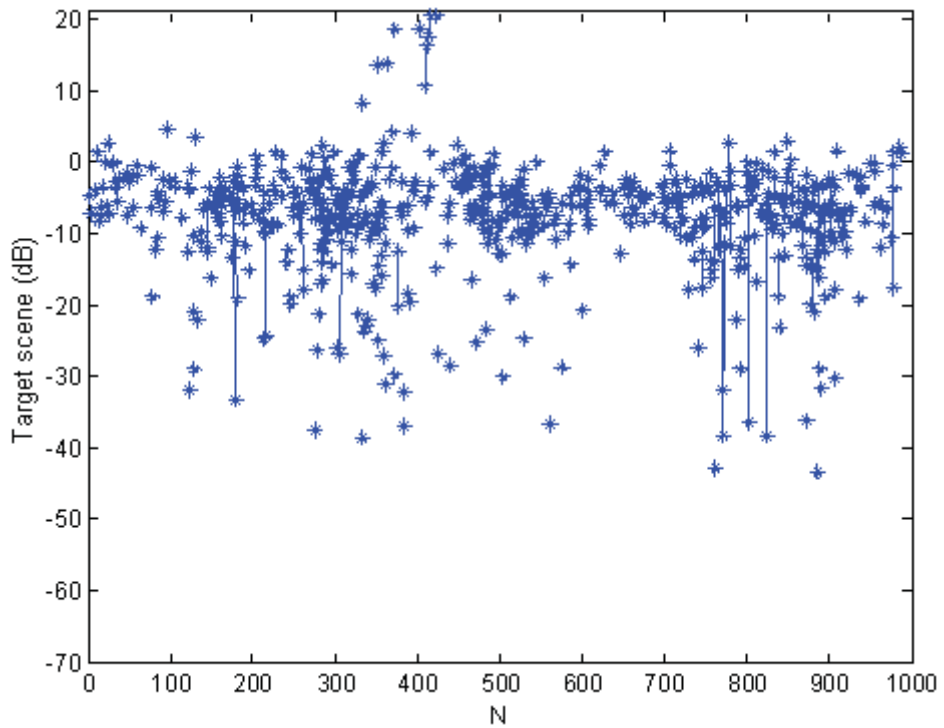


Figure 5-29 BAOMP simulation for  $N=1000$ ,  $M=200$ , no target and  $\alpha = 0.01$

c)  $\alpha = 0.05$ : FAR = 0:

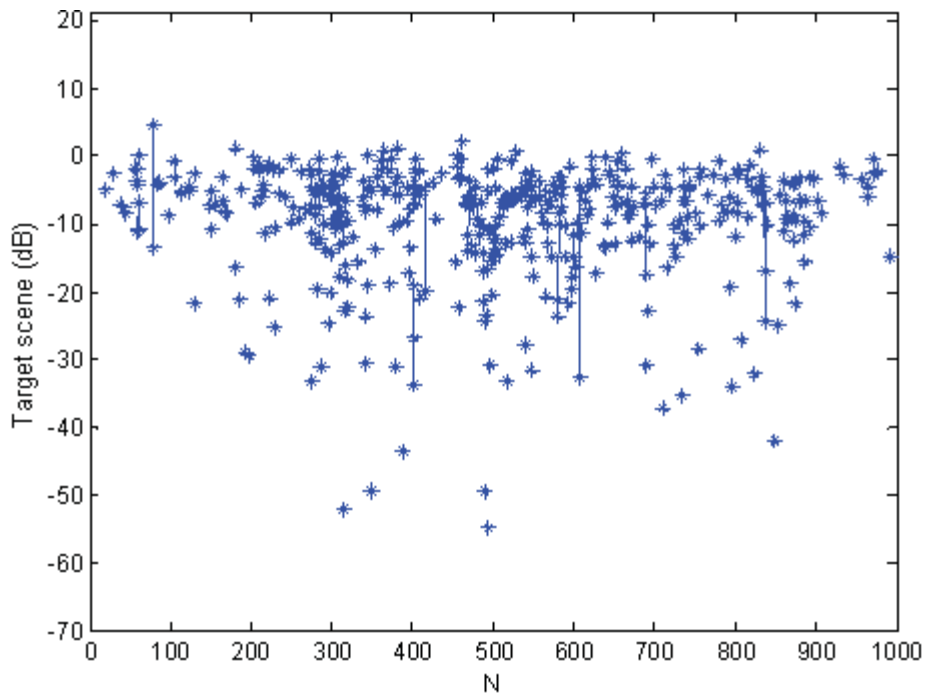


Figure 5-30 BAOMP simulation for  $N=1000$ ,  $M=200$ , no target and  $\alpha = 0.05$

d)  $\alpha = 0.1$ : FAR = 0:

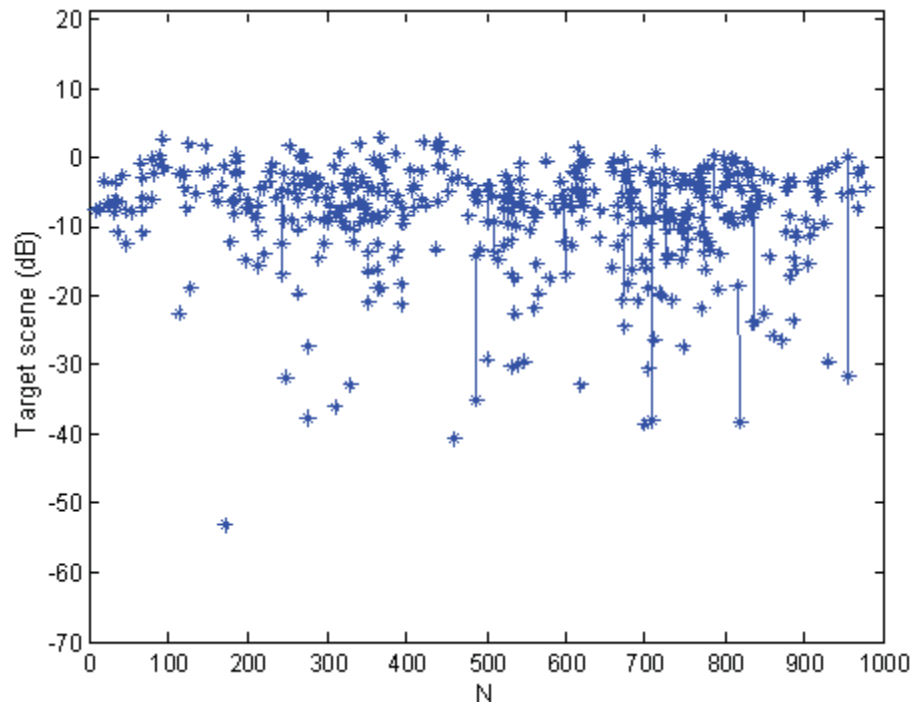


Figure 5-31 BAOMP simulation for  $N=1000$ ,  $M=200$ , no target and  $\alpha = 0.1$

### 5.2.8 Detection Threshold Calculations for Constant FAR

In this section, detection threshold values are calculated for constant FAR and different convergence threshold values, using the BAOMP algorithm. Depending on these results, the detection threshold that will be used for Pd calculations will be chosen indirectly, since the convergence threshold value that will be used in the simulations is chosen first, and then the corresponding detection threshold value is used for Pd calculations. These analyses show the change in the detection threshold by the change in the convergence threshold. The scenario is same as the Scenario 1, except there is no target, only noise is present, meaning  $K=0$ . The algorithm is run 100 times for each  $\varepsilon$  value with the same transmitted signal, but with different measurement matrices. At every run, the M rows of the measurement matrix are randomly chosen from N rows. For calculating threshold, there should be only noise no targets at the target scene. Threshold values are calculated for different  $\varepsilon$  values. The FAR is kept constant,  $FAR = 10^{-3}$ . Since  $N = 1000$  and the algorithm is run 100 times for each  $\varepsilon$  value,  $FAR = \frac{100}{1000*100} = 10^{-3}$ . This means that we should have 100 detections above the threshold. Threshold values are calculated by this way for each  $\varepsilon$ .

Simulations are done for 16 different  $\alpha$  values randomly distributed between  $10^{-3}$  and  $10^1$ , and threshold values are determined for each. As a result, threshold vs  $\alpha$  graph is obtained as shown in Figure 5-31. From the figure, we can say that the threshold value is stabilized at about 13.5dB when  $\alpha \geq 0.0316$ . That means choosing  $\alpha$  greater than this value does not affect the threshold value so much. When  $\alpha$  is smaller than that value, the detection threshold values are unsteady and become very high which means there are many false detections with large magnitudes. Therefore, we can say that the performance of the BAOMP algorithm is not good when  $\alpha$  is smaller than 0.0316. The threshold values found for  $\alpha \geq 0.0316$  is meaningful when we think of the threshold value in the classical method. It is defined as  $\text{Threshold} = \sqrt{-E\beta^2 \ln(P_{FA})}$  where E is the signal energy,  $\beta^2$  is noise power and  $P_{FA}$  is false alarm probability which is equal to FAR [17]. Depending on this simulation result, we can say that it is better to choose  $\alpha \geq 0.0316$ .

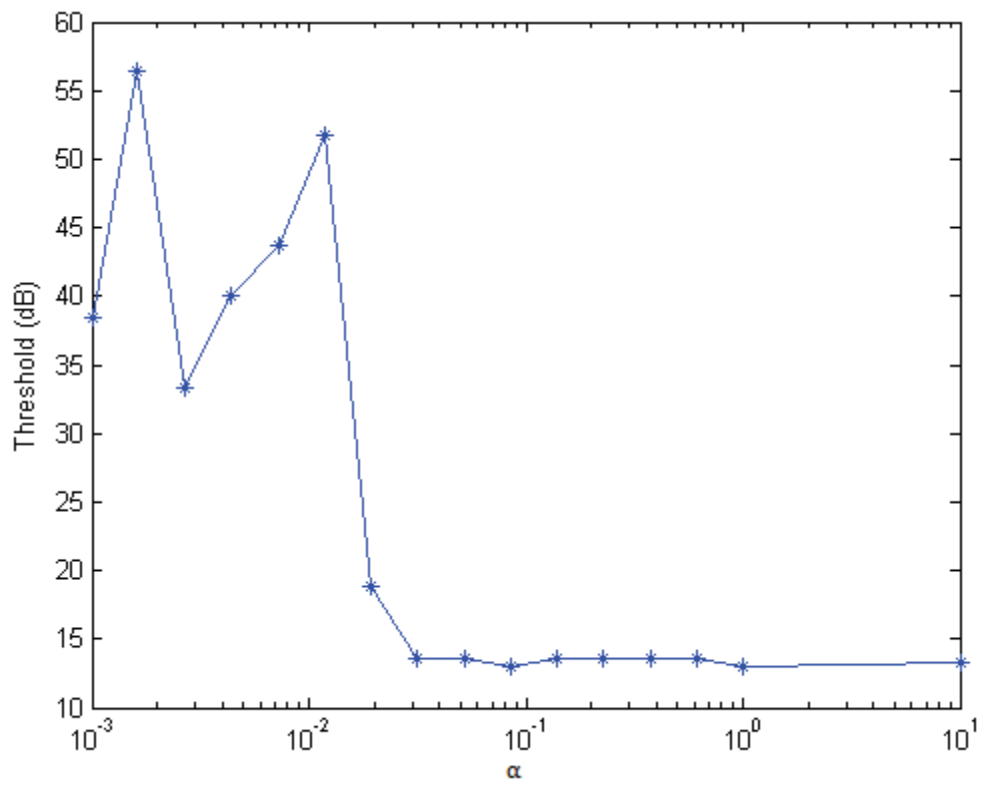


Figure 5-32 Detection threshold vs  $\alpha$  for constant FAR

### 5.2.9 Probability of Detection vs Convergence Threshold

In this section, by using the threshold values found in Section 5.2.9 for constant  $FAR=10^{-3}$ , the probability of detection is calculated for each  $\epsilon$ . The BAOMP algorithm is executed 100 times for Scenario 1, with  $N=1000$ ,  $M=200$ ,  $K=1$  and  $SNR=20dB$  for each  $\epsilon$ . The threshold values found for each  $\epsilon$  are used to calculate the probability of detection for each  $\epsilon$ .

For example, for  $\alpha = 0.01$ , we have the detections as shown in Figure 5-32. The threshold value found for  $\alpha = 0.01$  is 1.035. The number of detections at target's correct position with an amplitude greater than the threshold value is 72. This means that the probability of detection is 0.72 for this  $\alpha$  value.

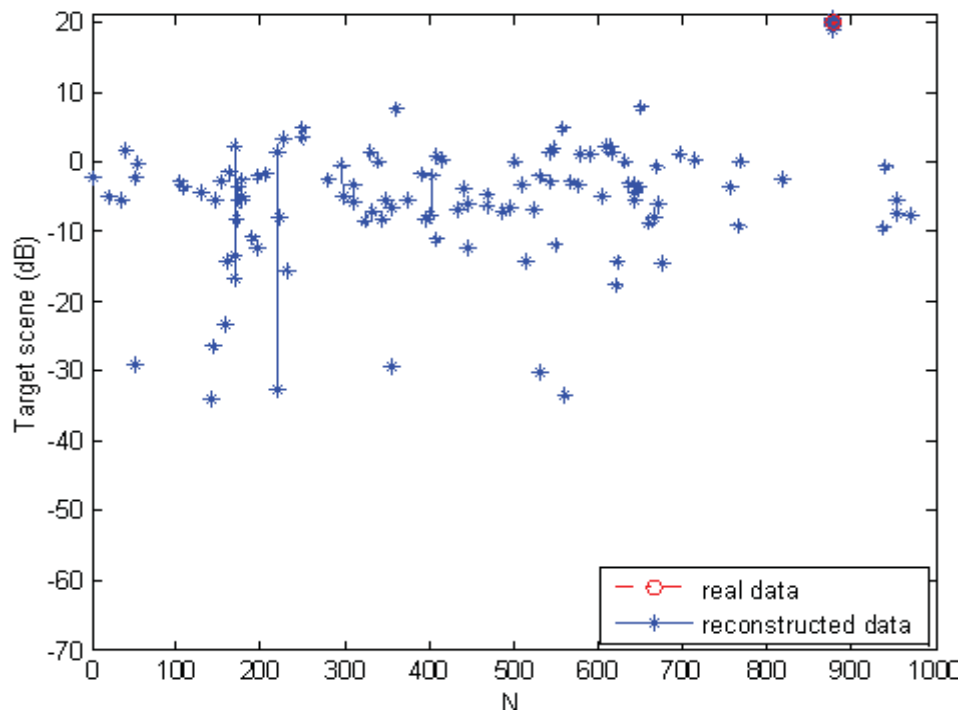


Figure 5-33 BAOMP simulation for  $N=1000$ ,  $M=200$ ,  $K=1$  with  $SNR=20dB$  and  $\alpha = 0.01$

The probability of detection values are calculated like the example for  $\alpha = 0.01$  for each  $\alpha$ . Then, probability of detection vs  $\alpha$  graph is obtained as shown in Figure 5-33. We can say that, exact recovery of the target scene is achieved when  $\alpha \geq 0.02$  since  $P_d=1$ .

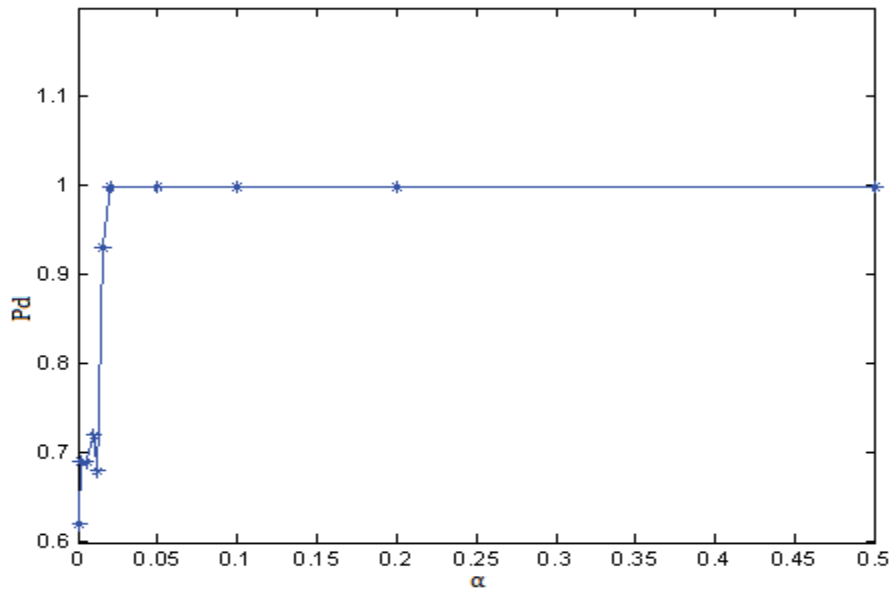


Figure 5-34 Pd vs  $\alpha$  for SNR=20dB

Figure 5-33 is for SNR=20dB. The same procedure is repeated for different SNR values by keeping everything else the same as SNR=20dB case. Then, probability of detection vs  $\alpha$  graph is obtained as shown in Figure 5-34 below. We can say that, for different SNR values, maximum reconstruction performance is achieved when  $\alpha \geq 0.0316$ . Choosing  $\alpha$  bigger decreases the number of iterations, so we decided to choose  $\alpha$  larger than this value.

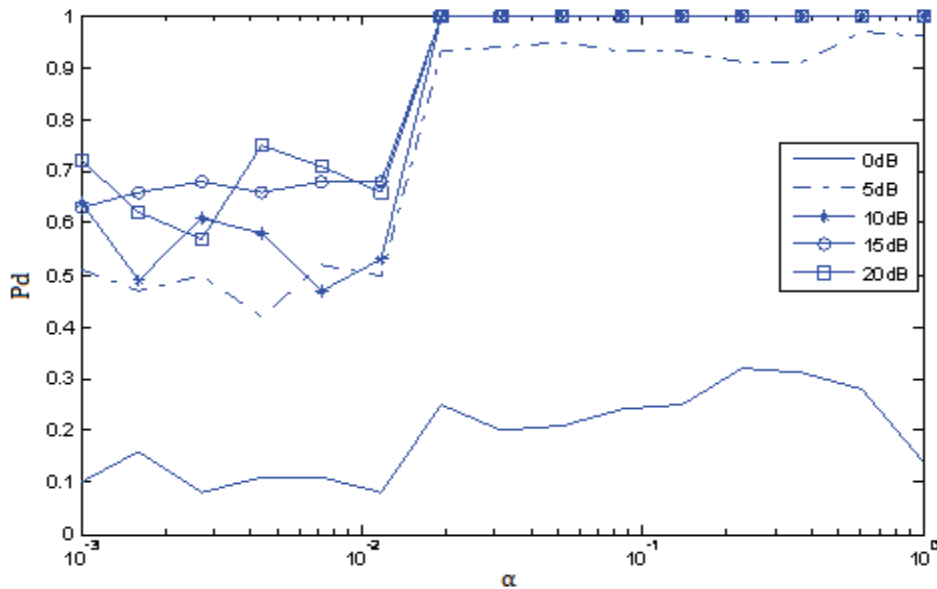


Figure 5-35 Pd vs  $\alpha$  for SNR values

Probability of Detection vs Convergence Threshold graph is also obtained only with a different transmitted signal to see whether the performance of the BAOMP algorithm gets better. The transmitted signal is generated by using 8 PSK. Probability of detection values are not better than the previous case. Therefore, the choice of using a random signal as the transmitted signal is still applicable.

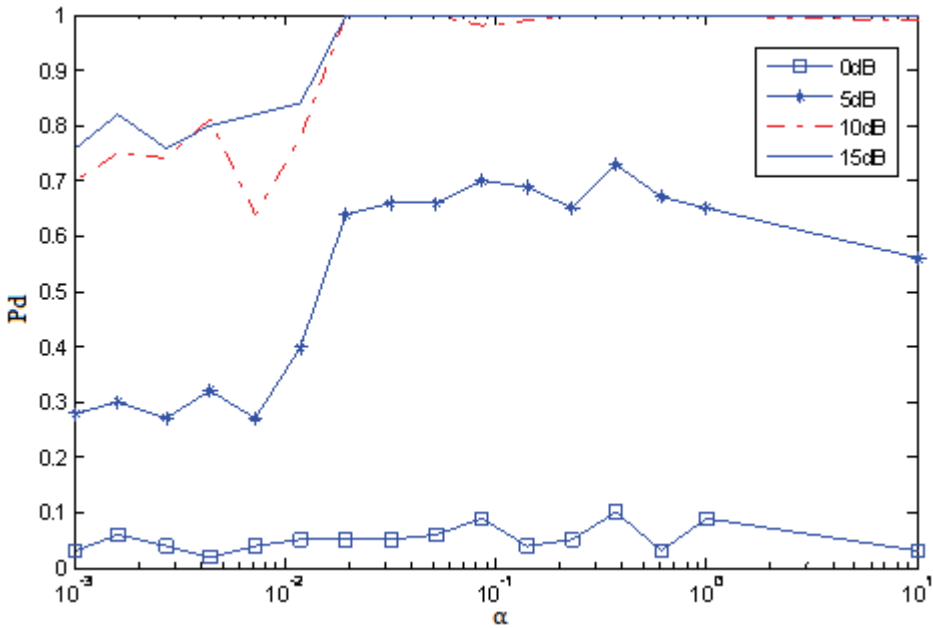


Figure 5-36 Pd vs  $\alpha$  for SNR values with 8 PSK transmitted signal

### 5.2.10 Probability of Detection (Pd) vs SNR

From Figure 5-34, the  $\alpha$  value that is the best to be used in the BAOMP algorithm for this transmitted signal is chosen as 0.6105. With this value, Probability of Detection vs SNR graph together with the classical detection result is obtained as shown below. Since we use  $N=1000$  and  $M=200$  in the BAOMP algorithm, this results in a SNR loss of  $200/1000=1/5$  which is equal to  $10\log_{10}(1/5)=-7\text{dB}$ . Therefore, when comparing Pd vs SNR graphs of the CS and the classical method, the graph obtained for the CS is shifted as  $-7\text{dB}$ . This shift is included in Pd vs SNR graphs.

**Scenario 2:** All data is complex. A random code of length 60 is used as transmitted signal, iid Gaussian noise added for noisy case,  $N=1000$ ,  $M=200$ ,  $K=1$  and  $\text{SNR}=10\text{dB}$ .

To find a more precise solution, the BAOMP algorithm is run 100 times for Scenario 2 with  $\alpha = 0.6105$ . The probability of detection value for  $\text{SNR}=10\text{dB}$  is calculated for each transmitted signal. The signal which gives the best probability of detection value is chosen as the transmitted signal. Threshold value is found as  $13.3290\text{ dB}$  for constant  $\text{FAR}=10^{-3}$ . Then, by using this transmitted signal and  $\alpha$  value, Pd vs SNR graph together with the classical detection result is obtained as shown below. We have the same performance with the classical method when  $\text{SNR} \geq 10\text{dB}$ . When  $\text{SNR} < 10\text{dB}$ , the performance of the CS with the BAOMP algorithm is slightly worse than the classical method.

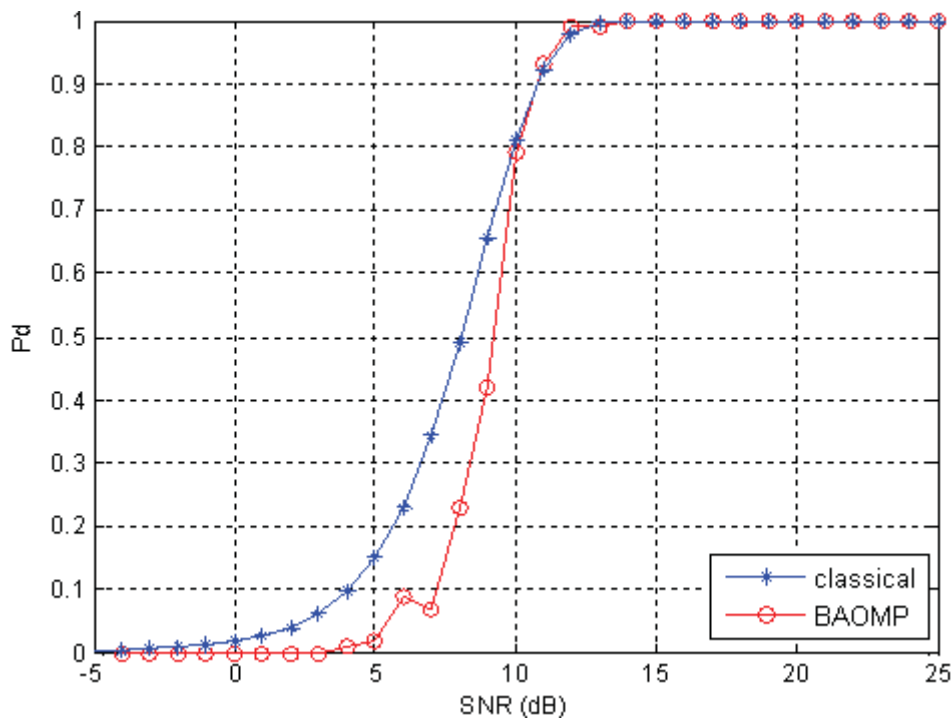


Figure 5-37 Pd vs SNR by choosing the transmitted signal as the signal which gives the best Pd for  $\text{SNR}=10\text{dB}$ ,  $\text{FAR}=10^{-3}$

We choose  $\text{SNR}=10\text{dB}$  in the previous simulation and the performance of the BAOMP algorithm is found to be same as the classical method for  $\text{SNR} \geq 10\text{dB}$ . We repeat the same

procedure by changing the chosen SNR value to see whether this result is a coincidence. When Scenario 2 is run 100 times for SNR=5dB instead of 10dB and the same procedure in the previous case is applied with  $\alpha = 0.6105$ , Pd vs SNR graph together with the classical detection result is obtained as shown below in Figure 5-37. The detection performance of CS method is now about 1dB worse than that of the classical method. A different result is obtained with SNR=5dB compared to SNR=10dB. That means there is no relation between the performance of the BAOMP algorithm being same as the classical method and the choice of the SNR value at the beginning of the procedure.

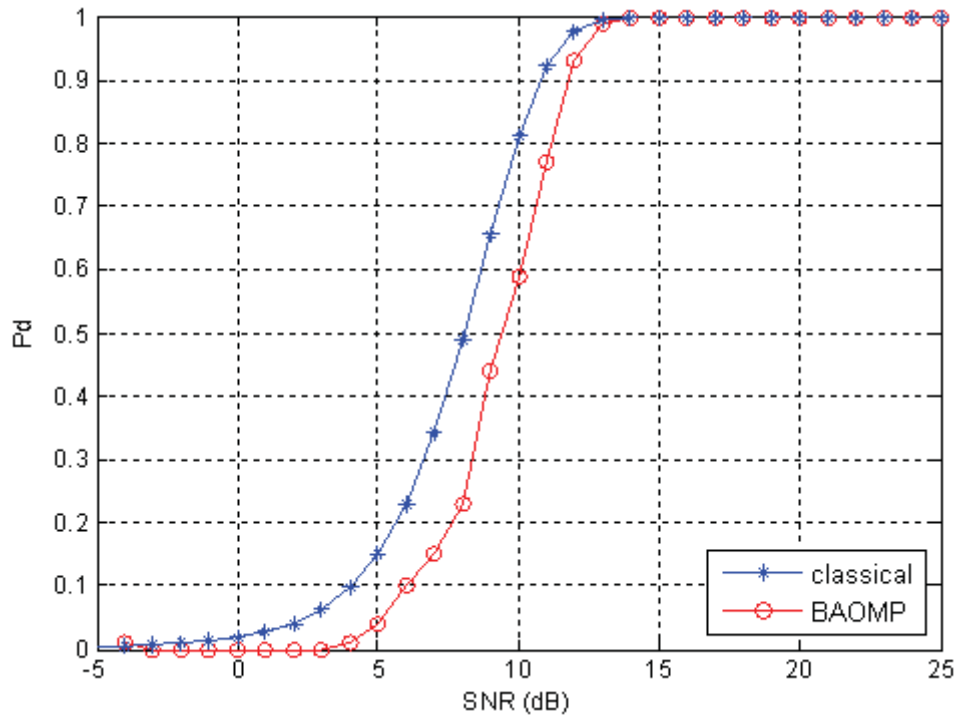


Figure 5-38 Pd vs SNR by choosing the transmitted signal as the signal which gives the best Pd for SNR=5dB, FAR= $10^{-3}$

### 5.2.11 False Detections Around the Target Position

This section analyzes whether the BAOMP algorithm makes false detections around the correct target position. For example, if there exists a target at 915th range bin, instead of looking at 915th range bin, we look at the 914th and 916th range bins, which we call '1\_shifted', to see whether there are any wrong detections. As a second case, we look at the 913, 914, 916 and 917th range bins, which we call '2\_shifted'. Probability of Detection vs SNR graphs for 1\_shifted and 2\_shifted cases are obtained with the same data used to obtain Figure 5-36. The graphs are added to the graph in Figure 5-36 as shown below in Figure 5-38. The Pd values for 1\_shifted and 2\_shifted cases are so close to zero, so we can say that the BAOMP algorithm does not make many wrong detections around the correct target position which is a good property.

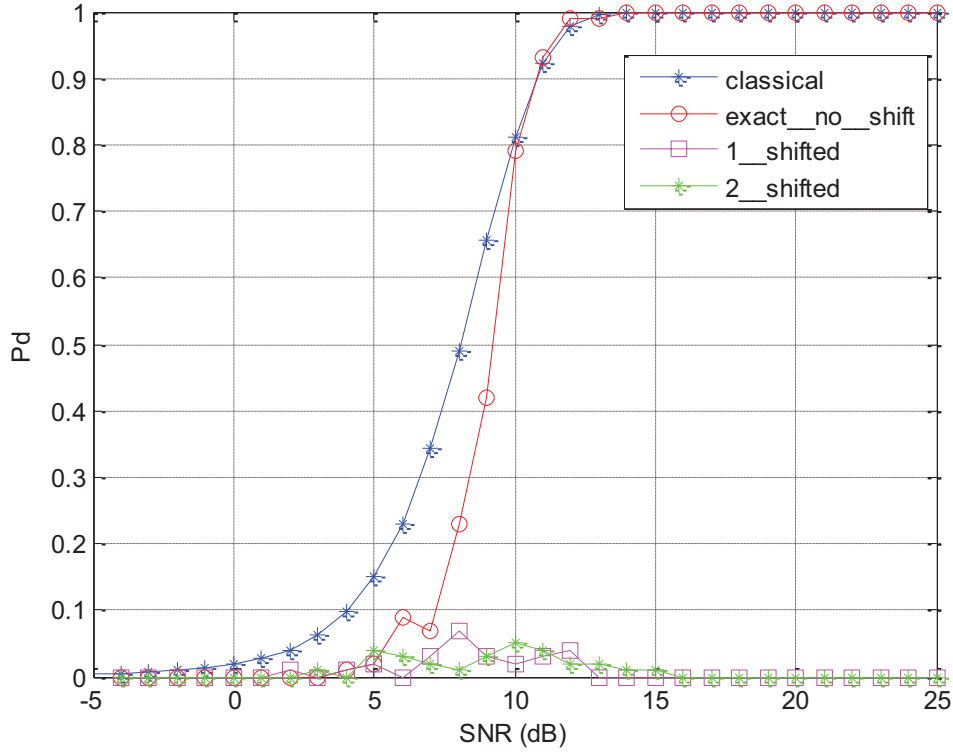


Figure 5-39 Pd vs SNR graphs for classical, exact target position, 1\_shifted target position and 2\_shifted target position cases, FAR= $10^{-3}$

### 5.2.12 Doppler Effect

The effect of Doppler to the performance of CS method is analyzed in this section.

Doppler effect is applied by adding the Doppler frequency shift to the transmitted signal. This means multiplication of the transmitted signal by  $e^{j2\pi f_i \text{PRI}}$  where PRI is pulse repetition interval and  $f_i$ 's are Doppler frequencies. We define PRF = 10000 Hz and  $\text{PRI} = \frac{1}{\text{PRF}} = \frac{1}{10000} = 10^{-4}$  second and  $f_i = i \cdot \left(\frac{\text{PRF}}{16}\right) = i \cdot \left(\frac{10000}{16}\right)$  for  $i = 0, 1, 2, \dots, 15$  for 16 Doppler case. For 32 Doppler frequencies, we have  $f_i = i \cdot \left(\frac{\text{PRF}}{32}\right) = i \cdot \left(\frac{10000}{32}\right)$  for  $i = 0, 1, 2, \dots, 31$ .

**Scenario 3:** Random Code of length 10 is used as transmitted signal which are the columns of  $N \times N$  convolution matrix  $\mathbf{A}$ , iid Gaussian noise added for noisy case,  $N=100$ ,  $M=20$ ,  $K=1$ . 16 pulses are transmitted. We have the  $N \times N$  convolution matrix  $\mathbf{A}$  formed by shifting the transmitted signal once at each column. This convolution matrix is multiplied by the term  $e^{j2\pi f_i \text{PRI}}$  for Doppler frequency shift. Since we have 16 pulses and 16 Doppler frequencies, a  $16N \times 16N$  matrix will be formed. First  $N$  rows are for the first transmitted pulse, second  $N$  rows (from  $(N+1)$  to  $(2N)$ th row) are for the second pulse, etc. First  $N$  columns are for the first Doppler frequency, second  $N$  columns are for the second Doppler frequency, etc. In our scenario, this means a  $1600 \times 1600$  matrix, and out of these 1600 rows  $16M=320$  rows will be randomly chosen. This results in a  $16M \times 16N = 320 \times 1600$  Measurement matrix. The form of

the 1600x1600 matrix in terms of the convolution matrix  $\mathbf{A}$  is shown below. The 16Mx16N measurement matrix is formed by randomly choosing 16M rows of this 1600x1600 matrix.

$$\begin{bmatrix} \mathbf{A} & \mathbf{A} & \cdots & \mathbf{A} & \mathbf{A} \\ \mathbf{A}e^{j2\pi f_1 \text{PRI}} & \mathbf{A}e^{j2\pi f_2 \text{PRI}} & \cdots & \mathbf{A}e^{j2\pi f_{15} \text{PRI}} & \mathbf{A}e^{j2\pi f_{16} \text{PRI}} \\ \vdots & \vdots & \ddots & \vdots & \vdots \\ \mathbf{A}e^{j14.2\pi f_1 \text{PRI}} & \mathbf{A}e^{j14.2\pi f_2 \text{PRI}} & \cdots & \mathbf{A}e^{j14.2\pi f_{15} \text{PRI}} & \mathbf{A}e^{j14.2\pi f_{16} \text{PRI}} \\ \mathbf{A}e^{j15.2\pi f_1 \text{PRI}} & \mathbf{A}e^{j15.2\pi f_2 \text{PRI}} & \cdots & \mathbf{A}e^{j15.2\pi f_{15} \text{PRI}} & \mathbf{A}e^{j15.2\pi f_{16} \text{PRI}} \end{bmatrix}$$

The SNR loss of -7dB explained in Section 5.2.10 is still exists here. Additionally, a processing gain of  $10\log_{10}(16)=12\text{dB}$  exists because of the transmission of 16 pulses. Therefore, when comparing Pd vs SNR graphs of the CS and the classical method for 16/32 Doppler and 16 pulse cases, the graph obtained for the CS is shifted  $12-7=5\text{dB}$ . This shift is included in Pd vs SNR graphs only. In other simulations below, this SNR shift is not included.

**16 Doppler, 16 Pulse Simulations:** Scenario 3 is run 100 times for 16 Doppler frequencies and 16 transmitted pulses.

- 1) One target is present at 90th bin at frequency= $f_1=0$  (90th range bin, 1th Doppler bin). Detection results for different SNR values are given below. For all of three SNR values used in the simulations, the detection probability is so close to 1.

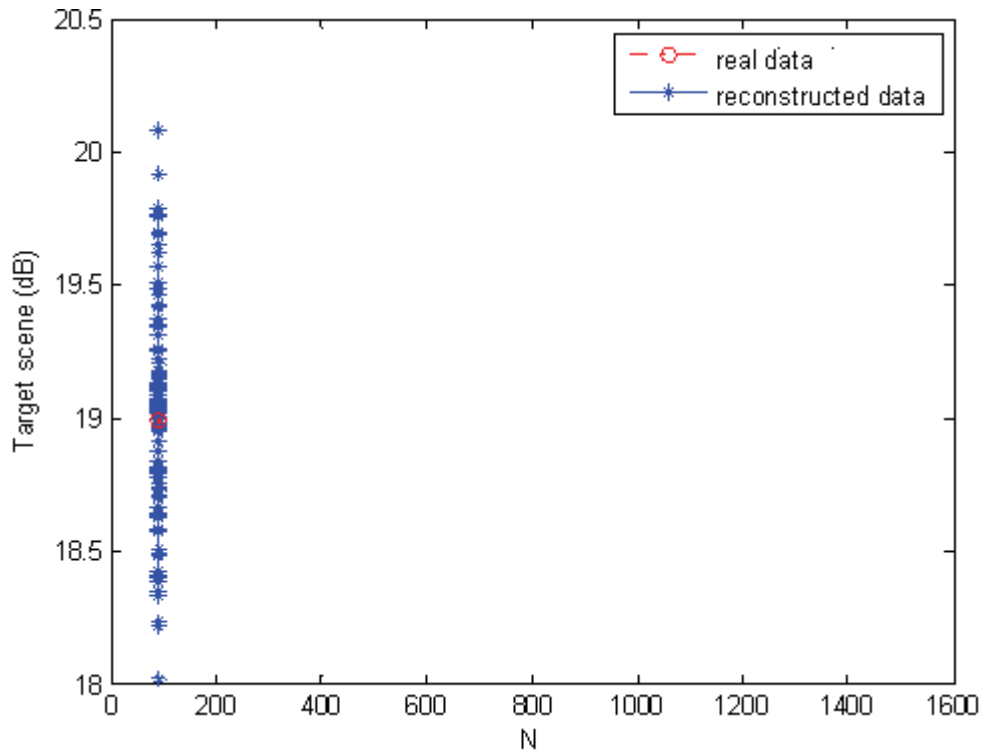


Figure 5-40 One target at 90<sup>th</sup> bin, 16 Doppler, 16 pulse, N=100, M=20, K=1 with SNR=22dB

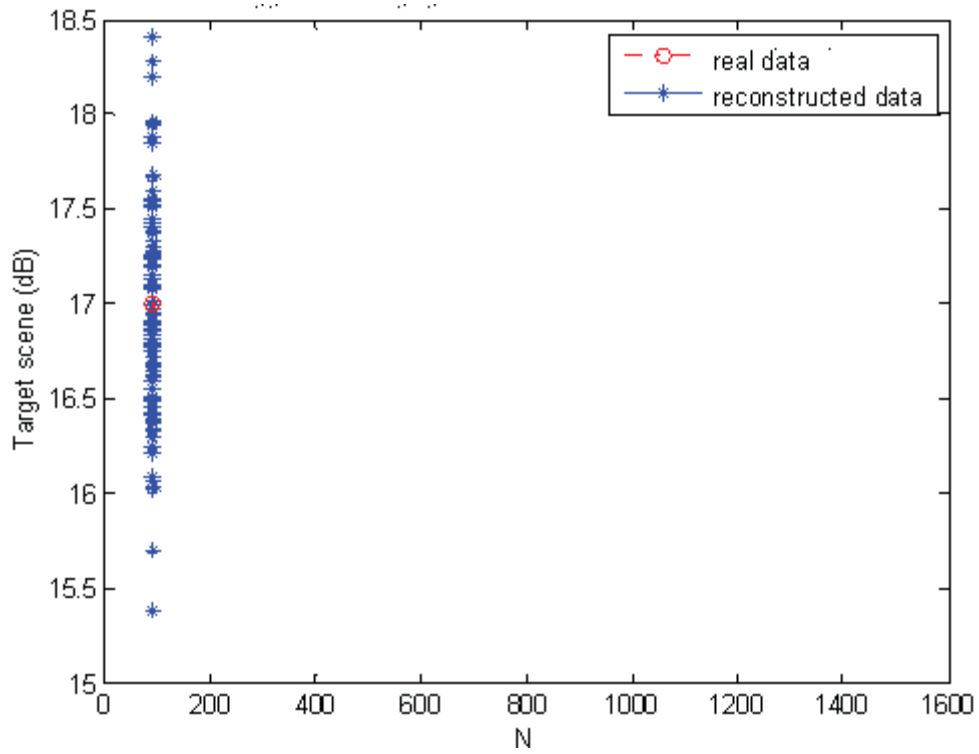


Figure 5-41 One target at 90<sup>th</sup> bin, 16 Doppler, 16 pulse, N=100, M=20, K=1 with SNR=17dB

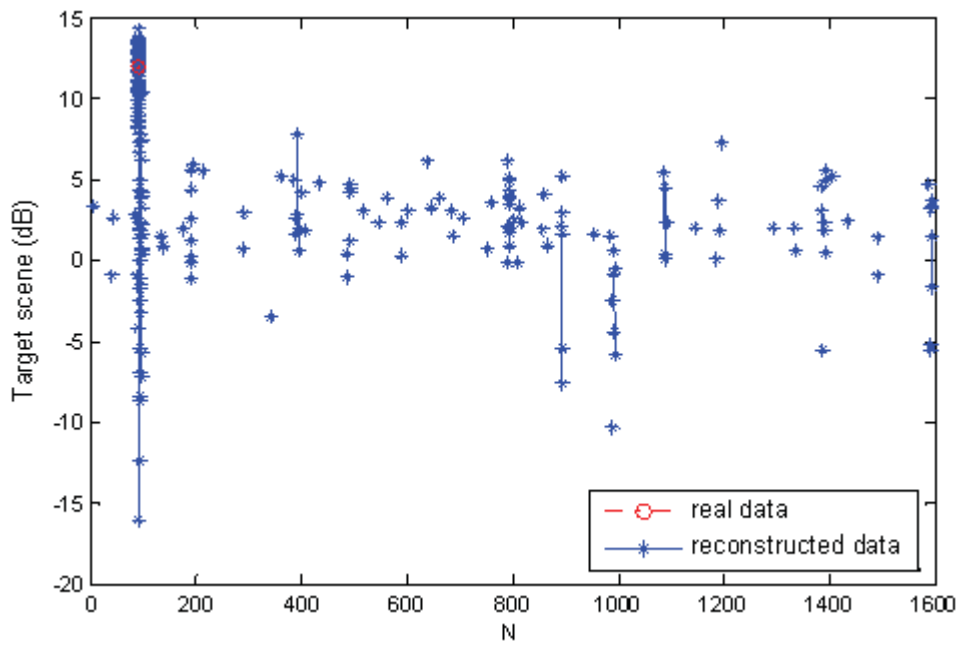


Figure 5-42 One target at 90<sup>th</sup> bin, 16 Doppler, 16 pulse, N=100, M=20, K=1 with SNR=12dB

- 2) One target is present at 750th bin at frequency= $f_g=4375$  Hz (50th range bin, 8th Doppler bin): For constant FAR =  $10^{-3}$ , threshold is found as 0.8948 and the probability of detection for the detection result in Figure 5-42 is found as 0.86. When SNR is increased to 15dB, the detection result is obtained as in Figure 5-43 and Pd=1.

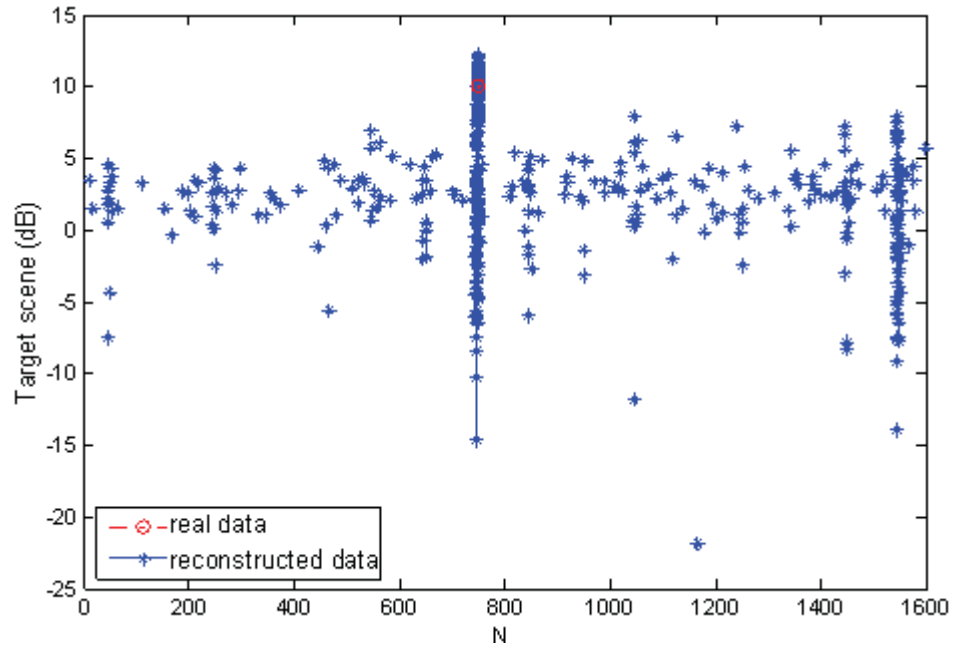


Figure 5-43 One target at 750<sup>th</sup> bin, 16 Doppler, 16 pulse, N=100, M=20, K=1 with SNR=10dB

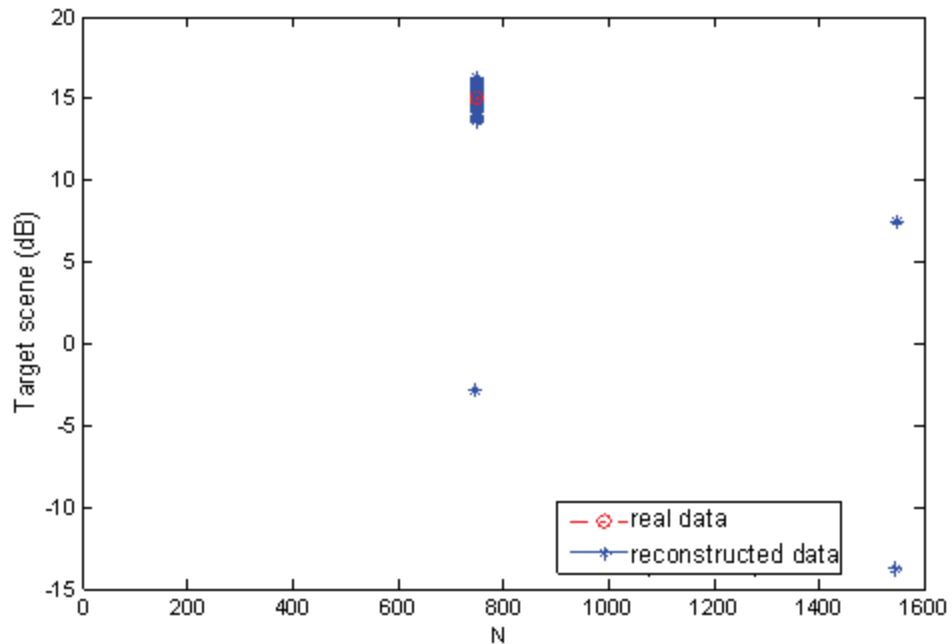


Figure 5-44 One target at 750<sup>th</sup> bin, 16 Doppler, 16 pulse, N=100, M=20, K=1 with SNR=15dB

**Pd vs SNR for 16 Doppler, 16 Pulses:** Probability of detection vs SNR graph together with the classical detection result is obtained for 16 Doppler, 16 pulse case as shown in Figure 5-44. The performance of CS method is about 2,5dB worse than the classical detection result.

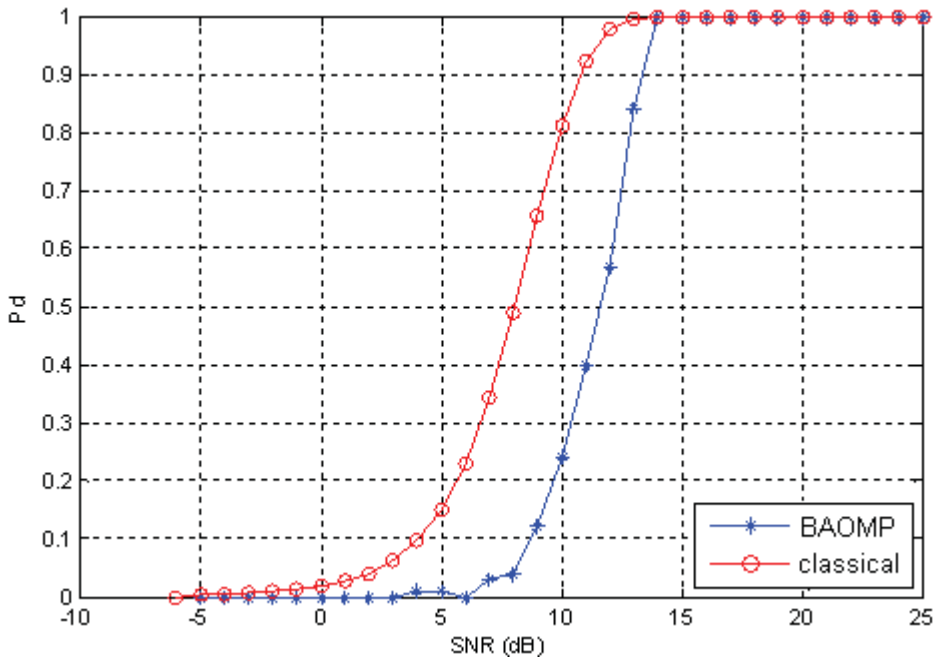


Figure 5-45 Pd vs SNR comparison for 16 Doppler, 16 pulses, FAR=10<sup>-3</sup>

**Threshold Determination:** The threshold value changes for every run of BAOMP algorithm for the same transmitted signal. To find a generalized threshold value; no target, only noise present case is run 10000 times for 16 Doppler 16 Pulse case, and the threshold value is found as 1.1768 for constant FAR = 10<sup>-3</sup>. Similarly, for 32 Doppler 16 Pulse case, the threshold value is found as 1.6116 for constant FAR = 10<sup>-3</sup>.

**32 Doppler, 16 Pulse Simulations:** Simulations performed for 16 Doppler, 16 pulse case are also performed for 32 Doppler, 16 pulse case. Scenario 3 is run 100 times for 32 Doppler frequencies and 16 transmitted pulses. Since we have 16 pulses and 32 Doppler frequencies, a  $16N \times 32N$  matrix will be formed. In our scenario, this means a  $1600 \times 3200$  matrix, and out of these 1600 rows  $16M=320$  rows will be randomly chosen. This results in a  $16M \times 32N = 320 \times 3200$  Measurement matrix.

- 1) One target is present at 2601<sup>th</sup> bin at frequency= $f_{27}=8125$  Hz (1<sup>th</sup> range bin, 27<sup>th</sup> Doppler bin). Detection result for SNR=10dB is given below. Probability of detection is found as 0.63.

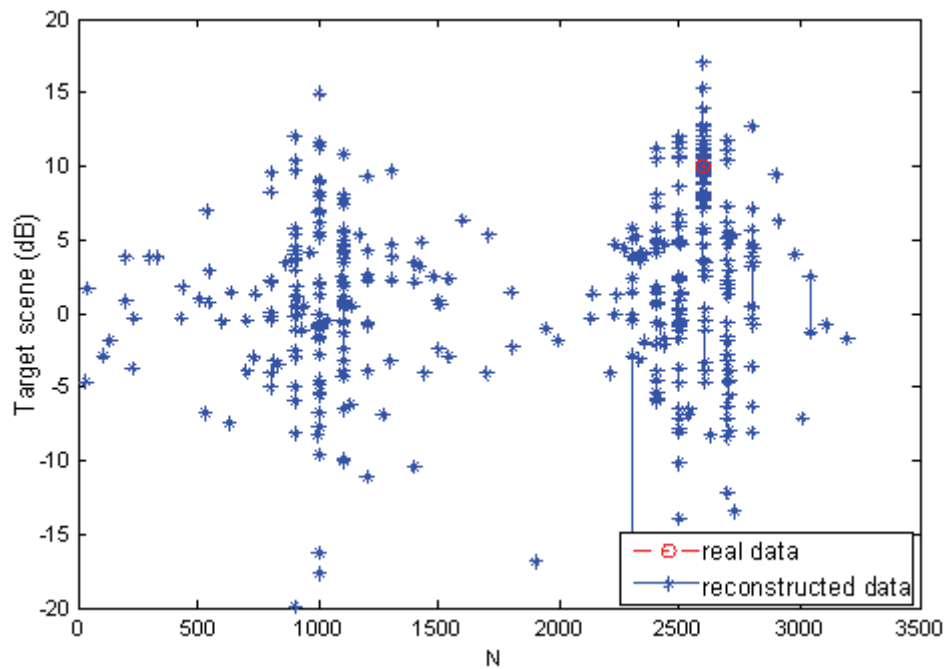


Figure 5-46 One target at 2601<sup>th</sup> bin, 32 Doppler, 16 pulse,  $N=100$ ,  $M=20$ ,  $K=1$  with SNR=10dB

- 2) **Single runs for SNR=10dB:** In Figure 5-45, the scenario is run 100 times and the total detection results are observed. To see the distribution of the detections in a single run, we run the same scenario once. We observe detections in a single run as shown in the figures below. On some runs the target is detected correctly, but on some other runs target cannot be detected and false alarms arise. False detections in a run are usually at bins close to each other.

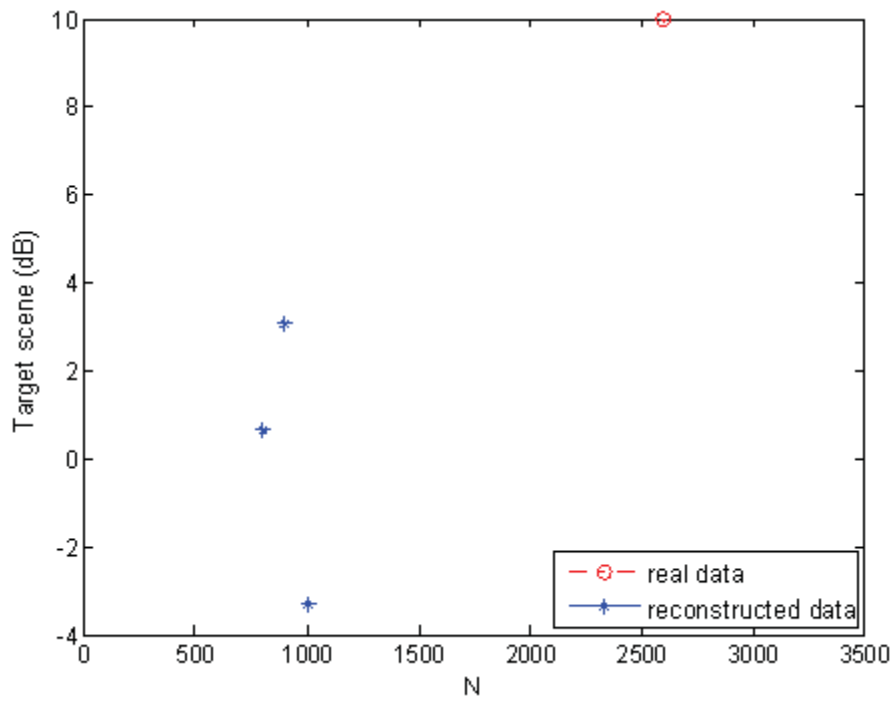


Figure 5-47 Single run for one target at 2601<sup>th</sup> bin, 32 Doppler, 16 pulse, N=100, M=20, K=1 with SNR=10dB

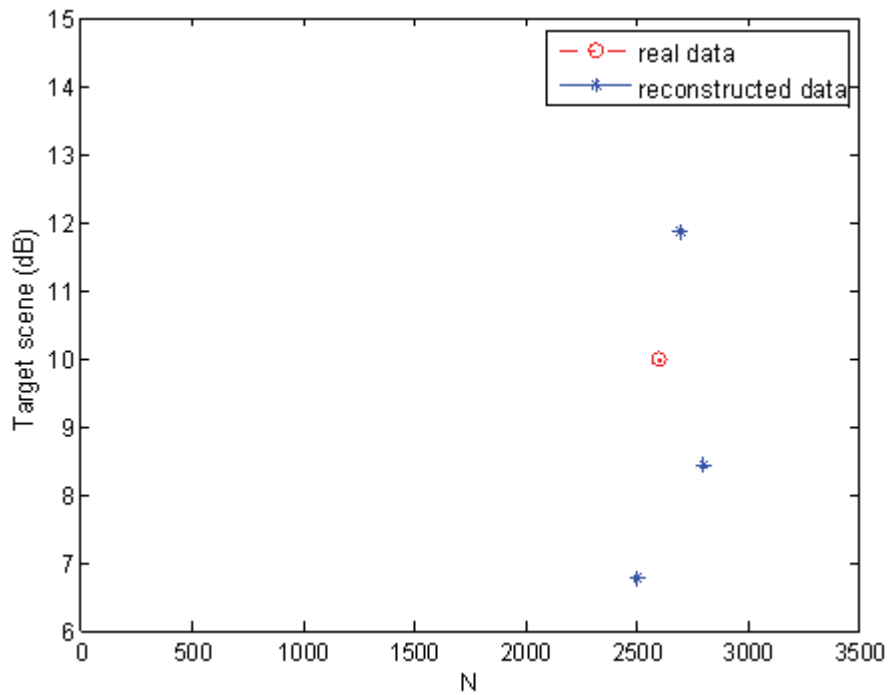


Figure 5-48 Single run for one target at 2601<sup>th</sup> bin, 32 Doppler, 16 pulse, N=100, M=20, K=1 with SNR=10dB

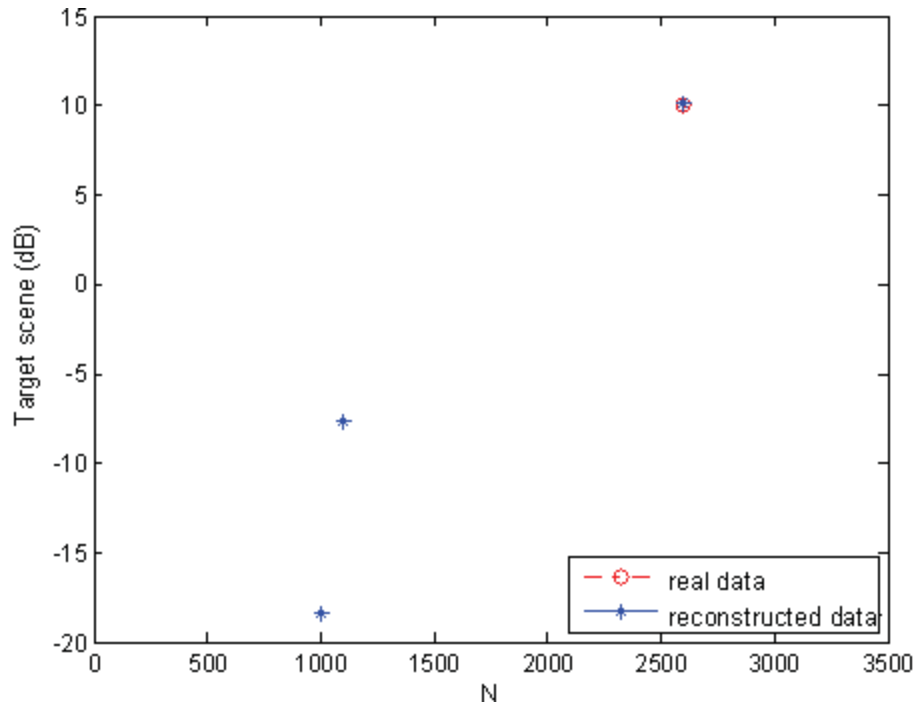


Figure 5-49 Single run for one target at 2601<sup>th</sup> bin, 32 Doppler, 16 pulse, N=100, M=20, K=1 with SNR=10dB

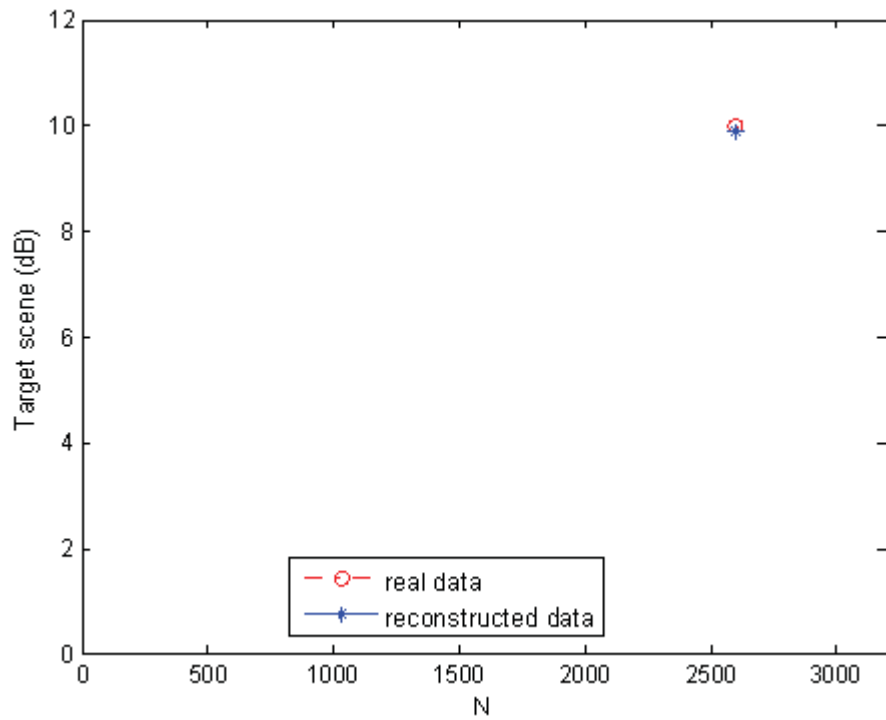


Figure 5-50 Single run for one target at 2601<sup>th</sup> bin, 32 Doppler, 16 pulse, N=100, M=20, K=1 with SNR=10dB

- 3) Same scenario in (1) is run with SNR=15dB. One target is present at 2601th bin at frequency= $f_{27}$ = 8125 Hz (1th range bin, 27th Doppler bin). Detection result for SNR=15dB is given below. Probability of detection is found as 0.81.

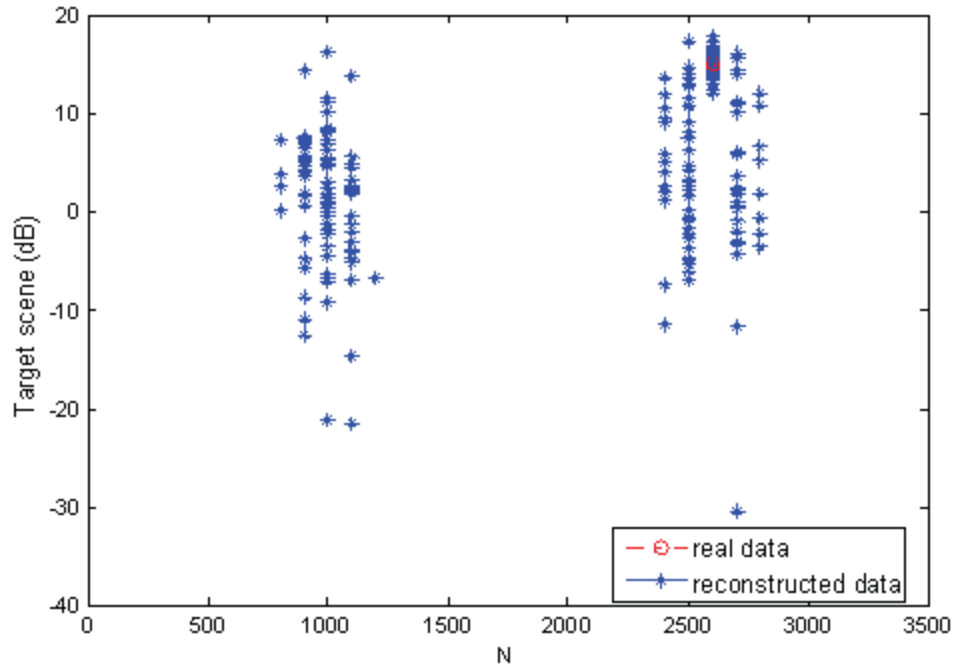


Figure 5-51 One target at 2601<sup>th</sup> bin, 32 Doppler, 16 pulse, N=100, M=20, K=1 with SNR=15dB

- 4) **Single runs for SNR=15dB:** The same analysis in (2) is done for SNR=15dB. At both runs below, the target is detected correctly, with some false detections.

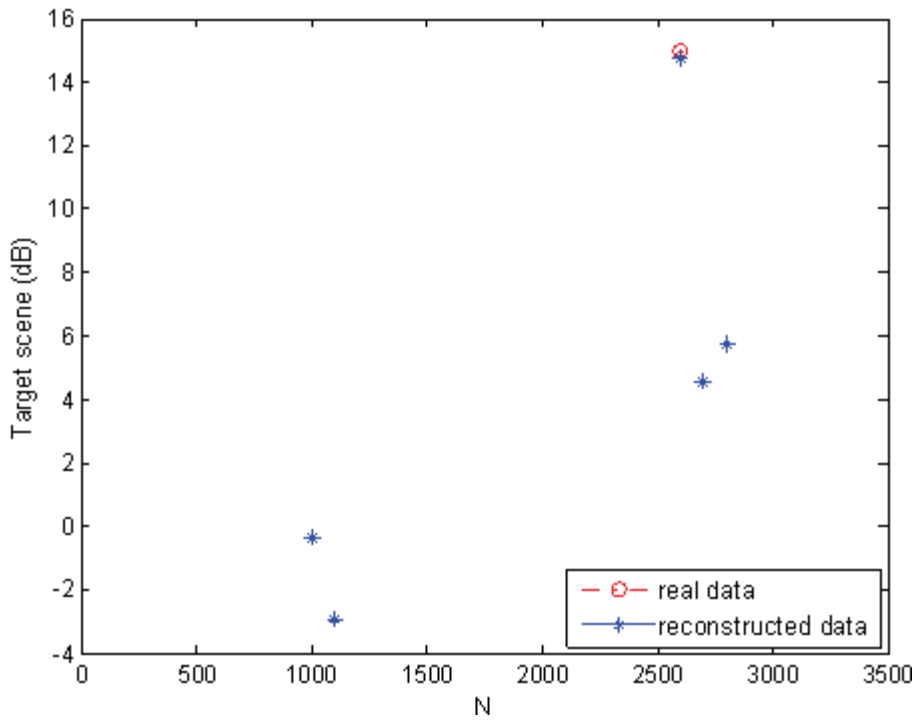


Figure 5-52 Single run for one target at 2601<sup>th</sup> bin, 32 Doppler, 16 pulse, N=100, M=20, K=1 with SNR=15dB

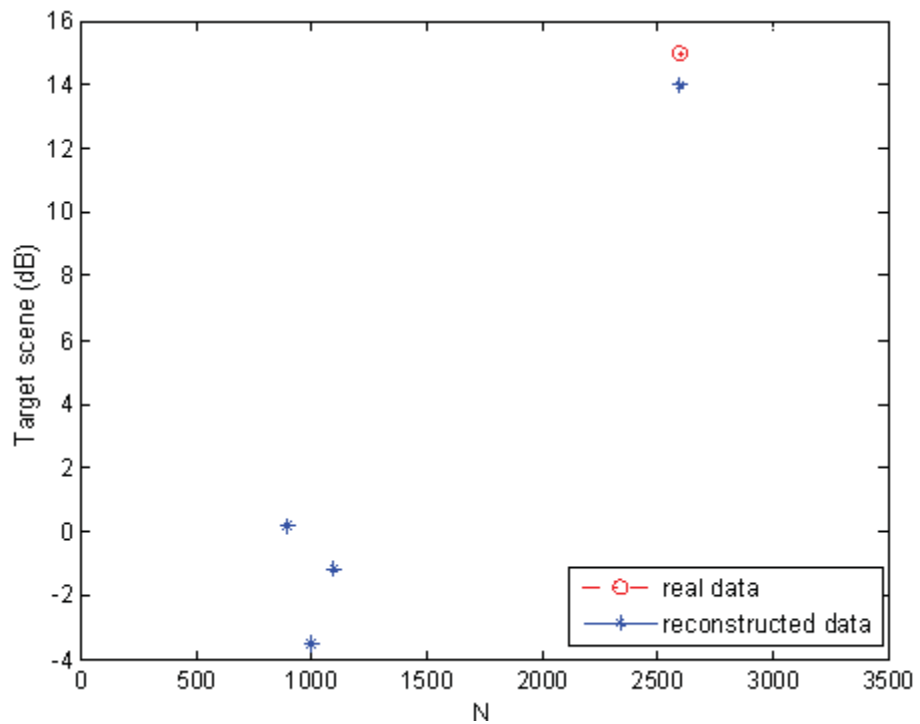


Figure 5-53 Single run for one target at 2601<sup>th</sup> bin, 32 Doppler, 16 pulse, N=100, M=20, K=1 with SNR=15dB

**Target at an offset Doppler frequency:** In all the above simulations in Section 5.2.13, the target possesses either zero Doppler frequency or Doppler frequency equal to a multiple of PRF/16. Now, a target at a frequency not equal to a multiple of PRF/16 exists. The detection performance of the BAOMP algorithm at detecting this target is analyzed. Scenario 3 is run 100 times for the same case in 32 Doppler, 16 pulse simulations. One target is present at 380th bin at frequency= 1000 Hz, and SNR=15dB. The probability of detection for the detection result in Figure 5-53 is found as 1. This result shows that targets at different frequencies, not on a multiple of PRF/16, can also be detected with the BAOMP algorithm.

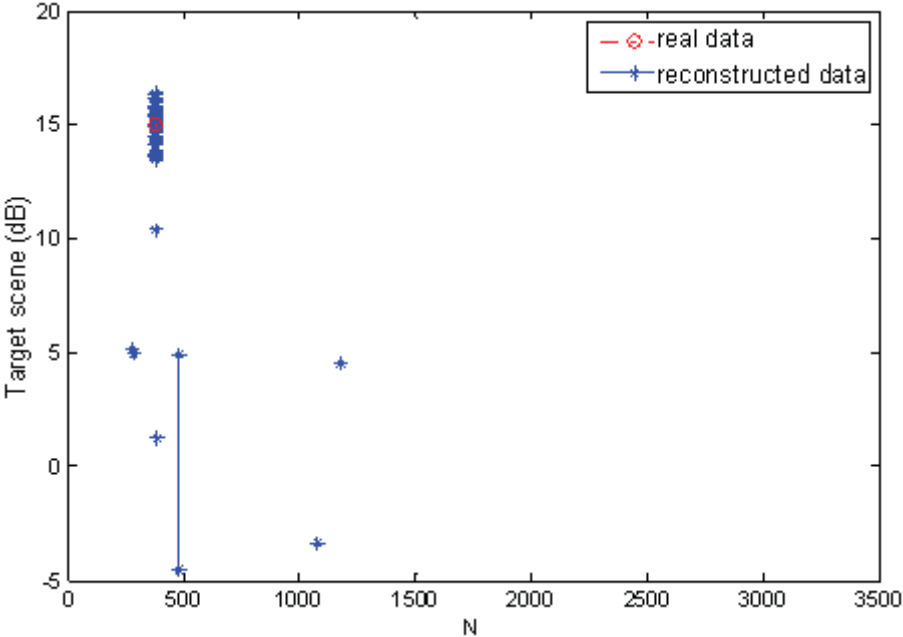


Figure 5-54 One target not at any Doppler frequency, 32 Doppler, 16 pulse, N=100, M=20, K=1 with SNR=15dB

**Pd vs SNR for 32 Doppler, 16 Pulses:** Probability of detection vs SNR graph together with the classical detection result is obtained as shown below in Figure 5-54 for 32 Doppler, 16 pulse case. The performance of CS method is about 4dB worse than the classical detection result.

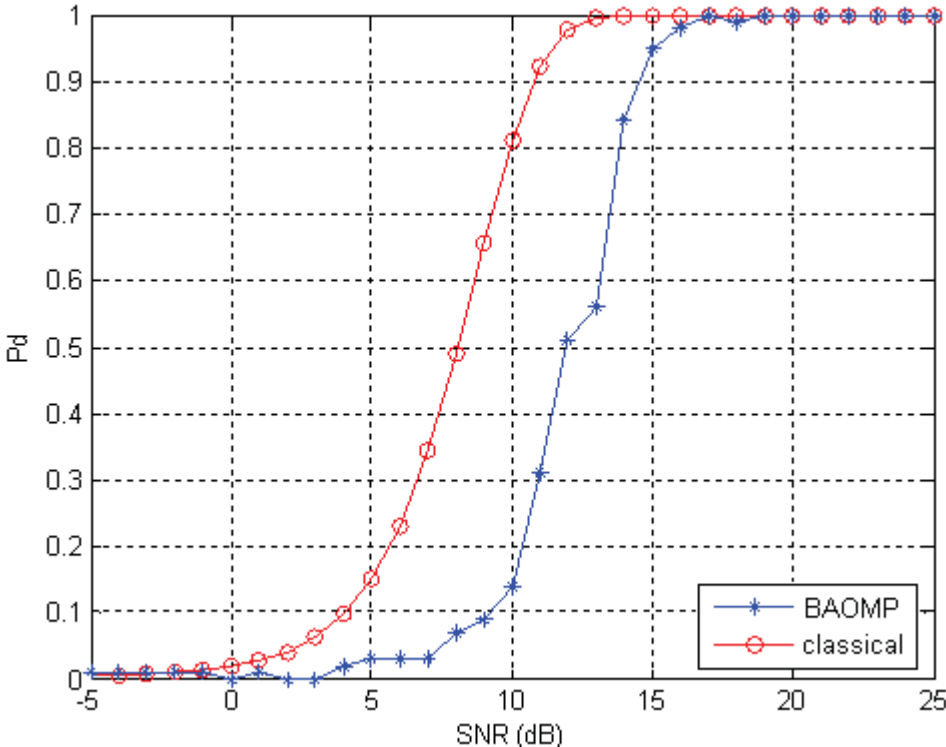


Figure 5-55 Pd vs SNR comparison for 32 Doppler, 16 pulses, FAR= $10^{-3}$

### 5.3 Summary of Simulation Results

The table below gives the summary of the simulations performed with their results.

#	Simulation	Result
1	Simulations for different transmitted signals (Alltop sequence, Barker Code, P4 Code and Random signal)	Among these transmitted signals, Barker Code is the worst. Others give similar results, so random signals are used in this thesis.
2	Choice of transmitted signal depending on the analyses of autocorrelation functions and Restricted Isometry Properties of different random signals of length-60	Autocorrelation function is not a measure of a good signal or a bad signal. The measure is the RIP. If the measurement matrix has smaller restricted isometry constant, the detection performance of the BAOMP is better.
3	OMP - BAOMP detection performance comparison	BAOMP finds the solution with a smaller number of iterations than OMP. CPU time of the BAOMP is also smaller than the OMP. The detection performance of the BAOMP is better than the OMP for noisy case.
4	Choice of $\alpha$ (the constant in the convergence threshold equation) depending on the analysis of its effect on the detection performance of the BAOMP	When $\alpha$ is greater than 0.05, exact recovery is observed.
5	Classical – $l_1$ Minimization – BAOMP detection performance comparison	The CS method (both $l_1$ minimization and BAOMP algorithm) gives better reconstruction results than the classical method, even by using a smaller number of measurements. Also, BAOMP has better detection performance than $l_1$

		minimization.
6	Detection of close targets	The CS with the BAOMP algorithm detects close targets at exactly correct positions.
7	FAR calculations for constant threshold value, no target - only noise present case with different convergence threshold (meaning different $\alpha$ values)	For $\alpha \geq 0.05$ , the BAOMP method detects no false alarms above the detection threshold, so FAR=0. Therefore, choosing $\alpha$ value greater than 0.05 is a good choice for the BAOMP algorithm.
8	Detection threshold calculations for constant FAR= $10^{-3}$ with different convergence threshold (meaning different $\alpha$ ) values	Detection threshold vs $\alpha$ graph is obtained for constant FAR. From the graph, one can say that the threshold value is stabilized at about 13.5dB when $\alpha \geq 0.0316$ , so choosing $\alpha$ greater than this value is better.
9	Probability of detection calculations for constant FAR= $10^{-3}$ and different SNR values with different convergence threshold (meaning different $\alpha$ ) values	Pd vs $\alpha$ graph is obtained for constant FAR. The graph shows that, for different SNR values, maximum reconstruction performance is achieved when $\alpha \geq 0.0316$ . Choosing $\alpha$ bigger decreases the number of iterations, so $\alpha$ is chosen larger than this value.
10	Classical and BAOMP probability of detection vs SNR graph comparison for constant FAR= $10^{-3}$ and with SNR loss of the CS method (7dB because of taking 200 measurements out of 1000) included	CS method with the BAOMP algorithm and classical method have the same performance when $SNR \geq 10dB$ . When $SNR < 10dB$ , the performance of the CS with the BAOMP algorithm is slightly worse than the classical method.
11	False detections around the target position when the BAOMP algorithm is used	The BAOMP algorithm makes very few wrong detections around the correct target position which is

		a good property.
12	The effect of Doppler to the performance of the CS	CS method also works when Doppler is present. This method can detect targets at an offset Doppler frequency. The performance of CS method is about 2.5dB worse than the classical detection result for 16 Doppler, 16 pulse case (processing gain of 12dB and SNR loss of -7dB are included).

**Table 1 Simulation Results Summary**

## CHAPTER 6

### CONCLUSION AND FUTURE WORK

This thesis has mainly focused on the usage of compressive sensing theory for radar target detection. First, the general compressive sensing theory is explained in detail. There are two conditions that should be satisfied in this theory: The target scene should be sparsely populated and the measurement matrix should be incoherent with any fixed basis. If these conditions are met, the target scene can be reconstructed by taking far fewer measurements or samples than traditional methods use.

While using the CS theory, there are two key points to consider:

- 1) The measurement matrix should be designed so that it satisfies the incoherence property. The choice of the transmitted signal is important since it generates the columns of the measurement matrix. In this thesis, the Alltop sequence, Barker coded, P4 coded and random signals are chosen as the transmitted signal. As a result, random signals are decided to be used as the transmitted signal. Also, the measurement matrix is chosen as the matrix which gives the best detection result out of 100 measurement matrices generated by 100 different transmitted signals.
- 2) The reconstruction algorithm to be used should be chosen. Three of the reconstruction algorithms;  $l_1$  minimization, OMP and BAOMP are described in this thesis. When the performances of these algorithms are compared, the best reconstruction algorithm is found to be the BAOMP.

A 1-dimensional, monostatic, far-field radar system is used in the thesis. The classical radar target detection procedure is explained. Then, the main aim of this thesis, which is the usability of the CS theory for reconstruction of target scene of a radar is explained. Radar target detection performance of the CS is better than the classical detection performance when appropriate conditions for CS are met. The same detection performance can be achieved by taking far less measurements than the classical detection. Also, the matched filter used in the classical detection is not used in the CS method.

In the BAOMP algorithm, there are some predefined constants. One of them is the convergence threshold which is one of the determining factors for the number of iterations in the BAOMP. The effect of this value on the performance of the BAOMP algorithm is analyzed and the convergence threshold value that gives the best detection result is chosen.

Detection of close targets is a problem in classical detection. In this thesis, CS method with the BAOMP algorithm is used to detect close targets. As a result, CS method can detect targets which are close to each other correctly. Also, analyses show that the CS method does not make false detections around the target position.

This thesis also includes the analysis of the detection threshold values under constant FAR and different convergence threshold values, using the BAOMP algorithm. With these detection threshold values, the probability of detection values are calculated for different SNR values. Probability of detection values of the CS for different SNR values are so close to that of the classical detection when the SNR loss which is proportional with the  $M/N$  ratio is compensated.

Finally, the effect of Doppler to the performance of the CS is analyzed for 16 Doppler, 16 pulse and 32 Doppler, 16 pulse cases. The results show that the CS method also works when Doppler is added. Therefore, when the appropriate conditions for CS are satisfied, CS method can be used for radar target detection.

In this thesis, a 1-dimensional, monostatic, far-field radar system is used. The target scene is designed to have maximum 1000 possible target locations. The analysis can be improved by using MIMO radars, increasing the maximum number of possible target locations, and adding the effects of clutter.

## REFERENCES

- [1] Richard G. Baraniuk, Compressive Sensing Lecture Notes, IEEE Signal Processing Magazine, July 2007
- [2] Graeme Pope, Compressive Sensing A Summary of Reconstruction Algorithms, Masters Thesis, Department of Computer Science Eidgenössische Technische Hochschule, Zürich, August 2008 to February 2009
- [3] Matthew Herman and Thomas Strohmer, Compressed Sensing Radar, IEEE International Conference on Acoustics, Speech and Signal Processing, 2008
- [4] Emmanuel J. Candès and Michael B. Wakin, An Introduction To Compressive Sampling, IEEE Signal Processing Magazine, March 2008
- [5] Stephen R. Becker, Practical Compressed Sensing: Modern Data Acquisition and Signal Processing Thesis, California Institute of Technology, Pasadena, California, 2011
- [6] Marco F. Duarte, Mark A. Davenport, Michael B. Wakin, and Richard G. Baraniuk, Sparse Signal Detection From Incoherent Projections, IEEE International Conference on Acoustics, Speech and Signal Processing, 2006
- [7] E. Candès, J. Romberg, and T. Tao, Robust Uncertainty Principles: Exact Signal Reconstruction From Highly Incomplete Frequency Information, IEEE Transactions on Information Theory, vol. 52, no. 2, pp. 489–509, February 2006
- [8] D. Donoho, Compressed Sensing, IEEE Transactions on Information Theory, vol. 52, no. 4, pp. 1289–1306, April 2006
- [9] Lokman Ayas, Ali Cafer Gürbüz, Sıkıştırılmış Algılamada Gerekli Ölçüm Sayısının Analizi, IEEE 18.Sinyal İşleme ve İletişim Uygulamaları Kurultayı, Diyarbakır, SIU2010
- [10] Emmanuel J. Candès, Compressive Sampling, European Mathematical Society, 2006
- [11] Dmitry Malioutov, Müjdat Çetin, Alan S. Willsky, A Sparse Signal Reconstruction Perspective for Source Localization With Sensor Arrays, IEEE Transactions on Signal Processing, Vol. 53, No. 8, August 2005
- [12] <http://cvxr.com/cvx/>
- [13] <http://users.ece.gatech.edu/~justin/11magic/>

- [14] Nazım Burak Karahanoğlu, Hakan Erdoğan, Compressed Sensing Signal Recovery via A\* Orthogonal Matching Pursuit, IEEE International Conference on Acoustics, Speech and Signal Processing, 2011
- [15] Joel A. Tropp, Anna C. Gilbert, Signal Recovery From Random Measurements Via Orthogonal Matching Pursuit, IEEE Transactions on Information Theory, vol. 53, no. 12, December 2007
- [16] H. Huang, A. Makur, Backtracking-Based Matching Pursuit Method for Sparse Signal Reconstruction, IEEE Signal Processing Letters, vol. 18, no. 7, pp. 391–394, July 2011
- [17] Mark A. Richards, Fundamentals of Radar Signal Processing, McGraw-Hill, 2005
- [18] Matthew A. Herman and Thomas Strohmer, High-Resolution Radar via Compressed Sensing, IEEE Transactions on Signal Processing, 2008
- [19] R. E. Blahut, W. Miller Jr., and C. H. Wilcox, Theory of Remote Surveillance Algorithms, in Radar and Sonar, Part I, ser. IMA Volumes in Mathematics and its Applications, Eds. NY: Springer-Verlag, vol. 32, pp. 1–65, 1991
- [20] K. Gröchenig, H. G. Feichtinger, and T. Strohmer, Uncertainty Principles for Time-Frequency Representations, in Advances in Gabor Analysis, ser. Applied and Numerical Harmonic Analysis, Eds. Boston: Birkhauser, pp. 11–30, 2003
- [21] A. W. Rihaczek, High-Resolution Radar, Boston: Artech House, 1996 (originally published: McGraw-Hill, NY, 1969)
- [22] Richard Baraniuk, Justin Romberg, Michael Wakin, Tutorial on Compressive Sensing, Information Theory and Applications Workshop, 2008
- [23] E. J. Candes and T. Tao, Decoding by Linear Programming, IEEE Transactions on Information Theory, 51(12):4203-4215, December 2005
- [24] E. J. Candes, The Restricted Isometry Property and Its Implications for Compressed Sensing, Comptes Rendus de l'Academie des Sciences, Paris, Serie I, 346 589-592, 2008
- [25] Anila Satheesh B., Deepa B., Subhadra Bhai, Anjana Devi S., Compressive Sensing for Array Signal Processing, IEEE Transactions on Information Theory, 2012